

INFORMATION TO USERS

This manuscript has been reproduced from the microfilm master. UMI films the text directly from the original or copy submitted. Thus, some thesis and dissertation copies are in typewriter face, while others may be from any type of computer printer.

The quality of this reproduction is dependent upon the quality of the copy submitted. Broken or indistinct print, colored or poor quality illustrations and photographs, print bleedthrough, substandard margins, and improper alignment can adversely affect reproduction.

In the unlikely event that the author did not send UMI a complete manuscript and there are missing pages, these will be noted. Also, if unauthorized copyright material had to be removed, a note will indicate the deletion.

Oversize materials (e.g., maps, drawings, charts) are reproduced by sectioning the original, beginning at the upper left-hand corner and continuing from left to right in equal sections with small overlaps. Each original is also photographed in one exposure and is included in reduced form at the back of the book.

Photographs included in the original manuscript have been reproduced xerographically in this copy. Higher quality 6" x 9" black and white photographic prints are available for any photographs or illustrations appearing in this copy for an additional charge. Contact UMI directly to order.

UMI

**A Bell & Howell Information Company
300 North Zeeb Road, Ann Arbor MI 48106-1346 USA
313/761-4700 800/521-0600**

UNIVERSITY OF ALBERTA

**3D MODELLING
FOR AN
INTRAOPERATIVE
STEREO-VISION
SYSTEM**

by

Jonathan Rasmusson



A thesis submitted to the Faculty of Graduate Studies and Research in partial fulfillment of the requirements for the degree of Master of Science.

**DEPARTMENT OF ELECTRICAL AND COMPUTER
ENGINEERING**

Edmonton, Alberta

SPRING 1998



**National Library
of Canada**

**Acquisitions and
Bibliographic Services**

**395 Wellington Street
Ottawa ON K1A 0N4
Canada**

**Bibliothèque nationale
du Canada**

**Acquisitions et
services bibliographiques**

**395, rue Wellington
Ottawa ON K1A 0N4
Canada**

Your file Votre référence

Our file Notre référence

The author has granted a non-exclusive licence allowing the National Library of Canada to reproduce, loan, distribute or sell copies of this thesis in microform, paper or electronic formats.

The author retains ownership of the copyright in this thesis. Neither the thesis nor substantial extracts from it may be printed or otherwise reproduced without the author's permission.

L'auteur a accordé une licence non exclusive permettant à la Bibliothèque nationale du Canada de reproduire, prêter, distribuer ou vendre des copies de cette thèse sous la forme de microfiche/film, de reproduction sur papier ou sur format électronique.

L'auteur conserve la propriété du droit d'auteur qui protège cette thèse. Ni la thèse ni des extraits substantiels de celle-ci ne doivent être imprimés ou autrement reproduits sans son autorisation.

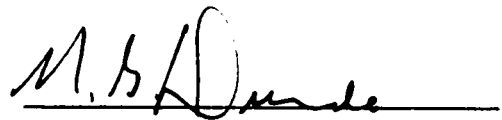
0-612-28980-X

Canada

University of Alberta

Faculty of Graduate Studies and Research

The undersigned certify that they have read, and recommend to the Faculty of Graduate Studies and Research for acceptance, a thesis entitled '*3D Modeling for an Intraoperative Stereo-Vision System*' submitted by *Jonathan Rasmuson* in partial fulfillment of the requirements for the degree of *Master of Science*.



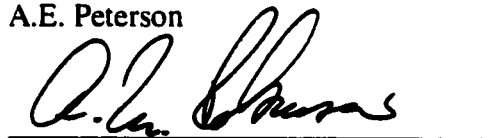
N.G. Durdle



V.J. Raso



A.E. Peterson



A.M. Robinson

Date: Nov. 26/97

Abstract

Success rates of scoliosis surgery are very dependent on the skill and experience of the surgeon. An objective measurement tool would provide surgeons with insight into the successes and failures of these surgeries. This work continues the development of an Operating Room Imaging System (ORIS) capable of tracking the three-dimensional (3D) motion of artificial markers rigidly attached to vertebrae during the surgical correction of scoliosis.

Accuracy experiments were conducted on ORIS. Small predetermined displacements and rotations were made to artificial markers mounted on the spinous processes of vertebra while results were recorded by the stereo-vision system. The system was determined to have an accuracy of +/- 1mm. This result was judged to be excellent and demonstrated that small millimetre displacements of artificial markers could be accurately detected by ORIS.

Because ORIS detects the position and orientation of artificial markers, a model was developed to relate the artificial markers to the vertebrae for visualization. Geometry, vector analysis, and stereo- radiographs were used to relate the artificial markers to the vertebrae. Experiments were done using stereo-radiographs and an electromagnetic digitizer to determine the orientation and position of vertebrae in a simulated operating room (OR) environment. Results demonstrated that the model performed as expected when supplied accurate data from an electromagnetic digitizer.

Stereo-radiographs however were deemed too inaccurate to provide the necessary data for the model.

Additional tools were added to the visualization stage of ORIS. Multiple simultaneous views of the spine were added. The user can view successive stages of the surgery also. Various 3D computer models of vertebra were developed to investigate optimal spine graphical representation. Surgeons were asked which model was most useful to them as a tool in spinal visualization. They favoured the more detailed models despite the longer rendering times.

Acknowledgements

Like any long piece of multi-disciplinary work, this work owns its success to a number of people. I would like to express my sincere gratitude to:

my supervisor, Dr. Nelson G. Durdle for his encouragement, guidance and support throughout my studies.

the very patient and accommodating Doug Hill and Jim Raso from the Glenrose Rehabilitation Technology Group for sharing their valuable expertise and knowledge in scoliotic research. I am extremely obliged to Doug and his system administrative skills at mounting faulty hard drives that had the knack for breaking down at the most inopportune times.

the Glenrose Radiology Department (Heather, Corey and Suzanne) for accommodating me and all those impromptu afternoon visits with my cameras, laptop and human spine model.

surgeon Dr. Mahood for his valuable feedback and insight into scoliotic surgery visualization.

Kevin Grant for his vast knowledge and insight into C and invaluable help in debugging software. Also to be thanked for many insightful discussions on the advantages of owning a Mac.

my friends : Derek, Roger, and Lawrence for all those colourful hockey discussions and letting me win the 1996-1997 NHL Hockey Draft (Go Gretzky!).

my wife Tannis whose love and encouragement kept me going when the going got tough.

grandma and grandpa Merle and Lloyd, and George for all your love, wisdom and insight into life and keeping things in perspective.

my parents Murray and Laurie for their undying love and guidance to make me who I am today - a very grateful person.

Table of Contents

1 INTRODUCTION	1
1.1 Objectives	1
1.2 Overview	2
2 BACKGROUND	4
2.1 Scoliosis	4
2.2 Intraoperative Monitoring	6
2.3 Stereo-vision in the Operating Room.....	7
2.4 Previous research on ORIS	11
2.4.1 <i>Camera modelling</i>	11
2.4.2 <i>Image Acquisition</i>	12
2.4.3 <i>Photogrammetry</i>	13
2.4.4 <i>Feature Detection</i>	14
2.4.5 <i>Feature Correspondence</i>	16
3 ACCURACY EXPERIMENTS.....	17
3.1 Displacement Experiments	17
3.1.1 <i>Displacement Experiment Results</i>	19
3.1.2 <i>Discussion of Displacement results</i>	21
3.2 Rotation Experiments.....	23
3.2.1 <i>Rotation of Kappa</i>	24
3.2.2 <i>Rotation Experiment Results</i>	26
3.2.3 <i>Discussion of Rotation Results</i>	29
4 TRIAD VERTEBRA GEOMETRIC MODEL	31
4.1 Background	32
4.2 Rotating a point about an arbitrary line in free space.....	36
4.2.1 <i>3D transformations</i>	36
4.2.2 <i>Algorithm for rotating a point about an arbitrary line in free space</i>	39
4.3 Triad vertebra model.....	41

4.4 Calculation of vertebra position and orientation.....	42
4.5 Model Experiments.....	46
4.5.1 <i>FOB Model Experiment</i>	47
4.5.1.1 Results and Discussion	50
4.5.2 <i>FOB X-ray Experiment</i>	58
4.5.2.1 Results and Discussion	60
5 VISUALIZATION	67
5.1 Background	67
5.2 ORIS software model and direct interface	69
5.3 Multiple stages of operation	71
5.4 Multiple views	72
5.5 Models of Vertebra.....	75
5.5.1 <i>Wire Frame model</i>	77
5.5.2 <i>Positional model</i>	78
5.5.3 <i>Orientation model</i>	80
5.5.4 <i>Geometric model</i>	82
5.5.5 <i>Rendering times</i>	84
5.5.6 <i>Comparison of models</i>	85
6 CONCLUSIONS AND RECOMMENDATIONS	87
6.1 Summary of Results.....	87
6.2 Recommendations for future work	89
6.3 Conclusions	92
REFERENCES	93
APPENDIX A SYSTEM SPECIFICATIONS	97
APPENDIX B SOFTWARE MODEL: SHOW-POINT	98
APPENDIX C TRIAD2VERT FLOWCHARTS.....	106
APPENDIX D DRAW MODULE FLOWCHARTS	117

List of Tables

Table 2.1 Equipment used to capture images..... 13

Table 3.1. Results of ORIS detecting 1,3,5 mm displacements in xyz..... 19

Table 3.2 ORIS measured displacements of +/- 1mm in x,y,z (m - mean, s.d. - standard deviation, e - mean absolute value of error). 20

Table 3.3 ORIS measured rotations about the x and y-axis..... 26

Table 3.4 ORIS measured rotations of +/- 1° about x,y,z axes (m - mean, s.d. - standard deviation, e - mean absolute value of error). 28

Table 3.5 ORIS measured rotations of +/- 15° about x,y,z axes (m - mean, s.d. - standard deviation, e - mean absolute value of error). 28

Table 3.6 ORIS measured rotations of +/- 30° about x,y,z axes (m - mean, s.d. - standard deviation, e - mean absolute value of error). 29

Table 4.1(a) FOB data before and after -3 cm displacement in z. 51

Table 4.1(b) FOB vertebra body orientation before and after -3 cm displacement in z. 51

Table 4.1(c) FOB vertebra body position before and after -3 cm displacement in z. 51

Table 4.1(d) Triad body orientation measured by ORIS before and after -3 cm displacement in z. 52

Table 4.1(e) Triad body position measured by ORIS before and after -3 cm displacement in z. 52

Table 4.1(f) Model calculated vertebra body orientation before and after -3 cm displacement in z. 52

Table 4.1(g) Model calculated triad vertebra position vector TB_0 before and after -3 cm displacement in z. 52

Table 4.2(a) FOB data before and after +10° rotation about the x-axis and displacement of +3.5 cm in y and +1 cm in z. 53

<i>Table 4.2(b) FOB vertebra body orientation before and after +10° rotation about the x-axis and displacement of +3.5 cm in y and +1 cm in z.</i>	<i>53</i>
<i>Table 4.2(c) FOB vertebra body position before and after +10° rotation about the x-axis and displacement of +3.5 cm in y and +1 cm in z.</i>	<i>53</i>
<i>Table 4.2(d) Triad body orientation measured by ORIS before and displacement of after +10° rotation about the x-axis and displacement of +3.5 cm in y and +1 cm in z.</i>	<i>54</i>
<i>Table 4.2(e) Triad body position measured by ORIS before and +10° rotation about the x-axis and displacement of +3.5 cm in y and +1 cm in z.</i>	<i>54</i>
<i>Table 4.2(f) Model calculated vertebra body orientation before and after +10° rotation about the x-axis and displacement of +3.5 cm in y and +1 cm in z. ...</i>	<i>54</i>
<i>Table 4.2(g) Model calculated triad vertebra position vector TB_0 before and +10° rotation about the x-axis and displacement of +3.5 cm in y and +1 cm in z. ...</i>	<i>54</i>
<i>Table 4.3(a) TB_0 measured results from FOB and X-RAY of non-rotated spine.</i>	<i>62</i>
<i>Table 4.3(b) B measured results from FOB and X-RAY of non-rotated spine.</i>	<i>62</i>
<i>Table 4.4(a) TB_0 measured results from FOB and X-RAY rotated spine.</i>	<i>62</i>
<i>Table 4.4(b) B measured results from FOB and X-RAY rotated spine.</i>	<i>62</i>
<i>Table 4.5 Amount of rotation detected by FOB and x-ray.</i>	<i>62</i>
<i>Table 4.6(a) Scaled x-ray non-rotated results.</i>	<i>65</i>
<i>Table 4.6(b) Scaled x-ray rotated results.</i>	<i>65</i>
<i>Table 5.1 Time to render each vertebra model (all times are in seconds).</i>	<i>84</i>

List of Figures

<i>Fig. 2.1 Conventional stereo setup.</i>	8
<i>Fig. 2.2 Epipolar geometry based on two stereo cameras.</i>	10
<i>Fig. 2.3 Peg board used in camera calibration.</i>	12
<i>Fig. 2.4 A triad mounted on the spinous process of a vertebra.</i>	15
<i>Fig. 3.1 Experimental setup used in displacement and rotation experiments. This setup was for rotational experiments. The rotating table vice would be replaced with another caliper for displacement experiments.</i>	18
<i>Fig. 3.2 Defining angles of rotation ϕ, ω and κ.</i>	23
<i>Fig. 3.3 3D plane made by triad balls.</i>	24
<i>Fig. 3.4 (a) a triad before rotation about the z-axis.</i>	26
<i>(b) a triad after rotation about the z-axis.</i>	26
<i>Fig. 3.5 Triad ball features become less visible at 40° angle rotations.</i>	27
<i>Fig. 4.1 Vertebra position and orientation are not the same as triad.</i>	32
<i>Fig. 4.2 Rigid body undergoing a rotation about CR_i.</i>	33
<i>Fig. 4.3 Rotating point P_3 by θ about an arbitrary line segment $P_1 P_2$.</i>	39
<i>Fig. 4.4 Geometric model of vertebra and triad.</i>	41
<i>Fig. 4.5 Calculating vertebra position $C_i = D_i - TB_i$.</i>	43
<i>Fig. 4.6 Calculating Stage I results based on Stage 0 results.</i>	44
<i>Fig. 4.7 The electromagnetic digitizer Flock Of Birds (FOB) used for making vertebra feature measurements.</i>	47
<i>Fig. 4.8 Caliper was used to accurately displace vertebra in FOB Model experiments.</i>	48
<i>Fig. 4.9 ORIS camera setup and Cartesian coordinate system for FOB Model experiment.</i>	49
<i>Fig. 4.10 Experimental setup used in FOB X-RAY experiments.</i>	59
<i>Fig. 4.11 X-rayed objects are enlarged when exposed onto film.</i>	64
<i>Fig. 5.1 Components of ORIS.</i>	70
<i>Fig. 5.2 Spine segment (T5-T9) displaying various stages of the spinal curvature.</i> ..	71
<i>Fig. 5.3 3D coordinate system in each display window.</i>	73

<i>Fig.5.4 Wire frame cube surrounding rotated spine.....</i>	<i>73</i>
<i>Fig. 5.5 Multiple simultaneous views of spine segment (T5-T9).</i>	<i>74</i>
<i>Fig. 5.6 Dominant features of vertebra.....</i>	<i>75</i>
<i>Fig. 5.7 Model of spine segment T5-T9 using wire frame model.</i>	<i>77</i>
<i>Fig. 5.8 Positional model of vertebra.</i>	<i>78</i>
<i>Fig. 5.9 Model of spine segment T5-T9 using positional model.</i>	<i>79</i>
<i>Fig. 5.10 Orientation model of vertebra.</i>	<i>80</i>
<i>Fig. 5.11 Model of spine segment T5-T9 using orientation model.....</i>	<i>81</i>
<i>Fig. 5.12 Geometric model representation of vertebra including spinous and transverse processes.</i>	<i>82</i>
<i>Fig. 5.13 Model of spine segment T5-T9 using geometric model.....</i>	<i>83</i>
<i>Fig. B.1 SHOW-POINT: Software Modules.</i>	<i>99</i>
<i>Fig. B.2 triad2vert software module and respective routines.....</i>	<i>100</i>
<i>Fig. B.3 draw software module and respective routines.</i>	<i>101</i>
<i>Fig. B.4 draw_spine software module and respective routines.</i>	<i>101</i>
<i>Fig. B.5 misc software module and respective routines.</i>	<i>102</i>
<i>Fig. B.6 drawing_area_callback software module and respective routines.</i>	<i>102</i>
<i>Fig. B.7 Read_data flowchart.....</i>	<i>103</i>
<i>Fig. B.8 Interpolate flowchart.</i>	<i>105</i>
<i>Fig. C.1 Vectorize flowchart.....</i>	<i>107</i>
<i>Fig. C.2 Rotate_x, Rotate_y, Rotate_z flowcharts.</i>	<i>110</i>
<i>Fig. C.3 Phi_omega_kappa flowchart.....</i>	<i>111</i>
<i>Fig. C.4 Angle flowchart.</i>	<i>113</i>
<i>Fig. C.5 Cross_product flowchart.....</i>	<i>114</i>
<i>Fig. C.6 Rotate_about_A flowchart.</i>	<i>115</i>
<i>Fig. D.1 CenterSpine flowchart.</i>	<i>118</i>
<i>Fig. D.2 InitVert flowchart.</i>	<i>119</i>
<i>Fig. D.3 WireFrame, position, geometric flowcharts.</i>	<i>120</i>
<i>Fig. D.4 Draw_triad flowchart.</i>	<i>121</i>
<i>Fig. D.5 Draw_xaxis, draw_yaxis, draw_zaxis flowchart.</i>	<i>122</i>

<i>Fig. D.6 Spotlight flowchart.</i>	123
<i>Fig. D.7 Draw flowchart.</i>	124
<i>Fig. D.8 Draw_spine flowchart.</i>	132
<i>Fig. E.1 RTS flowchart.</i>	135
<i>Fig. E.2 Reset flowchart.</i>	137
<i>Fig. E.3 Drawing_area_callback flowchart.</i>	139
<i>Fig. E.4 CascadeButton flowchart.</i>	141
<i>Fig. E.5 CascadePushButton flowchart.</i>	142
<i>Fig. E.6 CascadeToggleButton flowchart.</i>	143
<i>Fig. E.7 DisplayCB flowchart.</i>	144

1 INTRODUCTION

Scoliosis is an abnormal curvature of the spine with axial rotation of the vertebrae. In severe cases, surgery is used to correct the excess curvature and rotation of the spine. This work continues the development of an Operating Room Imaging System (ORIS) (Bhalla, 1995) capable of making intraoperative three-dimensional measurements of markers during scoliosis surgery.

The success of scoliotic surgeries depends on the skill and experience of the surgeon. There is currently no means of objectively measuring the procedure of surgical scoliosis correction. This led to the development of an imaging system capable of making accurate three-dimensional measurements intraoperatively. It is hoped that this tool will provide surgeons with further insight into the successes and failures of scoliotic operations.

1.1 Objectives

A three-dimensional intraoperative imaging system (ORIS) was created to provide surgeons with real-time feedback during surgery (Bhalla, 1995). Stereo video cameras were able to detect triad markers attached to specific vertebrae of a spine during a corrective operation. With the triad's 3D positions and orientations, it was possible to create a 3D model of the spine for display on a computer console.

Before ORIS can be accepted as a useful clinical tool, several areas required further research. The accuracy of ORIS needed to be determined. Attaching triad markers to vertebrae, to assist in feature detection, led to questions regarding the geometric relationship between the triad and the vertebra. Three-dimensional visualization tools needed to be interfaced with the current imaging system software. Further research into optimal 3D modelling of the spine was also required.

These motivations lead to the following objectives:

1. Determine the accuracy of ORIS.
2. Develop and test a mathematical model that relates the artificial triad markers to the vertebrae in a laboratory environment.
3. Investigate optimal ways of rendering a 3D spinal model.

1.2 Overview

Bhalla successfully demonstrated that intraoperative spinal measurements could be made using principles of computer vision. However, more work remained before ORIS can be accepted as a useful clinical tool. The following chapters address some of these remaining issues.

Chapter 2 provides background into the nature of scoliosis and how stereo-vision can be used in the Operating Room (OR) for monitoring scoliosis surgeries. A brief review of Bhalla's work is presented along with a review of the stereo-vision paradigm.

Chapter 3 explains the experiments performed to determine the spatial accuracy of ORIS. Translation and rotation experiments were done to test the ability of ORIS to detect changes in position and orientation of artificial triad markers. The experiments performed and respective results are presented.

Chapter 4 explains the mathematical model developed to relate the artificial triad markers and the vertebrae. Stereo x-rays were used to geometrically relate the vertebrae to their respective mounted markers. A detailed description of the model,

and the experiments performed to test its functionality are presented along with laboratory results.

Chapter 5 describes improvements made to the visualization stage of ORIS. Software has been added to simultaneously display multiple views of the spine. The capability to view multiple stages of surgery has also been added. Various geometric shapes used to represent the vertebra were explored to discover which ones were optimal at conveying visual information. Merits of the various models are compared and discussed.

Chapter 6 concludes this work by summarizing the research done, the current limitations of ORIS, as well as further areas of research.

2 BACKGROUND

2.1 Scoliosis

The word 'scoliosis' is derived from the Greek word meaning 'crookedness'. It is defined as abnormal lateral curvature of the spine. Most cases of scoliosis are detected during the rapid growth spurt of adolescence. The most common form of scoliosis is *idiopathic* scoliosis, meaning 'curvature without a cause' (Robin, 1973). This form accounts for 80-85% of cases. It tends to run in families, though it is not thought to be associated with a single gene. It is believed 10% of the adolescent population has some degree of scoliosis; however, most mild cases do not require treatment. Only 0.5% have scoliosis curves greater than 20° and less than 0.1% have scoliosis curves greater than 40°. Statistically, girls' spinal curves tend to grow more rapidly than boys'. For curves severe enough to warrant treatment, females outnumber males by 5:1.

Mild cases of scoliosis have little effect on the trunk other than causing slight asymmetric deformity on the shape of the spine. However, more severe cases with large scoliotic curves can impair proper functioning of the back. Posture imbalance (head no longer centered over pelvis) forces back muscles to work harder to maintain erect posture. This can lead to increased muscle fatigue and pain. Abnormal stresses on the discs in the spine may eventually cause arthritis. When the spine curves laterally, the vertebrae of the spine must also rotate correspondingly. This creates the most noticeable sign of scoliosis: the rib hump that projects from the plane of the back. Other symptoms of scoliosis include one shoulder blade (usually the right) higher than the other, an asymmetrical waistline, and an abnormally shaped back.

Few methods of measuring the severity of scoliosis exist. Orthopedists determine the magnitude of a scoliotic curve by measuring what is referred to as the Cobb angle (Asher, 1992) (Cobb, 1948). Lines are drawn on front-to-back radiographs parallel to the end plates of the highest and lowest vertebrae involved in a scoliotic curve. These vertebrae are the ones most angled in the curve. Another line is drawn perpendicular to each of these lines. The intersection of these two perpendicular lines produces the Cobb angle. Spinal curves with Cobb angles less than 10° are not considered scoliotic.

While widely accepted and used, the Cobb angle is a 2D measure that does not give the complete 3D picture of the deformity. Stereo-radiographs (x-rays), posterior-anterior (PA) and lateral, are the most common tools used to evaluate deformity and to plan surgery. Bracing and corrective surgery are most often used in treating scoliosis. The type of treatment used depends on the severity of the deformity (De Giorgi, 1992). In extreme cases (Cobb angle greater than 50°) surgery is performed. Invasive procedures involve rigidly attaching instrumentation to the spine where corrective forces are then applied to straighten the spine. One method of treatment, Cotrel-Dubousset (CD), is based on the belief that correction is primarily the result of derotations of vertebrae during instrumentation maneuvers (Morrissy, 1992) (Weinstein, 1994). Another form of treatment uses Harrington maneuvers that involve applying stretching forces to instrumentation attached to the spine, thereby straightening the spine. It is currently unclear which method is superior. Part of the uncertainty of which corrective method is better is because the conventional tools for measuring scoliosis, radiographs, are not reliable or convenient for intraoperative assessment of 3D correction. Unfortunately, there is no other widely used tool that does this.

2.2 Intraoperative Monitoring

Intraoperative measurements allow surgeons to closely monitor and record the corrections they make to the scoliotic spine during corrective surgery. If intraoperative monitoring could be made accurate, better quantitative analysis of the operation would offer surgeons improved insight into the successes and failures of these corrective operations. Features on the scoliotic spine are usually measured with stereo-radiographs. This procedure is both cumbersome and subject to many limitations. The radiographs themselves do not produce clear pictures and are subject to non-uniform distortions. Radiographs use radiation, which is undesirable for the patient. In addition, corrective instrumentation can obscure view of the vertebrae.

Bhalla defined the following requirements of an intraoperative measurement tool for scoliosis:

- it must satisfy all operating room constraints of safety and sterility
- it should make automatic on-line measurements and provide easily interpreted results in near real-time
- it should make accurate measurements in three dimensions (approx. 1-2 mm and 1°)
- it should have the capability to record and present visual results

Related research in this area has taken place (Labelle, 1995) (Treadwell, 1995). By drilling small holes on the spinal column as reference points, Labelle used an electromagnetic digitizer to record 3D positional point measurements. These measured points on vertebra were later used to create a 3D model of the spine. This left no opportunity for real-time feedback to the surgeon during an operation. This method is very labor intensive and prone to error due to the patient's breathing. These problems have lead to other directions of research for intraoperative monitoring - stereo cameras. Treadwell used single reflex cameras and traditional surveying

techniques to take stereo photographs of the spine during surgery. Before a 3D model of the spine could be created, the stereo photographs were processed and manually digitized. This does not satisfy the real-time monitoring requirement and photographs had to be manually processed leaving the results prone to human error and judgment.

It was the previously described requirements that lead to the development of the Operating Room Imaging System (ORIS) (Bhalla, 1995). ORIS uses calibrated stereo-video cameras with a frame grabber and computer to take intraoperative images during surgery and reconstruct a model of the spine.

2.3 Stereo-vision in the Operating Room

Stereo-vision permits the creation of 3D models by making use of two or more different views of a scene. Conventional stereo imaging uses two cameras laterally displaced to capture the stereo images. Figure 2.1 shows a conventional stereo setup. Two camera systems are shown with their respective image planes (I_L , I_R) and focal lengths (F_L , F_R). The 3D point P is projected onto each image plane at points P_L and P_R .

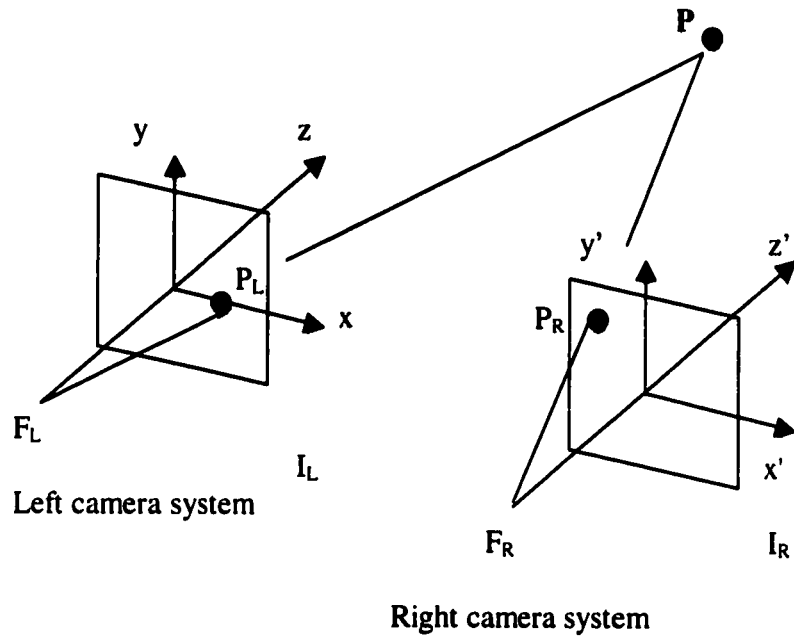


Fig. 2.1 Conventional stereo setup.

The cameras are calibrated if extrinsic and intrinsic parameters are known. With the location of P_L , P_R , and calibrated cameras, the location of P can be determined from its stereo projection.

The process involved in creating a 3D model from stereo images is referred to as the stereo paradigm (Banard and Fischler, 1982) (Dhond and Aggarwal, 1989). In its general form the computational stereo paradigm can be broken into the following areas:

- camera modelling
- image acquisition
- feature detection
- feature correspondence
- reconstruction

Camera modelling involves the attributes that describe the geometric properties of the cameras used to acquire the stereo images. These attributes (extrinsic and

intrinsic parameters) must be known to relate corresponding points in the stereo scene. Extrinsic camera parameters include the camera position (X_0, Y_0, Z_0) and camera orientation (ϕ, ω, κ). Intrinsic camera parameters include the focal length (f), principal image coordinates (x_0, y_0), radial distortion coefficients (K_1, K_2) and tangential distortion coefficients (P_1, P_2). The camera model also plays an important role in limiting the search area during correspondence.

Image acquisition is the stage where the stereo images are captured by the cameras. In the operating room (OR), stereo images are acquired nearly simultaneously to minimize changes occurring in the scene due to the breathing cycle of the patient.

Feature detection locates the features of interest in the stereo scene. These features are the points to be reconstructed in 3D. Usually 'interest operators' are used to locate features in one image that can be matched with confidence to the other image. In the OR, artificial triad markers attached to the spinous processes of vertebrae are the areas of interest. The small black balls of these triad markers are detected during feature detection.

Feature correspondence, or image matching, is the stage where features (triad marker balls) from one image are matched with the same features in the other image. The features to be matched are similar but differ slightly because of different points of view, occlusion, and lighting. Camera modelling also plays an important role in image matching. Knowing the camera model allows the search area to be greatly reduced, when looking for a corresponding feature, by making use of the epipolar constraint. Figure 2.2 shows how the epipolar plane and lines are constructed from a conventional stereo setup.

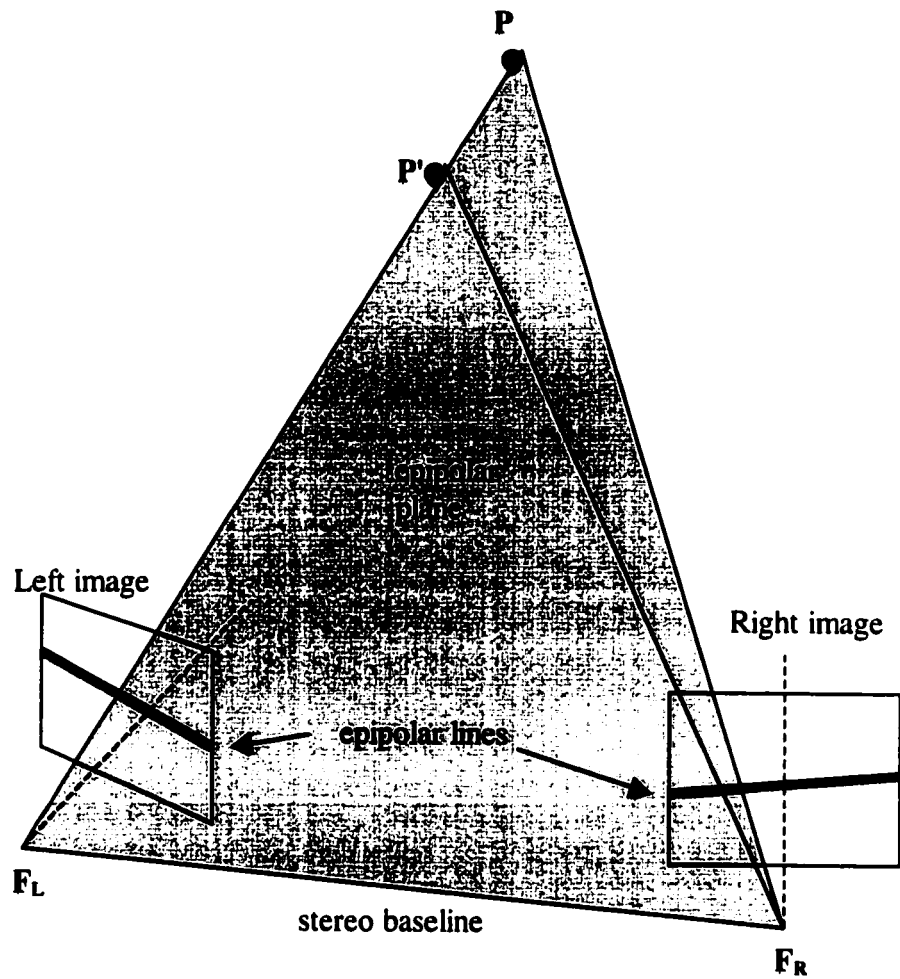


Fig. 2.2 Epipolar geometry based on two stereo cameras.

Any point P in 3D world space together with the focal points of two camera systems (F_L and F_R) forms the epipolar plane. The intersection of this plane with the respective left and right image planes form the epipolar lines. Every point on one image's epipolar line must have a corresponding point on the other images epipolar line. When the cameras are calibrated, knowing the range of distance from the cameras to P and P' reduces the size of the search area when looking for corresponding points between images. This reduction in computational complexity makes the epipolar line constraint an important tool in the stereo paradigm.

Once correspondence of features between images has been determined, reconstruction of the point in 3D can take place making use of camera geometry.

2.4 Previous research on ORIS

Bhalla implemented the previously discussed stereo paradigm (Bhalla, 1995). The following sections briefly explain how each section of the paradigm was implemented and applied to the stereo scene in the OR.

2.4.1 Camera modelling

Before accurate reconstruction of 3D object space coordinates from stereo 2D images can take place, the geometric relationship between the cameras must be known. The camera calibration method used by Peterson (Peterson, 1993) was used to model the system in the OR. This method makes use of the Direct Linear Transformation (Abdel-Aziz and Karara, 1971) (to obtain initial estimates of camera parameters), linearized collinearity equations (which yield final camera parameters on iteration), followed by least squares adjustment (to minimize errors) (Wolf, 1983).

A calibration peg board frame, shown in Figure 2.3, was created for the calibration procedure. This frame consists of 30 points (5 rows, 6 points/row) with widely varying heights (0-105 mm). Before acquiring stereo images in the OR, the calibration board was photographed by itself. Grid points were digitized and calibration procedures were run to deduce the camera parameters.

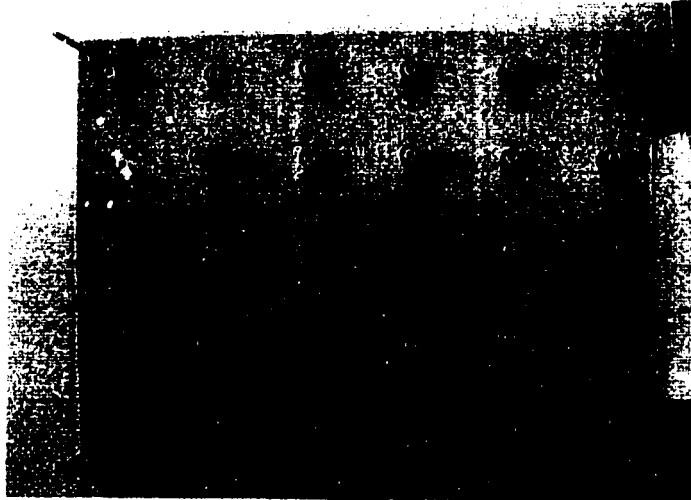


Fig. 2.3 Peg board used in camera calibration.

2.4.2 Image Acquisition

In an ideal machine vision application, fixed cameras are used to monitor objects of interest. This is not possible in the OR as the spine positions would constantly vary from scene to scene, and surgeons were opposed to permanently attaching cameras to modified bed posts as this would be an inconvenience to OR support staff. Mounting the cameras on the walls could not be done because the cameras were then too far away from the scene and features would be too small to detect. It was decided to use a mobile stereo-rig platform that could be wheeled into position before and after surgery. One disadvantage of the mobile rig is that the cameras must be calibrated for each session.

Camera calibration was done before surgery. Once all camera parameters were known, images could be captured. Table 2.1 lists the equipment used to capture the stereo images in the OR.

System Equipment	
Cameras	Sanyo VDC-2524, B/W, NTSC, video output
Camera Sensor	CCD frame transfer, 800x500 pix., 6.4x4.8 mm
Lenses	Tamron (f=6-16mm), variable aperture
Frame Grabber	Scion II Image Capture Card (640x480 pix.)
Captured Image	B/W, 640x480

Table 2.1 Equipment used to capture images.

2.4.3 Photogrammetry

Photogrammetry played an important part in the camera calibration procedure. The Direct Linear Transformation (Abdel-Aziz and Karara, 1971) was used to obtain initial estimates of the camera parameters. These parameters were then refined using linearized collinearity equations, which yielded final camera parameters on iteration. To minimize errors, these final parameters underwent least squares adjustment. Of the 13 camera parameters P1 and P2 (tangential distortion), x_0 and y_0 (principal image coordinates) were set to zero to help convergence in iteration to yield final parameters.

Once images had been acquired, it was often necessary to include processing steps before the images were suitable for feature detection. The following steps were taken to improve the quality of the stereo images.

To allow a greater depth of field, the aperture of the cameras was kept small. Consequently, images taken in the OR tended to be dark and features difficult to extract. A variac-controlled lamp was used to brighten the scene. However, this was not sufficient beyond the saturation of the camera sensor due to glare. Bhalla improved the contrast of the captured raw images by using a generalized form of gamma correction (Vernon, 1991).

Because of the computational burden involved in detecting features in stereo images, Bhalla reduced the size of his search area in images. By breaking the image up into segments, averages and standard deviations of pixel intensities were calculated. Applying thresholds to these segments, regions of interest could be identified. The region of interest (surgical field of view) was the region with the highest standard deviation and lowest average as this was the darker area. Areas of low standard deviation and high averages (white surgical drape surrounding image) were identified as regions of non-interest and were eliminated from the scene.

One consequence of gamma correction is the degradation of the signal-to-noise ratio (SNR) in the images. To improve the SNR and reduce the noise, Bhalla considered implementing the mean and median filters (Gonzalez and Wintz, 1987) but found the image edges to be unacceptably blurred and edge detail lost. A truncated median filter was used to represent the most probable value of any distribution (Davies, 1988, 1990). This filtering not only improves SNR, but also results in 'crisper' edges in the image which is useful for edge detection.

An important part of most image processing applications is edge detection. Edges provide valuable information for detecting features in stereo images. Bhalla examined Robinson masks and Canny edge detectors (Gonzalez and Woods, 1992) (Vernon, 1991) but found the computational cost too great. Bhalla choose the 3x3 Sobel detector (Davies, 1990). This is a differential type edge detector that is fast, efficient and accurate. It was used in all edge detection routines.

2.4.4 Feature Detection

Applying the stereo paradigm and computer vision algorithms to the operating room (OR) was complex. OR images were inconsistent and offered few well-defined features. Features could also be misinterpreted, as there is glare from blood, body fluids and reflective instrumentation. Bhalla simplified the feature detection problem

by attaching triads (Figure 2.4) to specified vertebrae. These were more readily identifiable as features for correspondence.



Fig. 2.4 A triad mounted on the spinous process of a vertebra.

The triad shown above is a three balled artificial marker that clamps onto the spinous process of the vertebra of interest. Because of the difficulty in extracting an individual vertebra from a scene, Bhalla reduced the problem to identifying where in the scene a three ball configuration could be found. The orthogonal configurations of the balls allow a position and orientation of a triad to be determined. This can then be related to the vertebra underneath. By attaching these triads to the spine and identifying their location and orientation, a model of the spine could be developed.

Template matching was used to identify triad ball features in the OR images. Templates of ball features were created based on gray level and edge-based images developed in the preprocessing stage of image acquisition. These templates were then

clustered into a two-level tree structure (Ramapriyan, 1976). The clustered templates were then applied to images and potential features were identified and recorded.

2.4.5 Feature Correspondence

To match triads from one stereo scene to another, camera and scene geometry were used with a number of constraints (Grimson, 1985) (Faugeras, 1993). A multilevel approach in the correspondence algorithm was used. A large candidate set of triad features was first obtained for a pair of stereo images. These candidates were identified based on epipolar geometry (Faugeras, 1993), system range, and the collinearity condition. The next level of correspondence refined this large initial candidate set using correlation-based measures. At the third and highest level of correspondence, triad features are created in 3D and tested for configurations matching the triad models. Heuristics and *a priori* knowledge were used to discard false triads so that only the number of triads known to be in the scene was kept.

3 ACCURACY EXPERIMENTS

The Operating Room Imaging System (ORIS), while functionally demonstrated, had not been tested for its accuracy and precision of measurements. This chapter explains the experiments performed to determine how accurately ORIS could detect translations and rotations of artificial triad markers in free space. Two types of experiments were performed. Displacement experiments determined the minimum distance a triad could be displaced before detection by ORIS. Rotation experiments determined the smallest angular change in triad orientation that ORIS could detect. The experimental procedures and results are presented.

3.1 Displacement Experiments

Displacement experiments were conducted to determine how accurately the displacement of triads in 3D space could be detected. Bhalla reported that the photogrammetric calibration techniques were capable of providing submillimetre 3D measurements (Bhalla, 1995). While the calibration results were promising, further testing of ORIS was required to measure the functional accuracy.

To detect these displacements, a minimum of two triads were required to be a part of the stereo scene. Two triads were essential because of the way ORIS correspondence software determines the location of a triad in 3D free space. All triad positions and orientations were measured relative to a reference triad. This triad was chosen by the software to be the one expected to undergo the least amount of displacement in the scene. All other triad measurements were reported relative to the reference triad. The experimental setup for testing the displacement and rotational experiments is shown in Figure 3.1.

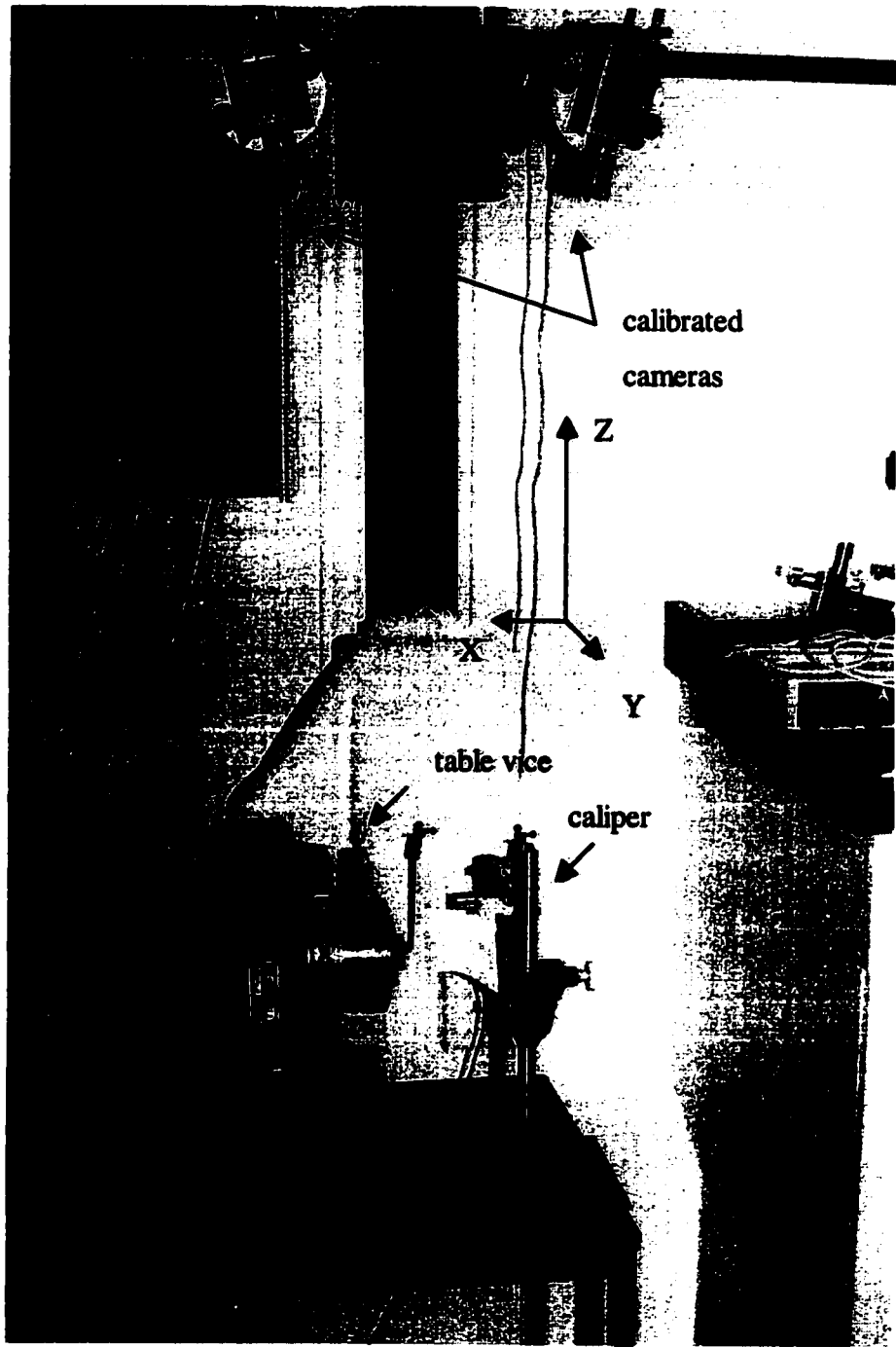


Fig. 3.1 Experimental setup used in displacement and rotation experiments. This setup was for rotational experiments. The rotating table vice would be replaced with another caliper for displacement experiments.

Two calipers were used to firmly hold the two triads in the calibrated stereo scene. The calipers were capable of 0.1 mm displacements. Small 3D displacements were made to one triad, while the other remained fixed. Displacements were only made in one direction at a time (i.e. x, y or z). Images were captured using a pair of Sanyo VDC-2524 cameras with a Tamron Variable Focal Length (6-16mm) lens, and a Scion II Image Capture Card installed in a Macintosh computer.

3.1.1 Displacement Experiment Results

To avoid repeating the same displacement experiment in the stereo scene, the triads were moved to different locations throughout the scene. Displacements were made along the positive and negative directions of the xyz axes to prevent bias of displacement in a single direction.

To ensure the cameras were properly calibrated and ORIS was functioning, preliminary displacement experiments (1, 3, 5 mm) were performed. Results are shown below in Table 3.1.

ORIS measurements (x,y,z in mm)			
displace	X	Y	Z
1 mm	0.97	0.89	0.52
3 mm	2.63	2.80	2.76
5 mm	5.09	5.01	4.68

Table 3.1. Results of ORIS detecting 1,3,5 mm displacements in xyz.

These preliminary results served as a confirmation that the system was calibrated and working properly. They also demonstrated that ORIS was detecting displacements at approximately the millimetre level. Further +/-1 mm experiments

were done with a larger sample size of $n=10$. Five of the ten displacements were made along the negative axes while the remaining five were made in the positive direction. The measured displacement, mean, standard deviation, and mean absolute value of error (Johnson, 1994) for displacements of ± 1 mm in x,y,z are reported in Table 3.2.

ORIS measurements (x,y,z in mm)			
n	X	Y	Z
1	0.60	1.00	0.25
2	0.64	0.76	0.09
3	1.33	0.65	1.81
4	0.55	1.29	1.22
5	1.42	1.88	1.64
6	-0.40	-0.58	-2.40
7	-0.97	-1.59	-0.39
8	-1.89	-0.36	-1.35
9	-1.64	-0.32	-2.11
10	-1.24	-0.48	-0.02
m	1.07	0.89	1.13
s.d.	0.51	0.53	0.88
e	0.44	0.46	0.78

Table 3.2 ORIS measured displacements of ± 1 mm in x,y,z (m - mean, s.d. - standard deviation, e - mean absolute value of error).

3.1.2 Discussion of Displacement results

The large standard deviations, with an average of 0.64 mm, indicated that ORIS was not very precise in its 1 mm measures. Mean absolute value of error was calculated as:

$$e = \frac{\sum_{i=1}^n |1 - |x||}{n} \quad (3.1)$$

where n is the number of samples and x is the ORIS measured x,y,z displacement.

The average mean of 1.06 mm demonstrated that 1mm displacements could be detected but not very precisely as indicated by the large standard deviations. This does not mean ORIS is an inaccurate system. The ability of ORIS to detect a displacement in the order of 1 mm was a very good result. Taken in the context of the spinal corrective surgery, 1 mm displacements are very small.

The three-dimensional accuracy was calculated as:

$$3D_{accuracy} \approx \sqrt{e_x^2 + e_y^2 + e_z^2} \quad (3.2)$$

These results show that ORIS has a 3D accuracy of approximately +/- 1mm.

Differences in standard deviations and mean absolute value of error between measurements made along the x,y,z axes can be explained. The x and y-axis form a plane that remains at a constant distance from the cameras for any value of x or y. Therefore, a displacement made in the x direction can be as precisely detected as an equivalent displacement made in the y direction. The z-axis however runs through the camera baseline. Changes in z are less readily detectable to the cameras because of

less geometric change in the stereo scene. Displacing an object in the x or y direction produces a more visible result than displacing the object an equivalent distance in the z direction. The mean absolute value of error shows that error was greater along the z-axis than the x and y-axis. Translations of triads along the z-axis, are more difficult to detect than those along the x and y-axis. Hence the larger standard deviation and mean errors in z measurements.

It should also be noted that the standard deviation of reconstructed points will vary throughout the image. This accounts for the difference in standard deviations along the x and y-axis. This is often referred to as dilution of position (DOP) in photogrammetry (Peterson, 1997). The x and y 3D measurements are a function of the 2D image coordinates, the camera location and orientation, tangential and radial lens distortions, and the resolution of the frame grabber. Each of these parameters has its own degree of error. As 3D point measurements were made throughout the stereo scene, the errors associated with these parameters will propagate, thus changing the overall error of the 3D measurement. This change of error results in a varied standard deviation depending on the location within the scene. While x and y 3D measurements should be equally precise, they will vary slightly due to the geometry of the experiment.

3.2 Rotation Experiments

Rotation experiments were performed to determine how accurately ORIS could detect changes in orientation of artificial triad markers in free space. Vertebra orientation information is required for the 3D modelling of the spine.

To describe the orientation of a triad in free space, each axis in the object space Cartesian coordinate system (x,y,z) was assigned an angle of rotation (ϕ, ω, κ) about its axis. These angles of rotation were used to describe the orientation of a triad in free space (Figure 3.2).

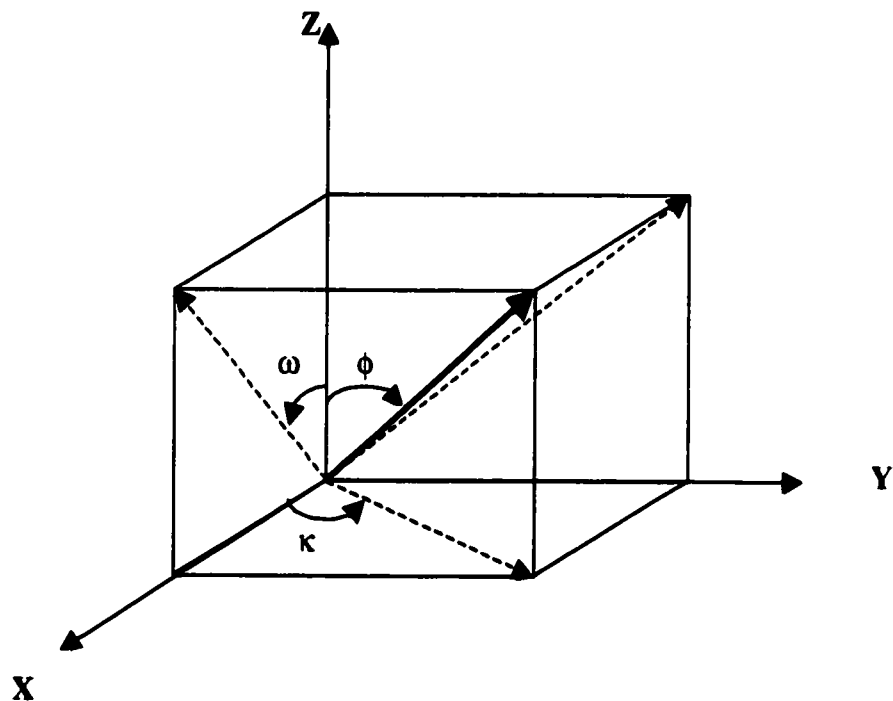


Fig. 3.2 Defining angles of rotation ϕ, ω and κ .

The rotation and displacement experiments were very similar. One of the calipers used to hold a triad in the displacement experiment was replaced with a rigidly fixed rotating table vice. This table vice held the triad that was to undergo

rotation. The vice was very precise in measuring rotation in dms (degrees, minutes, seconds). By holding one triad fixed in a caliper, and rotating the other triad by a known number of degrees, a difference in triad orientation of the rotated triad was measured.

3.2.1 Rotation of Kappa

Rotation experiments involving κ were performed in the same manner as ϕ and ω . However it was found that regardless of the magnitude of the rotation about the z-axis, ORIS failed to detect the relative change in orientation. Further investigation as to why rotations could be detected about ϕ , ω and not κ lead to the discovery that the method used by ORIS to calculate orientation was not sufficient to detect changes in rotations about all three axes. Figure 3.3 shows a planar view of a three-ball triad and the vectors used to describe its orientation.

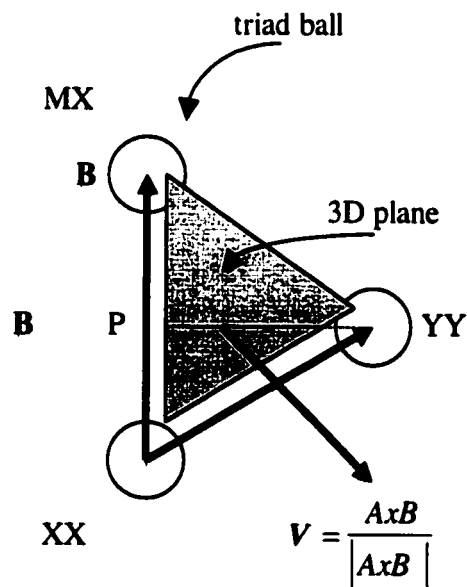


Fig. 3.3 3D plane made by triad balls.

The three triad ball features in Figure 3.3 form a 3D plane. By creating two vectors, **A** (YY-XX) and **B** (MX-XX) and taking the cross product, a normal vector **V** to the 3D plane was found. This vector described the orientation of the triad in free space. The orientation was reported as rotations about the x,y, and z-axis (ϕ, ω and κ). A single 3D vector in space, describing the orientation of the triad, does not contain enough information to describe a change in orientation about all three axes of rotation. There is only enough information to report changes about two of the axis (ϕ and ω). Another angle is required before changes in rotation about κ can be described.

This can be demonstrated with the following example. Assume the 3D plane of a triad is parallel to the *xy* plane and the normal vector **V** to be parallel to the z-axis. To rotate the triads about the z-axis (κ) would report no change in the 3D normal vector **V**. The vector would still be pointing in the same direction, along the z-axis. To detect rotations in the *xy* plane, another angle must be used to keep track of rotations parallel to the plane of the triad.

The following solution was implemented (see Figure 3.4). The vector **B**, used to calculate the normal vector **V**, was also used to keep track of rotations about the z-axis. This vector acted like a steering vector, keeping track of which way the projection of **V** was pointing in the *xy* plane. By rotating in the *xy* plane about the z-axis, it is possible to compare **B** with **B'** before and after the rotation. The difference will be the magnitude of the rotation κ about the z-axis.

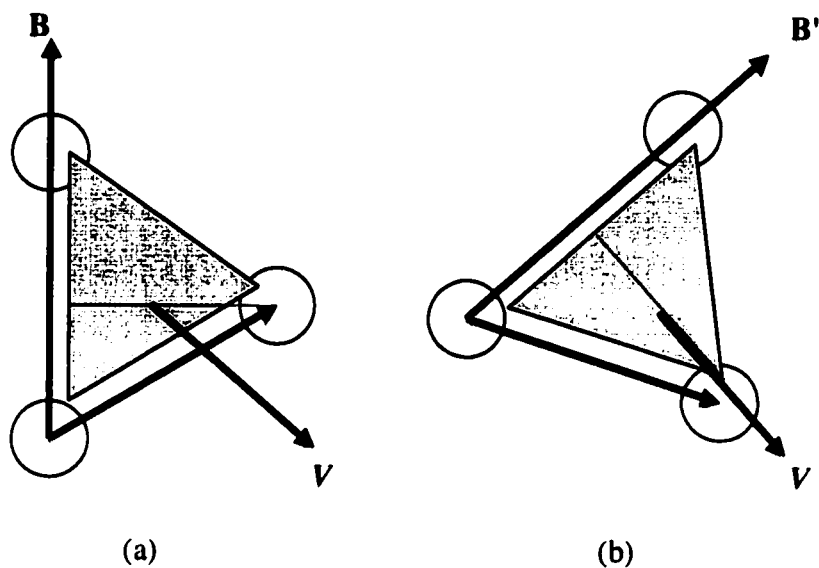


Fig. 3.4 (a) a triad before rotation about the z-axis.
 (b) a triad after rotation about the z-axis.

With this additional vector **B**, rotations are now detectable about all three axes.

3.2.2 Rotation Experiment Results

Preliminary rotations of 1°, 3°, 5°, 10°, 20°, 30°, 40° about all three axes were performed to confirm calibration and ORIS functionality. Preliminary results for ϕ and ω are shown in Table 3.3.

ORIS measurements (ϕ, ω in degrees)		
angle	ϕ	ω
1°	2.82	0.52
3°	1.67	3.25
5°	6.62	4.61
10°	10.63	13.25
20°	21.28	20.25
30°	33.67	30.53
40°	48.09	32.48

Table 3.3 ORIS measured rotations about the x and y-axis.

It is important to note ORIS had trouble detecting rotations at 40° . At large angles the triad ball features become less visible and occlusion can occur as shown in Figure 3.5. At extreme angles, ORIS had difficulty detecting all three triad balls accurately. Occasionally ORIS would not be able to detect all three balls and the triad would be falsely discarded. To simulate typical OR triad rotations, further testing was completed rotating triads $\pm 1^\circ$, $\pm 15^\circ$ and $\pm 30^\circ$ about all three axes. A sample size of $n=10$ was used. Results showing the measured angle, the mean, standard deviation and mean absolute value of error for measurements about each axis are shown in the Tables 3.4, 3.5, and 3.6.

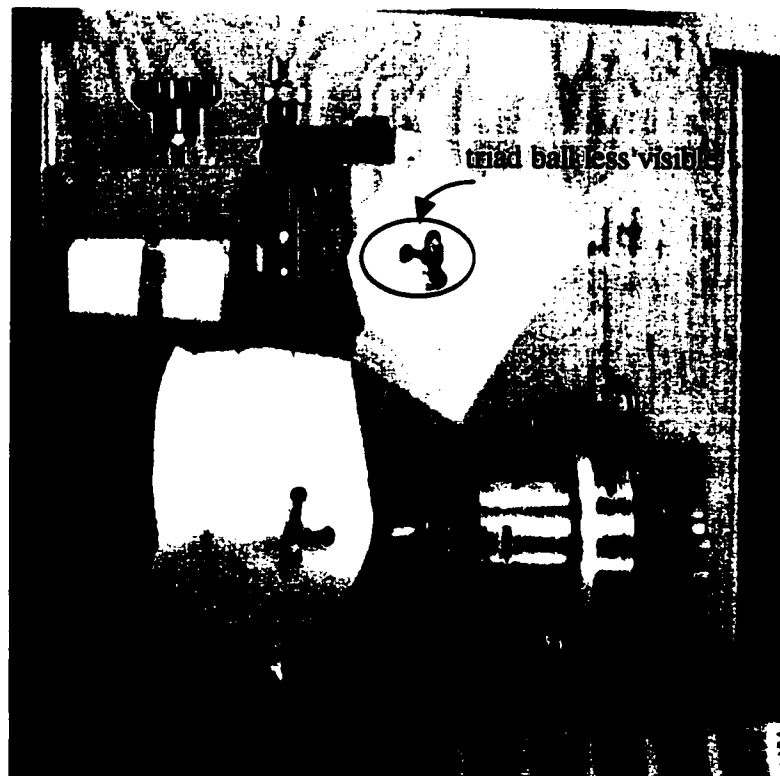


Fig. 3.5 Triad ball features become less visible at 40° angle rotations.

ORIS measurements (ϕ, ω, κ in degrees)			
n	ϕ	ω	κ
1	1.82	1.92	1.19
2	1.80	0.27	0.65
3	0.30	0.45	1.71
4	0.65	1.11	1.92
5	1.54	0.99	0.54
6	-1.53	-0.26	-1.27
7	-1.86	-0.33	-0.38
8	-2.02	-1.61	-1.93
9	-0.37	-0.78	-0.63
10	-0.34	-1.86	-1.37
m	1.22	0.96	1.16
s.d.	0.72	0.65	0.58
e	0.69	0.54	0.52

Table 3.4 ORIS measured rotations of $\pm 1^\circ$ about x,y,z axes (m - mean, s.d. - standard deviation, e - mean absolute value of error).

ORIS measurements (ϕ, ω, κ in degrees)			
n	ϕ	ω	κ
1	14.57	15.19	15.81
2	14.35	15.76	15.25
3	17.04	16.88	16.04
4	18.34	15.03	15.65
5	13.71	13.33	16.41
6	-15.05	-12.76	-17.66
7	-12.87	-12.93	-14.25
8	-13.15	-15.92	-14.40
9	-14.97	-12.84	-12.75
10	-16.16	-17.00	-13.99
m	15.02	14.76	15.22
s.d.	1.73	1.67	1.41
e	1.30	1.22	1.14

Table 3.5 ORIS measured rotations of $\pm 15^\circ$ about x,y,z axes (m - mean, s.d. - standard deviation, e - mean absolute value of error).

ORIS measurements (ϕ, ω, κ in degrees)			
n	ϕ	ω	κ
1	26.41	28.99	32.83
2	34.44	26.01	30.42
3	30.94	30.73	31.71
4	32.49	32.68	30.17
5	34.59	33.34	29.92
6	-31.68	-28.60	-31.21
7	-27.85	-28.84	-28.84
8	-30.57	-33.06	-27.38
9	-33.42	-34.51	-28.15
10	-32.63	-31.03	-29.70
m	31.50	30.78	30.03
s.d.	2.68	2.66	1.64
e	2.65	2.29	1.23

Table 3.6 ORIS measured rotations of $\pm 30^\circ$ about x,y,z axes (m - mean, s.d. - standard deviation, e - mean absolute value of error).

3.2.3 Discussion of Rotation Results

The results from Tables 3.4, 3.5 and 3.6 indicate that measurements of small angles ($\pm 1^\circ$ and $\pm 15^\circ$) are more accurate than large ones ($\pm 30^\circ$) on the basis of the absolute value of error. The average mean absolute error in the small angle rotations demonstrates this. One degree rotations were taken in a range of $\pm 10^\circ$ about the z-axis while $\pm 15^\circ$ and $\pm 30^\circ$ rotations were taken in a larger area of $\pm 35^\circ$ about the z-axis. The size of the rotation about the z-axis was significant because the orientation of the triad plane relative to the z-axis determines how visible the triad balls were. The less deviation from the z-axis the more visible the triad balls, hence more accurate detection. Because 1° measures were more aligned with the z-axis, they provided better results.

The absolute value of error demonstrated ORIS could accurately detect and measure rotations of $\pm 1^\circ$, $\pm 15^\circ$, and $\pm 30^\circ$. As angles of rotation approached 40° , the triad ball features became less identifiable to the stereo-video cameras. This resulted in less accurate detection and matching of ball features in images and consequently less accurate 3D reconstruction. It was found that when rotating triads through angles larger than 35° , triad ball features were not consistently detected. This led to the incorrect elimination of a triad feature by the correspondence software.

These experiments constrained changes in rotation to one axis at a time. In the OR, rotations will take place about all three axes as the movement of triads will be more complicated. However, because the stereo paradigm is always reduced to detecting features in a 2D image plane, as long as features can be identified, they can be accurately reconstructed regardless of what translation or rotation made prior to their detection. For this reason, similar results would be expected if tested in the OR.

Using equation (3.2), the angular accuracy of ORIS can be summarized as follows :

$1^\circ \pm 0.58^\circ$ Range $\pm 10^\circ$ off z-axis.

$15^\circ \pm 1.60^\circ$ Range $\pm 35^\circ$ off z-axis.

$30^\circ \pm 2.06^\circ$ Range $\pm 35^\circ$ off z-axis.

The above rotational results are of sufficient accuracy. However, detection accuracy falls off as angles approach 40° due to occlusion of triad balls.

4 TRIAD VERTEBRA GEOMETRIC MODEL

To display a 3D model of the spine, the position and orientation of the vertebrae are required. ORIS makes use of triad markers, mounted on the spinous processes of vertebrae, to aid in feature detection of the OR (operating room) scene. A relationship between the triads and vertebrae must be established before a 3D model of the spine can be displayed.

This chapter describes the model developed to relate the position and orientation of the triad to the vertebra. A geometric model was designed to define the orientation and location of a vertebra in relation to a triad mounted on its spinous process. Stereo-radiograph x-rays (Posterior-Anterior (PA) and lateral) were used to obtain the geometric relationship between the triads and vertebrae. Vertebral position and orientation can be calculated for any stage of surgery based on information received from stereo-radiographs combined with triad position and orientation data returned from ORIS.

The first part of the chapter gives background on related research and justifies the development of the geometric model. Next is a description of the algorithm used to keep track of the position and orientation of vertebrae in the developed model. The complete model and solution are then presented. The last two sections describe the experiments used to verify the functionality of the model and determine its potential in a clinical environment.

4.1 Background

ORIS can accurately determine the position and orientation of triads (± 1 mm). Before the 3D spine can be rendered, the position and orientation of the vertebrae must be calculated.



Fig. 4.1 Vertebra position and orientation are not the same as triad.

Figure 4.1 shows that a triad of known position and orientation can not be directly interpreted as a vertebra of the same position and orientation. The center of the vertebra is clearly at a different XYZ position compared to the triad xyz position. The orientation may be different as well. Therefore, a relationship was sought to calculate the position and orientation of any vertebra, given the position and orientation of the triad mounted on its spinous process.

In studying rigid bodies, Spiegelman developed a method of describing the movement of one rigid object relative to another (Spiegelman, 1987). Figure 4.2 shows how a rigid body that has undergone a rotation can be described. Two points on the body (A and B) and an angle of rotation θ about the CR_i (the instantaneous

center of rotation) are required. Relative to the current situation, point A would be the vertebra position, and point B would be the triad position. Together A and B would form one rigid body assuming A is rigidly attached to B. This method requires that both positions on the rigid body (at least two are required) be known. While stereo-graphic x-rays can provide a geometric relationship between vertebrae and triads (A and B), the magnitude of the CR_i angle is required to calculate the location of the new vertebra location. Because the instantaneous center of rotation angle (CR_i) was not readily obtainable, this method was deemed unsuitable.

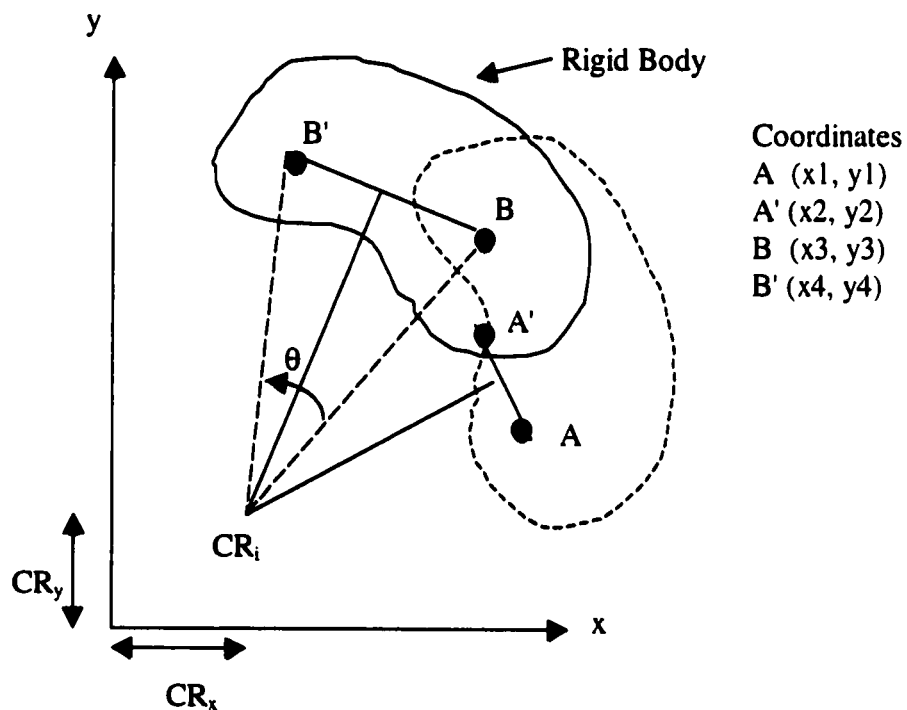


Fig. 4.2 Rigid body undergoing a rotation about CR_i .

The tracking of vertebral body motion during an operation using an optical tracking system has been researched (Glossop and Hu, 1997). Glossop mounted a seven-LED rigid body to the top of a Schanz pin. These pins are used in spinal corrective procedures to provide secure and reliable fixation for the unstable spine.

The screws, mounted with the infrared light emitting diodes (IREDs), were tracked by measuring their respective positions using an array of three custom cameras mounted on a one metre boom. While successful, this method has a drawback in that it violates the non-invasiveness requirement of ORIS. It was necessary to predrill the spinous process to insert the 5 mm Schantz pins, which were attached to the IRED body trackers. This is very invasive and is not desirable. Further, there was no attempt to relate the IREDs to the vertebrae they were mounted on. Only the relative displacement of IREDs was measured.

Another potential solution involved making assumptions about the dimensions of the vertebra (based on the sex and age of the patient) and required the surgeon to mount the triad onto the vertebra in some known manner. With the approximate dimensions of the vertebra, the exact dimensions of the triad, and an estimation of the vertebra's position relative to the triad, a calculation could be made approximating the vertebra position and orientation. This solution was not pursued for the following reasons:

1. A protocol for mounting triads onto spinous process would be required.
2. Compounding of assumptions would make model prone to error.

Even if a protocol were established whereby surgeons could mount the triads onto the spinous processes of the vertebrae in some known manner, there are too many gross approximations required. Variations in vertebral shape, vertebral body dimensions, and deformations of the spinous processes do not allow reasonable assumptions to be made regarding the dimensions of vertebra. As these inaccuracies compound it would not be possible to accurately determine the location and orientation of vertebrae. This made developing a protocol for mounting triads on vertebrae undesirable.

These reasons contributed to the development of the following solution. Stereo x-rays were used (PA and lateral) to measure the distances separating the triads and vertebrae, and the orientation of the vertebrae. With this information it was possible to track vertebrae positions and orientations as the triads underwent translations and rotations during surgery. By maintaining their relative differences in distance and orientation, it was possible to calculate the position and orientation a vertebrae given triad positions and orientations. With this solution, the surgeon was not limited in how the triad was mounted on the vertebra. The stereo x-rays uniquely describe the relationship between the triads and vertebrae for that specific operation. This would be much more accurate and all required data can be measured. This solution is now presented in greater detail.

4.2 Rotating a point about an arbitrary line in free space

Rotating a point about an arbitrary line in free space forms the basis of the solution used to predict the positions and orientations of vertebrae relative to their respective triads. Because the triad positions and orientations change for each stage of the operation, a way of monitoring changing vector orientations was required. Maintaining spatial positions and orientations of objects relative to one another can be achieved using the algorithm to rotate points about arbitrary lines in free space (Buchanan, 1996). Before the solution is presented in detail, the theory describing 3D rotations and translations in free space is presented.

4.2.1 3D transformations

Three-dimensional points and their respective transformations are usually described by matrix notation. A single 3D point can be represented by:

$$\begin{bmatrix} x \\ y \\ z \end{bmatrix} \quad (4.2)$$

Similarly, using matrix notation, a point 3D point V can be translated (T), scaled (S) and rotated (R) :

$$\begin{aligned} V' &= V + T \\ V' &= VS \\ V' &= VR \end{aligned} \quad (4.3)$$

To be able to treat all these transformations in a consistent manner so they can easily be combined into one transformation matrix, homogeneous coordinates are used. In homogeneous systems a fourth coordinate is added to a point. A point $V(x,y,z)$ becomes $V(X,Y,Z,w)$ for any scale factor $w \neq 0$. Represented in 3D Cartesian coordinates :

$$\begin{aligned}x &= X / w \\y &= Y / w \\z &= Z / w\end{aligned}\tag{4.4}$$

A useful property of homogeneous coordinates is that they are orthogonal (Foley *et al.*, 1993). Transformations on coordinates and objects preserve their physical properties. For example, the sides of a square maintain their parallelism when rotated and scaled. These are called rigid body transformations (Watt, 1989).

The homogeneous transformation matrix for scaling is:

$$S = \begin{bmatrix} S_x & 0 & 0 & 0 \\ 0 & S_y & 0 & 0 \\ 0 & 0 & S_z & 0 \\ 0 & 0 & 0 & 1 \end{bmatrix}\tag{4.5}$$

S_x, S_y and S_z are the scaling factors along the x, y and z axes. Applying this transformation to every point would scale an image. For uniform scaling:

$$S_x = S_y = S_z$$

Similar 3D transformations for translation (T) and rotation (R) about the x, y and z axes are:

$$T = \begin{bmatrix} 1 & 0 & 0 & 0 \\ 0 & 1 & 0 & 0 \\ 0 & 0 & 1 & 0 \\ T_x & T_y & T_z & 1 \end{bmatrix} \quad (4.6)$$

$$R_x = \begin{bmatrix} 1 & 0 & 0 & 0 \\ 0 & \cos\theta & \sin\theta & 0 \\ 0 & -\sin\theta & \cos\theta & 0 \\ 0 & 0 & 0 & 1 \end{bmatrix} \quad (4.7)$$

$$R_y = \begin{bmatrix} \cos\theta & 0 & -\sin\theta & 0 \\ 0 & 1 & 0 & 0 \\ \sin\theta & 0 & \cos\theta & 0 \\ 0 & 0 & 0 & 1 \end{bmatrix} \quad (4.8)$$

$$R_z = \begin{bmatrix} \cos\theta & \sin\theta & 0 & 0 \\ -\sin\theta & \cos\theta & 0 & 0 \\ 0 & 0 & 1 & 0 \\ 0 & 0 & 0 & 1 \end{bmatrix} \quad (4.9)$$

4.2.2 Algorithm for rotating a point about an arbitrary line in free space

To show how a point can be rotated about an arbitrary line, consider the following (Buchanan, 1996). Let P_1 and P_2 be the ends of a line segment about which the rotation of point P_3 will take place by angle θ as shown in Figure 4.3.

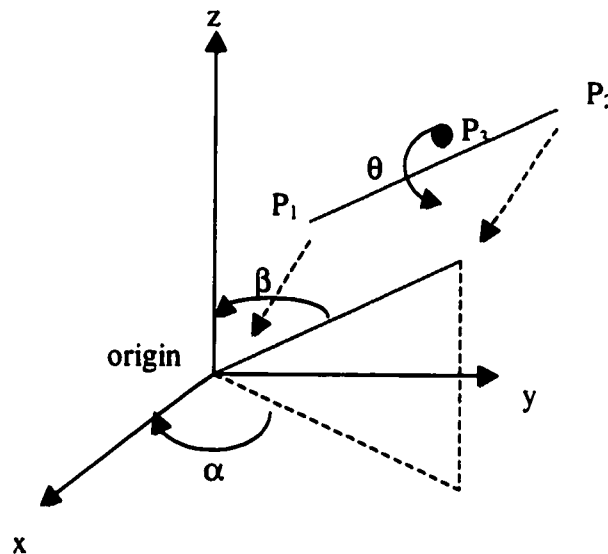


Fig. 4.3 Rotating point P_3 by θ about an arbitrary line segment $P_1 P_2$.

The solution breaks down the problem into the following five steps:

1. Translate line segment P_1P_2 to the origin (T_{P_1}).
2. Rotate point P_2 about the z -axis by α so that line segment is in zx -plane ($R_{z\alpha}$).
3. Rotate point P_2 about the y -axis by β so that line segment runs along the z -axis ($R_{y\beta}$).
4. Rotate P_3 about the z -axis by θ ($R_{z\theta}$).
5. Repeat steps 3,2 and 1 rotating and translating in the opposite directions ($R_{y\beta}^{-1}R_{z\alpha}^{-1}T_{P_1}^{-1}$).

The problem is simplified by using 3D transformations to reduce the problem to a series translations and rotations. The line segment P_1P_2 is aligned along the z-axis through the translations and rotations described above. Once aligned, the desired rotation of θ is performed about the z-axis in step 4. To return the line segment to its original configuration, the translations and rotations that brought P_1P_2 into alignment with the z-axis must be undone.

All these transformations can be combined into one transformation matrix.

$$M = T_{P_1} R_{z\alpha} R_{y\beta} R_{z\theta} R_{y\beta}^{-1} R_{z\alpha}^{-1} T_{P_1}^{-1}$$

4.3 Triad vertebra model

This section defines the vectors used to model the vertebra triad relationship. Figure 4.4 shows a vertebra body with the associated vertebra and triad vectors.

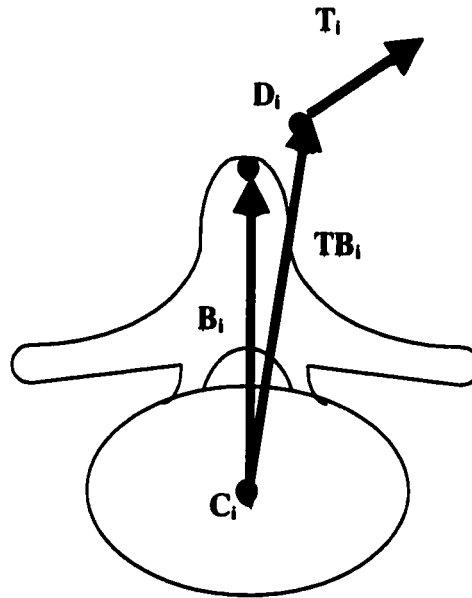


Fig. 4.4 Geometric model of vertebra and triad.

The positions of the *ith* vertebra and triad are defined as vectors C_i and D_i respectively. C_i is the center of the vertebral body while D_i is the intersecting joint linking the triad balls. The vector T_i defines the triad orientation (the plane formed by the three triad balls) and the vertebral body orientation is B_i (defined as the vector pointing from the center of the vertebra to the top of the spinous process). Vector TB_i relates the triad position to the vertebra position.

4.4 Calculation of vertebra position and orientation

To calculate the position and orientation of the vertebra at any stage of surgery, the previous stage's triad and vertebra positions and orientations were used. It was necessary to use the previous stage's results to calculate the current stage vertebra position because of the way a change in orientation of a 3D vector is described in free space. Equations 4.10 and 4.11 demonstrate how the cross product can be used to describe the rotation of a vector from one orientation to another. Let \mathbf{T}_i^0 be an arbitrary triad vector for Stage0 and \mathbf{T}_i^1 be an arbitrary triad vector for Stage1 of surgery. Vector A is the cross product of \mathbf{T}_i^0 and \mathbf{T}_i^1 and θ is the magnitude of the angle between \mathbf{T}_i^0 and \mathbf{T}_i^1 . When a triad undergoes a change in orientation from one stage to the next, the rotation of that triad in free space (\mathbf{T}_i^0 rotated to \mathbf{T}_i^1) can be described by rotating \mathbf{T}_i^0 about the vector A by angle θ . This rotation is used to describe triad orientations from one stage to the next. If a change in triad orientation can be described this way, changes in vertebra orientations can be described in a similar manner. Because triad vector \mathbf{T}_i^0 rotates about vector A in free space, the algorithm to rotate a point about an arbitrary line in free space was required.

$$A = T_i^0 \times T_i^1 \quad (4.10)$$

$$\theta = \sin^{-1} \left[\frac{|T_i^0 \times T_i^1|}{|T_i^0| \cdot |T_i^1|} \right] \quad (4.11)$$

At each stage of surgery, the information calculated by ORIS is the position (\mathbf{D}_i) and orientation (\mathbf{T}_i) of the triads mounted on the spinous processes of the vertebrae. The vertebra position and orientation could be calculated if the position vector \mathbf{TB}_i was known. Using PA and lateral x-rays, the position of the vertebra in relation to the triad (\mathbf{TB}_i) can be measured. If the triad orientation \mathbf{T}_i and position vector \mathbf{TB}_i are known, the position of the vertebra \mathbf{C}_i can be determined by subtracting \mathbf{TB}_i from \mathbf{D}_i as shown in Figure 4.5.

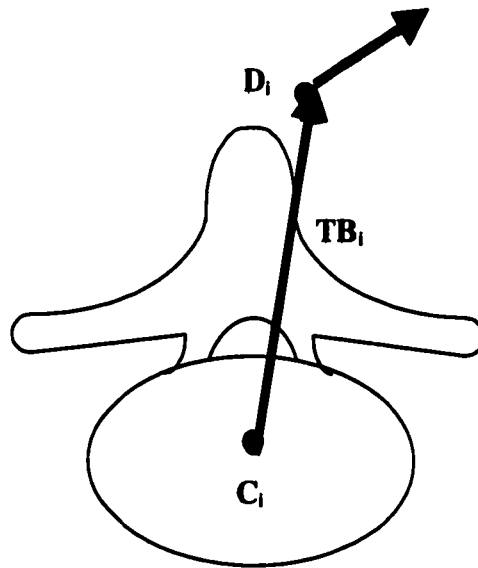


Fig. 4.5 Calculating vertebra position $C_i = D_i - TB_i$.

Figure 4.6 shows an example of how the current-stage vertebra position and orientation results were obtained from the previous-stage results. Initially, assume that Stage0 is completely modelled and that measurements D_0 , T_0 , TB_0 , B_0 , and C_0 are all known.

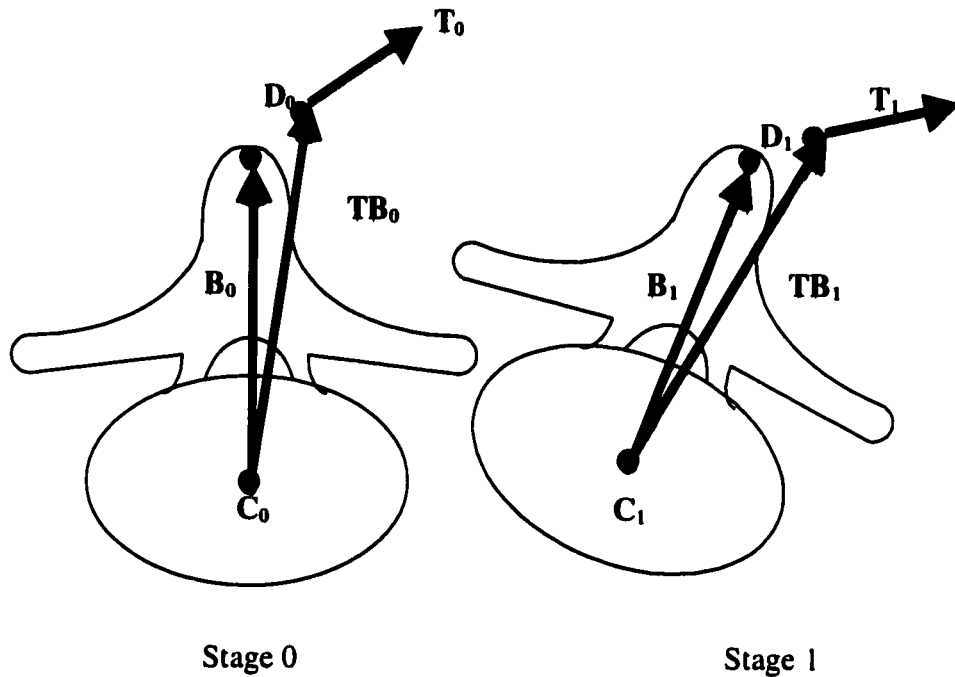


Fig. 4.6 Calculating Stage1 results based on Stage 0 results.

To calculate the position and orientation of the vertebra (C_1 and B_1) in the next stage of the surgery, Stage1, the following was done. Triad orientation vectors T_0 and T_1 were used to calculate the vector of rotation, A , and angle of rotation θ . By rotating Stage0 vertebra orientation vector B_0 about A by θ , Stage1 vertebra orientation vector B_1 was obtained. Similarly, rotating Stage0 positional vector TB_0 about A by θ gave TB_1 . All rotations assume that the triads are rigidly attached to the spinous processes of the vertebrae. Using the triad location returned from ORIS (D_1) the vertebra position of Stage1 was determined as:

$$C_1 = D_1 - TB_1 \quad (4.2)$$

In this way Stage1 vertebrae positions and orientations were calculated. The assumption made earlier that all Stage0 data was known is justified as follows. \mathbf{TB}_0 , \mathbf{C}_0 and \mathbf{B}_0 are calculated from the stereo-radiographs. ORIS determines the triad position and orientation information of both stages (\mathbf{T}_0 , \mathbf{T}_1 , \mathbf{D}_0 , and \mathbf{D}_1). Unknown Stage1 vertebra position and orientation \mathbf{C}_1 and \mathbf{B}_1 were calculated as described. Consecutive stages were calculated in an identical manner, using the previous-stage results to calculate the current-stage information.

4.5 Model Experiments

From now on the terms 'the model' and 'the triad to vertebra prediction software model' will be used interchangeably. To test the model's capability of predicting vertebrae positions and orientations, two sets of experiments were performed. The objective of the first experiment was to test the functionality of the model. An electromagnetic digitizer called the Flock of Birds (FOB) (Ascension Technology Corporation, 1997) was used to make measurements on a 3D scene containing two vertebrae. The FOB acted as a laboratory replacement for the stereo x-rays. By making accurate (0.1" RMS) 3D measurements with the FOB, data normally provided by the x-rays was generated by the electromagnetic digitizer and passed onto the model. The FOB also measured the vertebra position and orientation after a known displacement had been made to one of the vertebra. The model predicted the new vertebra location and orientation, based on the measurements provided by FOB. These results were then compared to the FOB measurements made after the vertebra had been displaced.

The second experiment addressed the issue of determining how successful the model could predict vertebrae positions and orientations when x-ray data was used. The concern with using data provided from x-rays was regarding the accuracy of the measurements. Once stereo x-rays were taken, key vertebral points on the x-rays were marked. These points were digitized into a computer program (IDIO_9) which calculated the distances between the points. These results would then be passed to the model, which would predict the vertebra position and orientation. The accuracy with which measurements could be made on these x-rays would provide insight into the accuracy of the model.

4.5.1 FOB Model Experiment

The objective of this experiment was to compare the results of the model with the results measured by the electromagnetic digitizer Flock of Birds (FOB) shown in Figure 4.7. FOB measured the positions and orientations of a vertebra in a scene before and after it had been displaced. FOB also measured the necessary data (TB_0 and B_0) that would be provided by the stereo x-rays for the model.

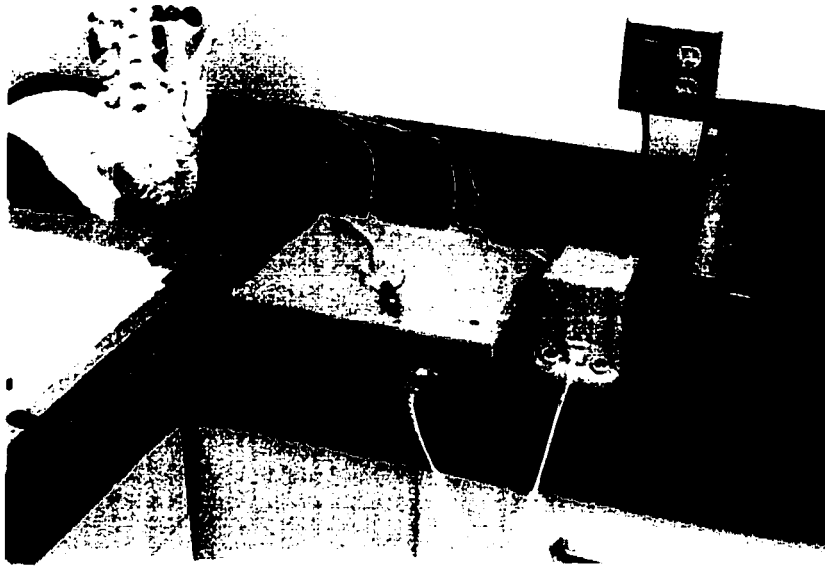


Fig. 4.7 The electromagnetic digitizer Flock Of Birds (FOB) used for making vertebra feature measurements.



Fig. 4.8 Caliper was used to accurately displace vertebra in FOB Model experiments.

A plastic model spine held a stationary triad in the scene. A caliper (capable of submillimetre displacements) held the other triad undergoing displacement (Figure 4.8). Measurements were made on the triad undergoing displacement using the FOB. The stereo cameras then captured the scene and ORIS processed the images to produce triad position and orientation information (Figure 4.9). The triad held by the caliper was then displaced. FOB measurements were made, and ORIS again processed the stereo images to produce the new triad position and orientation. Required FOB data (\mathbf{TB}_0 and \mathbf{B}_0) from the initial scene was input into the model. Results of the model were then compared with measured FOB data.

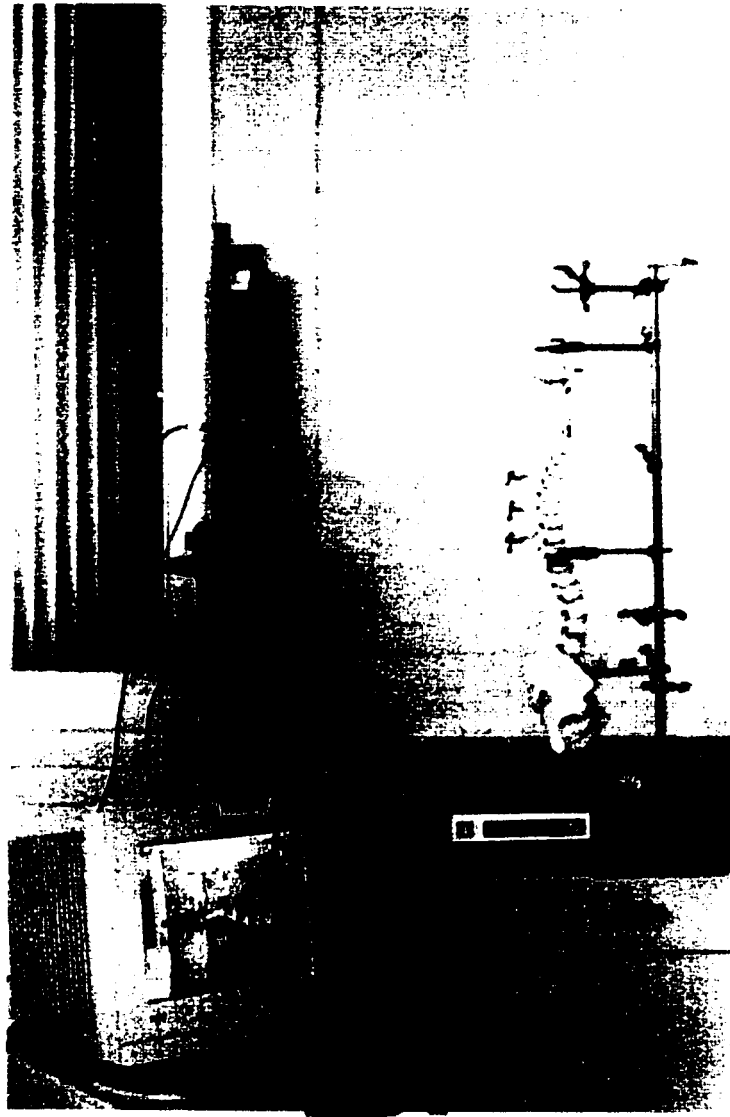


Fig. 4.9 ORIS camera setup and Cartesian coordinate system for FOB Model experiment.

4.5.1.1 Results and Discussion

To see how the model would perform in a complex scenario, two sets of results were obtained. Since displacement along the z-axis was the most difficult to detect for ORIS, the first experiment displaced the caliper triad -3 cm along the z-axis toward the cameras. The second set of results tested the model's ability to predict vertebral position and orientation when a triad had undergone rotation and translation. For this case the triad in the scene was rotated about the x-axis by $+10^\circ$ and displaced +3.5 cm in the y direction and +1 cm in the z direction.

Table 4.1(a) shows the FOB data of measured vertebra features for the -3 cm z-axis displacement experiment. Tables 4.1(b) and 4.1(c) show the vertebra orientation and position measured by FOB. Tables 4.1(d) and 4.1(e) show the triad orientation and position measured by ORIS. Tables 4.1(f) and 4.1(g) show the model calculated vertebra body orientation and the triad to vertebra position vector \mathbf{TB}_0 . Tables 4.2(a)-(g) show analogous results corresponding to the $+10^\circ$ rotation about the x-axis displaced by +3.5 cm in y and +1 cm in z experiment.

Measured FOB Vertebra Vectors (x,y,z in mm)			
	BEFORE		
Vector	X	Y	Z
C	347.1	123.4	261.8
D	314.1	123.3	197.2
TB0	-33.0	-0.1	-64.6
B	-10.8	1.4	-40.4
	AFTER		
C	347.1	124.8	233.6
D	313.5	124.2	167.9
TB0	-33.6	-0.6	-65.7
B	-11.5	0.7	-39.1

Table 4.1(a) FOB data before and after -3 cm displacement in z.

Vertebra Body Orientation (ϕ, ω, κ in degrees)			
Stage	ϕ	ω	κ
BEFORE	174.4	-196.4	-175.6
AFTER	174.6	-197.3	-174.8
delta	0.2	-0.9	0.8

Table 4.1(b) FOB vertebra body orientation before and after -3 cm displacement in z.

Vertebra Body Position (x,y,z in mm)			
Stage	X	Y	Z
BEFORE	347.1	123.4	261.8
AFTER	347.2	124.8	232.2
delta	0.1	1.4	-29.6

Table 4.1(c) FOB vertebra body position before and after -3 cm displacement in z.

Triad Body Orientation (ϕ, ω, κ in degrees)			
Stage	ϕ	ω	κ
BEFORE	161.5	-178.8	-168.5
AFTER	160.1	-179.7	-167.8
delta	-1.4	-0.9	0.7

Table 4.1(d) Triad body orientation measured by ORIS before and after -3 cm displacement in z.

Triad Body Position (x,y,z in mm)			
Stage	X	Y	Z
BEFORE	-7.3	-2.8	-44.4
AFTER	-6.5	-3.5	-13.2
delta	0.8	-0.7	31.2

Table 4.1(e) Triad body position measured by ORIS before and after -3 cm displacement in z.

Vertebra Body Orientation (ϕ, ω, κ in degrees)			
Stage	ϕ	ω	κ
BEFORE	174.9	-194.3	-173.1
AFTER	176.1	-196.4	-175.4
delta	1.2	-2.1	-2.3

Table 4.1(f) Model calculated vertebra body orientation before and after -3 cm displacement in z.

TB0 (x,y,z in degrees)			
Stage	X	Y	Z
BEFORE	-33.1	0.0	-64.5
AFTER	-35.1	0.4	-66.7

Table 4.1(g) Model calculated triad vertebra position vector TB_0 before and after -3 cm displacement in z.

Measured FOB Vertebra Vectors (x,y,z in mm)			
	BEFORE		
Vector	X	Y	Z
C	345.6	148.5	280.5
D	306.5	140.4	222.7
TB0	-39.1	-8.1	-57.8
B	-20.8	3.4	-60.4
	AFTER		
C	345.8	113.5	289.1
D	307.0	94.1	231.5
TB0	-38.8	-19.4	-57.6
B	-19.8	12.9	-59.2

Table 4.2(a) FOB data before and after $+10^\circ$ rotation about the x-axis and displacement of $+3.5$ cm in y and $+1$ cm in z.

Vertebra Body Orientation (ϕ, ω, κ in degrees)			
Stage	ϕ	ω	κ
BEFORE	176.8	-199.0	-170.7
AFTER	185.9	-198.5	-169.9
Delta	9.1	0.5	0.8

Table 4.2(b) FOB vertebra body orientation before and after $+10^\circ$ rotation about the x-axis and displacement of $+3.5$ cm in y and $+1$ cm in z.

Vertebra Body Position (x,y,z in mm)			
Stage	X	Y	Z
BEFORE	345.6	148.5	280.5
AFTER	345.8	183.4	291.5
delta	0.2	34.9	11.0

Table 4.2(c) FOB vertebra body position before and after $+10^\circ$ rotation about the x-axis and displacement of $+3.5$ cm in y and $+1$ cm in z.

Triad Body Orientation (ϕ, ω, κ in degrees)			
Stage	ϕ	ω	κ
BEFORE	163.8	-179.6	-163.7
AFTER	172.5	-178.5	-164.2
delta	8.7	1.1	-0.5

Table 4.2(d) Triad body orientation measured by ORIS before and displacement of after $+10^\circ$ rotation about the x-axis and displacement of $+3.5$ cm in y and $+1$ cm in z.

Triad Body Position (x,y,z in mm)			
Stage	X	Y	Z
BEFORE	-8.0	-2.0	-73.0
AFTER	-7.8	44.6	-52.3
delta	0.2	46.6	20.7

Table 4.2(e) Triad body position measured by ORIS before and $+10^\circ$ rotation about the x-axis and displacement of $+3.5$ cm in y and $+1$ cm in z.

Vertebra Body Orientation (ϕ, ω, κ in degrees)			
Stage	ϕ	ω	κ
BEFORE	178.1	-201.3	-169.0
AFTER	186.4	-199.7	-171.3
delta	8.3	1.6	-2.3

Table 4.2(f) Model calculated vertebra body orientation before and after $+10^\circ$ rotation about the x-axis and displacement of $+3.5$ cm in y and $+1$ cm in z.

TBO (x,y,z in degrees)			
Stage	X	Y	Z
BEFORE	-39.1	-8.1	-57.8
AFTER	-38.5	-18.1	-55.5

Table 4.2(g) Model calculated triad vertebra position vector TB_0 before and $+10^\circ$ rotation about the x-axis and displacement of $+3.5$ cm in y and $+1$ cm in z.

Because the accuracy of the cameras was determined in Chapter 3 (+/- 1 mm) and the FOB was a highly accurate measurement device (0.1" RMS), one set of results for each experiment was deemed sufficient. The experimental results showed that the triad to vertebra model performed as expected. The -3 cm displacement in z experiment contained no rotation. This is confirmed in Tables 4.1(b), 4.1(d), 4.1(f) where there is little difference in orientation measured. The magnitude of the displacement is verified in Table 4.1(c) and Table 4.1(e) where the vertebra and triad are reported to have moved -29.6 mm and -31.2 mm respectively.

The FOB and model vertebra orientations (Table 4.1(b) and Table 4.1(f)) after the -3 cm displacement in z were:

$$\text{FOB vertebra orientation } (\phi, \omega, \kappa) = (174.6^\circ, -197.3^\circ, -174.8^\circ)$$

$$\text{Model vertebra orientation } (\phi, \omega, \kappa) = (176.1^\circ, -196.4^\circ, -175.4^\circ)$$

$$\text{Difference } \Delta(\phi, \omega, \kappa) = (1.5^\circ, 0.9^\circ, -0.6^\circ)$$

This small difference in vertebra orientation may be attributed to the combined contribution of error in FOB, ORIS and human error in equipment operation and data collection. Human error comes from making measurements with the FOB.

To compare the vertebral body positions after the -3 cm displacement the position vector \mathbf{TB}_0 was used. This position vector kept track of the position and orientation of the vertebra relative to the triad. Comparing the \mathbf{TB}_0 vector determined how accurately the model could predict vertebra body position.

The position vectors after displacement for FOB and the model (Table 4.1(a) and Table 4.1(g)) were:

$$\text{FOB } \mathbf{TB}_0(x,y,z) = (-33.6, -0.6, -65.7) \text{ (mm)}$$

$$\text{Model } \mathbf{TB}_0(x,y,z) = (-35.1, 0.4, -66.7) \text{ (mm)}$$

$$\text{Difference } \Delta(x,y,z) = (-1.5, 1.0, -1.0) \text{ (mm)}$$

The small difference indicated that the model was functioning as expected. Similar comparisons between vertebra orientation and position were made with the results from the $+10^\circ$ rotation about the x-axis with a displacement of +3.5 cm in the y direction and +1 cm in the z direction. Table 4.2(b) and Table 4.2(d) measured angles of rotations of $+9.1^\circ$ and $+8.7^\circ$. The $+10^\circ$ rotation about the x-axis was crudely made using marked laminated millimetre graph paper. An accurate rotation of 10° was not a primary concern. ORIS and the FOB would both be making measurements on the same displaced scene and it was their relative differences in measurements to each other that was of interest. The $+10^\circ$ rotation served only as a means to complicate the scene.

Table 4.2(c) verified a vertebral displacement of +3.5 cm in y and +1 cm in z while Table 4.2(e) showed triad displacement of +46.6 mm in y and +20.7 mm in z. Triad displacements were more pronounced than vertebra displacement because the triad mounted on the spinous process of the vertebra is further away from the caliper vertex of rotation.

The FOB and model vertebra orientations (Table 4.2(b) and Table 4.2(f) after the +10° rotation were:

$$\text{FOB vertebra orientation } (\phi, \omega, \kappa) = (185.9^\circ, -198.5^\circ, -169.9^\circ)$$

$$\text{Model vertebra orientation } (\phi, \omega, \kappa) = (186.4^\circ, -199.7^\circ, -171.3^\circ)$$

$$\text{Difference } \Delta(\phi, \omega, \kappa) = (0.5^\circ, -1.2^\circ, -1.4^\circ)$$

The position vectors after rotation for FOB and the model (Table 4.2(a) and Table 4.2(g) were:

$$\text{FOB TB}_0 (x, y, z) = (-38.8, -19.4, -57.6) \text{ (mm)}$$

$$\text{Model TB}_0 (x, y, z) = (-38.5, -18.1, -55.5) \text{ (mm)}$$

$$\text{Difference } \Delta(x, y, z) = (0.3, 1.3, 2.1) \text{ (mm)}$$

The small difference in both sets of results demonstrated that the model was correctly calculating the new vertebra position and orientation. The differences between values can be attributed to the combined system error in FOB, ORIS and human error in equipment manipulation and data collection.

4.5.2 FOB X-ray Experiment

The objective of the FOB x-ray experiment was to investigate how accurately x-rays could be used to measure the vectors required for the model (\mathbf{TB}_0 and \mathbf{B}). With the functionality of the model demonstrated in the previous section, this experiment was necessary because stereo x-rays will be used in the OR to provide the model with its initial position and orientation. The FOB was used in place of the x-rays in the first experiment because it was a highly accurate measurement tool, which helped demonstrate the functionality of the model.

The experimental procedure was similar to the previous experiment. The differences being that there were no displacement of rigid bodies in the scene (since this was tested in the first experiment) and only the triad vertebra position vector \mathbf{TB}_0 and the vertebra orientation \mathbf{B} were measured. Stereo x-rays were taken of a human-scale plastic model spine with a triad mounted on one of its spinous processes (Figure 4.10). The x-rays were digitized (using IDIO_9 software (Hill, 1997)) to obtain the vectors \mathbf{TB}_0 and \mathbf{B} . The FOB was again used to measure \mathbf{TB}_0 and \mathbf{B} . X-ray and FOB results were then compared.

To aid triad ball feature identification in digitization, triads were covered with reflective tape. This made the triad balls more radio opaque and hence more visible to x-rays. The author and clinical staff empirically determined x-ray exposure levels (6.4 mAs @56 kV lateral, 10 mAs @56 kV PA) to provide a diagnostic image similar to the one surgeons would see in the OR.

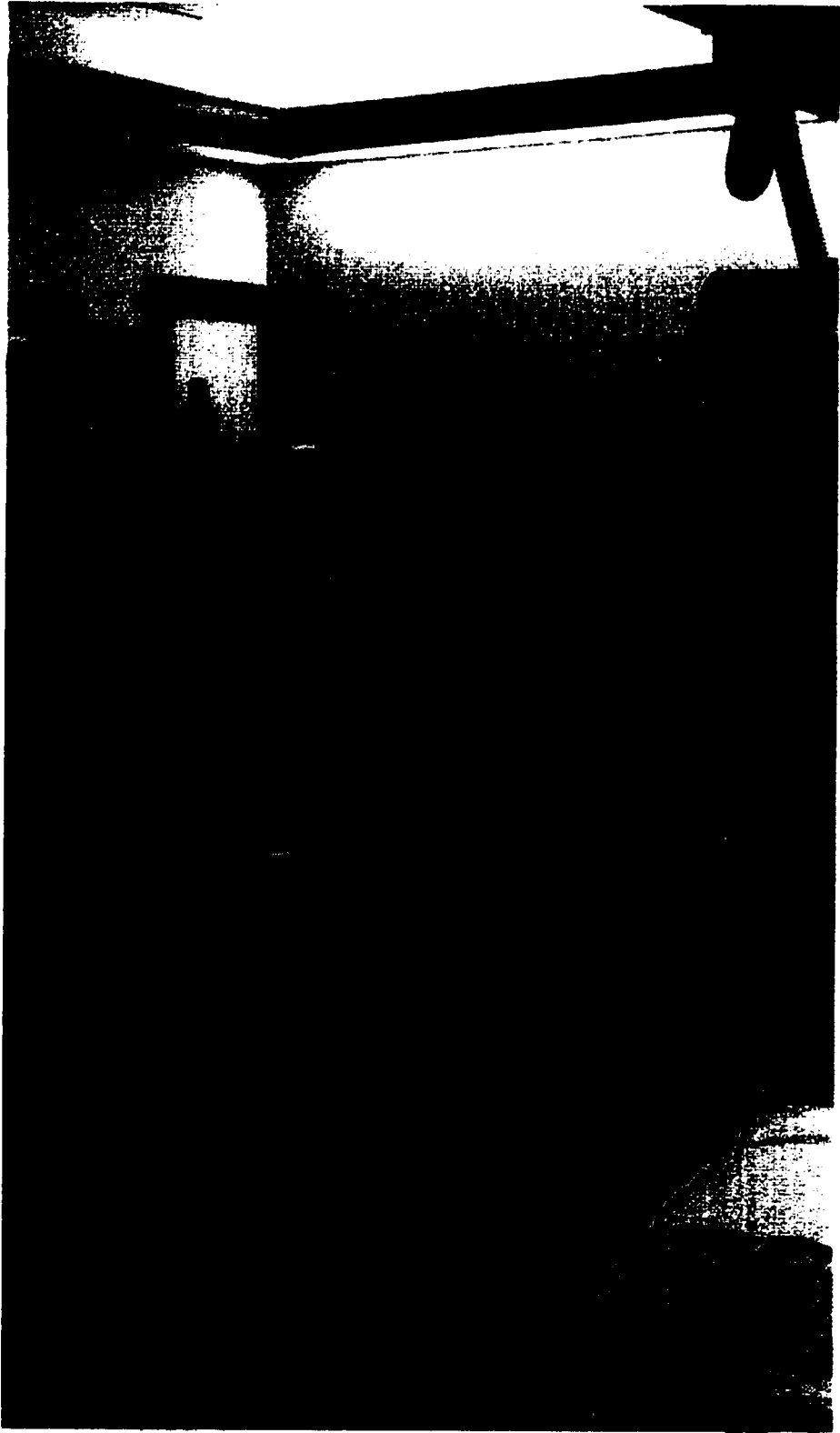


Fig. 4.10 Experimental setup used in FOB X-RAY experiments.

4.5.2.1 Results and Discussion

As in the previous experiment, because the accuracy of the cameras was determined in Chapter 3 (+/- 1mm) and the FOB was a highly accurate measurement device (0.1" RMS), one set of results was obtained for each experimental setup. Two setups were tested. The first simulated the posture a typical patient would be in when stereo x-rays are taken. The second setup rotated the spine +10° about the z-axis. The purpose of the rotation was to make the x-rays less than ideal thereby making digitization more prone to error. As in the FOB Model experiment, this was a crude rotation of 10° made with laminated millimetre grid paper. Results for both experimental setups are presented in Tables 4.3(a), 4.3(b) for the non-rotated case and Tables 4.4(a), 4.4(b) for the rotated case. Table 4.5 shows the amount of rotation detected by the FOB and the x-rays.

Required model data, triad vertebra positional vector **TB** and vertebra body orientation **B**, were obtained from stereo-graphic x-rays as follows. By locating the small metallic cube from which the triad balls originate, the triad position was identified. To locate the vertebra body center, four points were identified and marked on each corner of the vertebra body feature. These points were then averaged to give the vertebra position. With the triad and vertebra position, the triad vertebra vector **TB** could now be measured. This method was used for both the PA and lateral x-rays.

The vertebra orientation was measured in a similar way. With the center of the vertebra defined, one more point was digitized halfway between the two digitized points in the direction of the spinous process. The two digitized points were determined visually from the x-rays so that the orientation of the vertebra corresponded to that defined in the triad vertebral model. Using the same procedure in measuring **TB**, the vector **B** was determined. This vector was then expressed in

polar form $\phi\omega\kappa$. All points were digitized using a Hewlett Packard 9874A Digitizer with a resolution of 25 microns. Results were calculated using IDIO_9 software.

Measured TBO vector (x,y,z in mm)			
	x	y	z
TBO_{FOB}	-6	-84	-39
TBO_{XRAY}	-12	-108	-42
delta	-6	-24	-3

Table 4.3(a) TB_0 measured results from FOB and X-RAY of non-rotated spine.

Vertebra orientation B (ϕ, ω, κ in DDD)			
	ϕ	ω	κ
B_{FOB}	250	-255	-215
B_{XRAY}	260	-262	-217
delta	10	-7	-2

Table 4.3(b) B measured results from FOB and X-RAY of non-rotated spine.

Measured TBO vector (x,y,z in mm)			
	x	y	z
TBO_{FOB}	-8	-82	-38
TBO_{XRAY}	-8	-105	-42
delta	0	-23	-4

Table 4.4(a) TB_0 measured results from FOB and X-RAY rotated spine.

Vertebra orientation B (ϕ, ω, κ in DDD)			
	ϕ	ω	κ
B_{FOB}	252	-258	-204
B_{XRAY}	260	-263	-211
delta	8	-5	-7

Table 4.4(b) B measured results from FOB and X-RAY rotated spine.

Measured rotation (ϕ, ω, κ in DDD)			
	ϕ	ω	κ
FOB	-2	-3	11
X-RAY	0	-1	6
delta	2	2	-5

Table 4.5 Amount of rotation detected by FOB and x-ray.

Table 4.5 shows FOB measured a +11° rotation about the z-axis while the x-rays measured +6°.

The differences in vertebra orientation **B** between FOB and x-rays were:

$$\Delta\mathbf{B} (\phi, \omega, \kappa \text{ in DDD}) = (10^\circ, -7^\circ, -2^\circ) \text{ non-rotated case}$$

$$\Delta\mathbf{B} (\phi, \omega, \kappa \text{ in DDD}) = (8^\circ, -5^\circ, -7^\circ) \text{ rotated case}$$

While rotational differences of 2°-7° were acceptable, the 8°-10° difference in rotation about the x-axis was cause for concern. The primary differences in vertebra orientation were caused by measurement inaccuracies in digitizing stereo-radiographs. When studying the effects of radiographic landmark identification on the accuracy of three-dimensional reconstruction of the human spine, Andre found that there were problems in identifying exactly the same landmarks between pairs of stereo radiographs (Andre, 1992). Results showed that radiographic identification errors were typically 2 mm, causing reconstruction errors of up to 5mm. Using this as a guide, the measurements made from radiographs translated into orientation errors of +/-10°. These results were consistent with Andre's findings.

The differences in **TB₀** between FOB and x-rays were:

$$\Delta\mathbf{TB}_0 (x, y, z \text{ in mm}) = (-6, -24, -3) \text{ non-rotated case}$$

$$\Delta\mathbf{TB}_0 (x, y, z \text{ in mm}) = (0, -23, -4) \text{ rotated case}$$

While differences between TB_0 results were quite small in x and z , the -23 mm and -24 mm difference measured in y for both the rotated and non-rotated case was unacceptable. The largest contributor to this error (besides radiograph measurement inaccuracy) was the inherent distortion caused by exposing an object on a x-ray film set at a distance ΔD back from the object. Figure 4.11 shows how the object shadow exposed on x-ray film is not of the same dimensions as the original object.

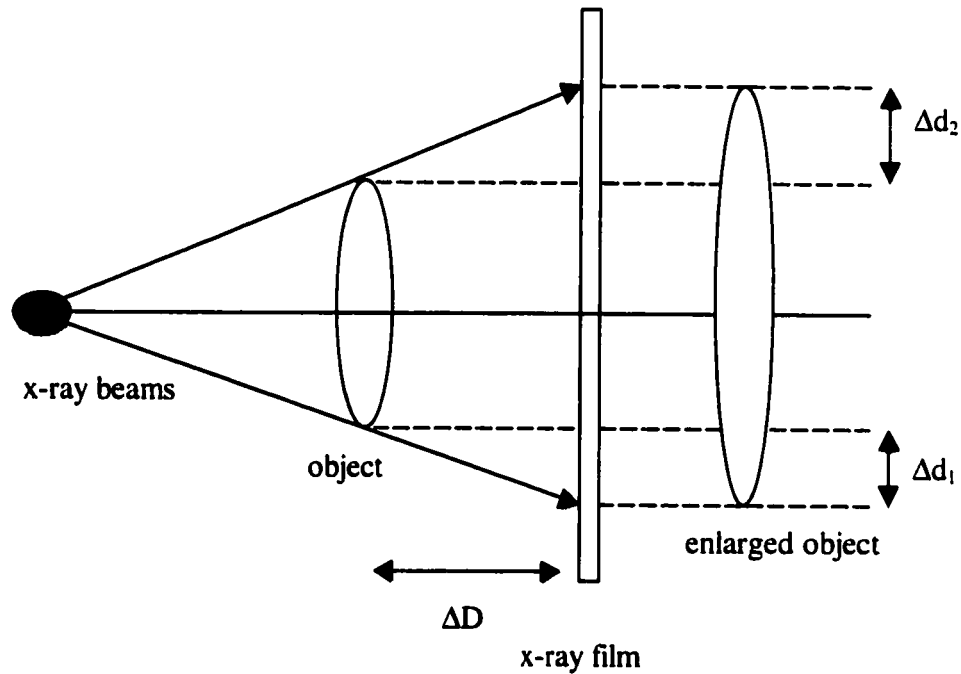


Fig. 4.11 X-rayed objects are enlarged when exposed onto film.

When a distance of ΔD separates an object from the x-ray film, the projected object image is larger than the actual object ($\Delta d_1, \Delta d_2$). After making measurements to the experimental scene, it was found that regions of interest in the radiographs were magnified 25%. To account for this scaling, the TB_0 x-ray values were scaled down 25% and the following results in Table 4.6(a) and 4.6(b) were produced.

Measured \mathbf{TB}_0 vector (x,y,z in mm)			
	x	y	z
\mathbf{TB}_{FOB}	-6	-84	-39
$\mathbf{TB}_{\text{XRAY}}$	-9	-81	-32
delta	-3	3	7

Table 4.6(a) Scaled x-ray non-rotated results.

Measured \mathbf{TB}_0 vector (x,y,z in mm)			
	x	y	z
\mathbf{TB}_{FOB}	-8	-82	-38
$\mathbf{TB}_{\text{XRAY}}$	-6	-79	-32
delta	2	3	6

Table 4.6(b) Scaled x-ray rotated results.

With scaling the difference in the measured y component showed much improvement at 3 mm. This demonstrated that x-ray magnification played a significant part in the obtained x-ray results. The same scaling was not applied to the orientation vectors \mathbf{B} because the relative orientation would not have changed with equal scaling in x,y,z.

The differences of 6-7 mm in z indicated significant inaccuracies remained in digitized x-rays. Digitization errors occur between the FOB and x-rays in measuring common vertebral features. There will always be a difference between the true and measured values. As reported earlier (Andre, 1995) it is difficult to measure common features between stereo-radiographs. This error alone contributes up to +/- 5mm in error. Further, while the FOB may be a highly accurate measurement tool, measurements manually made by a human observer will also contribute error in any observation.

These results demonstrated that while x-ray data could be used to obtain the \mathbf{TB}_0 and \mathbf{B} vectors required for the triad vertebra model, the systematic errors would have to be removed before measurements of sufficient accuracy could be made. The

error associated with making measurements using x-rays precludes reconstruction accuracies of +/- 1 mm.

5 VISUALIZATION

Visualization is the final stage of ORIS. The visualization stage renders the 3D model of the spine based on the information gathered from the stereo cameras. This chapter does not focus on the graphical user interface (GUI) development for ORIS. Rather, its objective is to explore various methods of displaying the 3D spinal model.

The chapter starts with a literature review of previous research in the field of 3D modelling. The various components of ORIS and their interaction with the visualization stage is then covered. Following this is a description of how stages of the operation can be presented and viewed as well as a section discussing how multiple views of the spine have been incorporated into the display. The final section explores the use of different models to best represent the vertebrae of the spine. Vertebra models and their respective merits are discussed.

5.1 Background

Three-dimensional modelling of objects and physical science is a topic covering many different areas of research. For instance, robots can now autonomously navigate themselves by modelling their 3D environment (Akbarally, 1996) (Behringer, 1995). Whether it is modelling heat transfer in thermodynamics (Han, 1996) or analyzing the varying material properties of human bones for finite element analysis (Mehta, 1996), 3D modelling has become an invaluable way of using visualization as a tool for gaining insight into complex problems and phenomena. With stereo-vision in the OR, a 3D representation of the human spine has been modelled to allow surgeons to record and view maneuvers made during scoliosis surgery.

Visualization software for the display of the human spine has been researched in the past (Chu, 1995) (Vandegriend, 1995) (Sultan, 1995)(Landry *et al.*, 1997). In

studying deformation patterns of scoliotic vertebrae, Landry constructed a 3D model of deformed vertebra using multiple thin (1 mm) contiguous CT slices. Measurements were then made on the 3D model to quantify various scoliotic vertebra deformations. It is hoped that the quantification of vertebral deformations will aid in the definition of deformation patterns of the vertebrae in the expression of scoliosis (Landry, 1997).

Sultan created a 3D computer animation model of the spine to provide the clinician with a 3D graphical visualization of the spinal correction process. The animation model interpolates the geometric transformations of the spine between two known states and displays the results as an animated computer model. While this animated model may be useful to surgeons as an offline visualization tool, questions regarding the accuracy of the model prevent it from making accurate intraoperative spinal measurements.

Vandegriend and Chu's visualization software was used to display vertebrae positions and orientations from stereo-radiographs. One of the motivations in the development of ORIS visualization software was the ability to read data directly produced from the detection/matching software (Bhalla, 1995). Eventually, the detection/matching and visualization software will be combined into a single package allowing real-time visual feedback of the spine in the OR.

The visualization package developed dealt with the following areas not previously addressed:

- Direct interface with Bhalla detection/matching software.
- Ability to display various stages of spinal corrective operation.
- Simultaneous multiple views of spine.
- Exploration of various geometric vertebra representations.

5.2 ORIS software model and direct interface

As discussed in Chapter 2, ORIS is made up of several sections each responsible for a different stage of the stereo paradigm. Figure 5.1 shows how these various components of ORIS interact. The visualization component of ORIS receives input from two sources. Triad information for each stage of the operation is passed from the matching correspondence software (Bhalla, 1995) and vertebra triad model information (\mathbf{TB}_0 and \mathbf{B}) is read from the stereo x-rays.

With these inputs, the visualization software calculates the vertebrae positions and orientations based on the stereo x-ray and triad data. Linear interpolation is performed on the remaining vertebrae between attached triads. Preliminary tests showed that linear interpolation gave more realistic representations than cubic splines and polynomial interpolation when triads were placed on every second vertebra. Cubic splines were found to be excessively 'stiff' due to their non-local coefficient calculating nature (Press, 1988). Polynomial interpolation took an unacceptable amount of computation and found to offer no improvement.

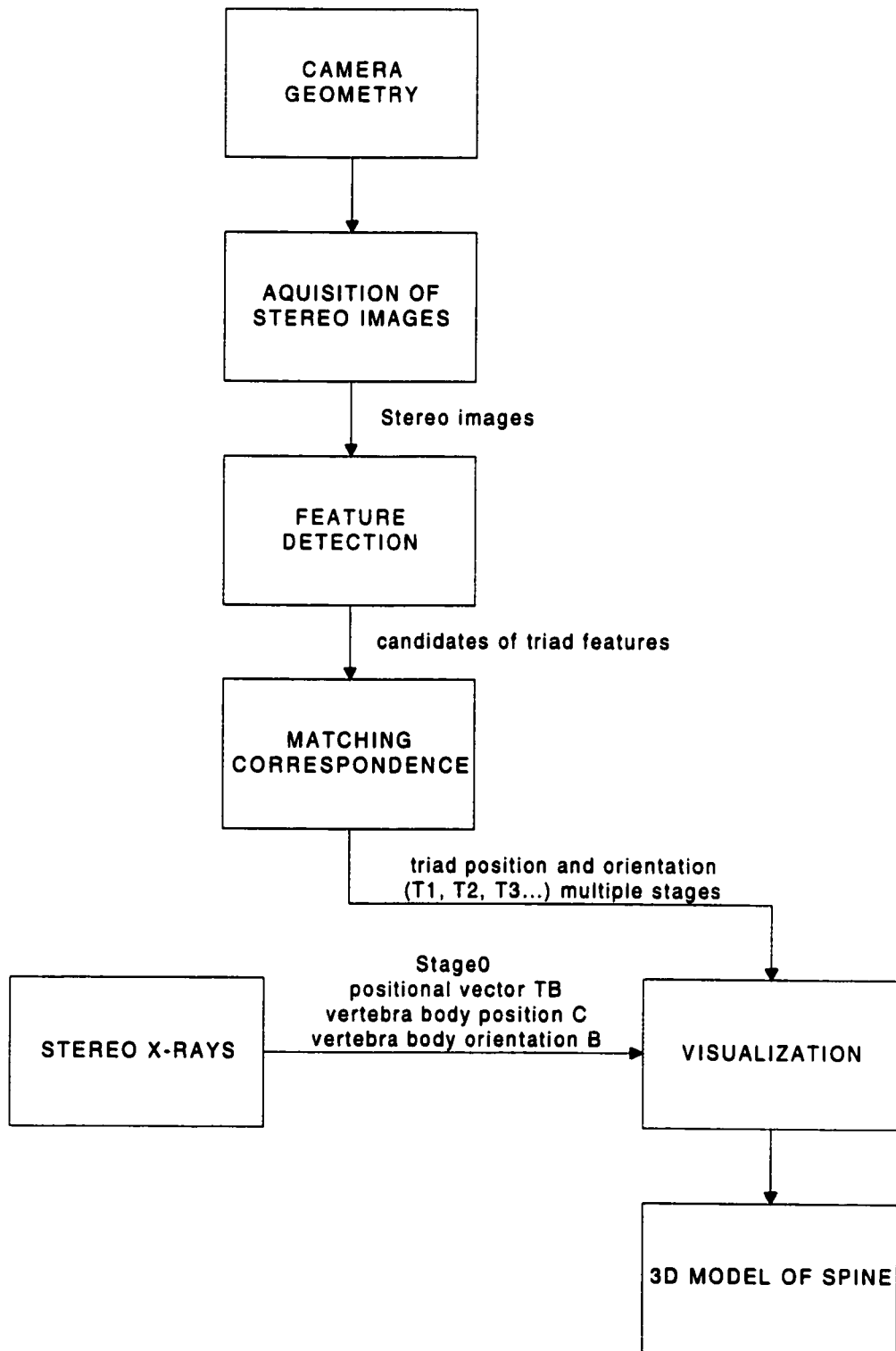


Fig. 5.1 Components of ORIS.

5.3 Multiple stages of operation

A stage is defined as a point where stereo images are captured and processed. To allow the physician to view various stages of an operation, features were added to process data from three sets of stereo images and be loaded for visualization. A surgeon may now view progress made through the operation, by bringing up successive stages of images. This is an important addition to the visualization software (Mahood, 1997).

Figure 5.2 shows images depicting three stages of a spine segment (T5-T9). Stage0 represents the initial uncorrected spine, while Stage1 and Stage2 show the laboratory simulated results of progressive spinal corrections.

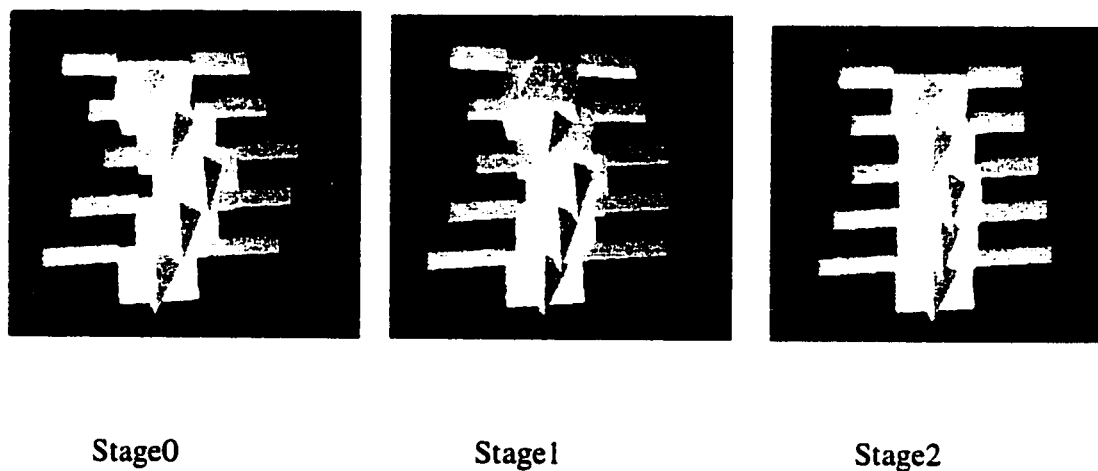


Fig. 5.2 Spine segment (T5-T9) displaying various stages of the spinal curvature.

5.4 Multiple views

To give the surgeon the opportunity to view the spine from various positions, simultaneous multiple views were incorporated into the display. This allowed surgeons to view the spine from multiple positions simultaneously. Two views important to the surgeon are PA (Posterior Anterior) and lateral. Initially two windows, displaying the PA and lateral view, were used to display the spine. Windows were added to allow two more orthogonal views of the spine. These windows allowed the surgeon to view the spine from four views simultaneously.

Initially the four orthogonal views of the spine were presented with each window capable of altering its view through user interface controls. By manipulating slider bars, the user can rotate the spine to the desired point of view (POV). The rotation can be thought of as a virtual camera that rotates around the spine allowing the user to change their POV (Durdle, 1997). However, comments from surgeons suggested that four simultaneously changing views was disorienting (Mahood, 1997). Often users would lose their sense of direction and not be able to set up the view windows for the type of spinal configuration desired. This problem was addressed in two ways.

First, three of the four windows were made static (not capable of changing POV) leaving one window dynamic. Figure 5.3 shows the coordinate system used in each window. The top left and right windows displayed PA and lateral views of the spine respectively. The bottom right window showed a caudad view (head to toe) and the bottom left window was free for user manipulation. This allowed a comparison of multiple views simultaneously without the user getting disoriented. By manipulating the bottom left window the user can compare the stationary PA, lateral, and caudad views with the non-stationary dynamic window.

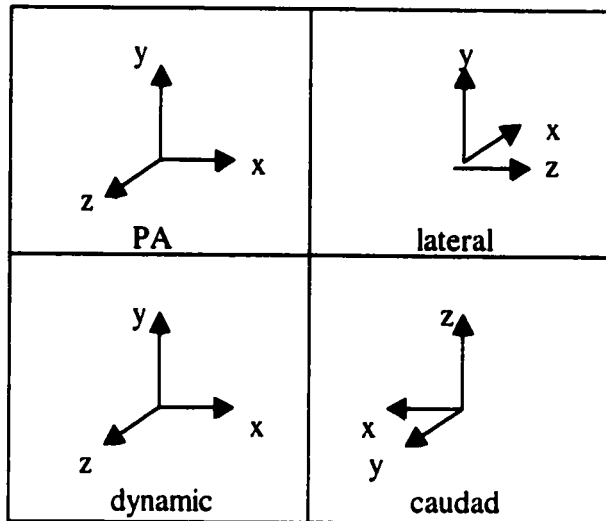


Fig.5.3 3D coordinate system in each display window.

Secondly, to give a frame of reference in the dynamic window, a wire frame cube was drawn surrounding the spine. The cube, shown in Figure 5.4, is rendered flush to the PA and lateral planes of the spine, as these were most useful for comparison as frames of reference. This provides a visual indication of how much rotation has been applied to the POV.

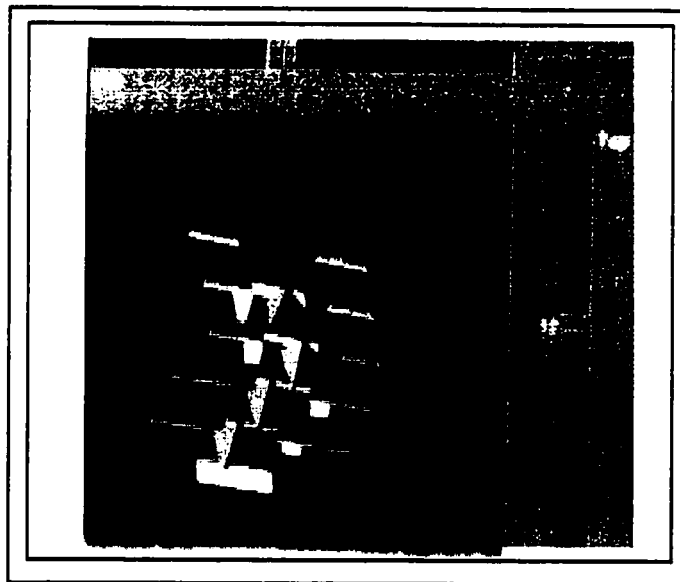


Fig.5.4 Wire frame cube surrounding rotated spine.

Figure 5.5 displays an example of what the spine looks like in each window. The view point configurations were chosen to offer the surgeon the most useful points of view for any given spine. This multiple view system allows the surgeon to view the spine from various points of view simultaneously.

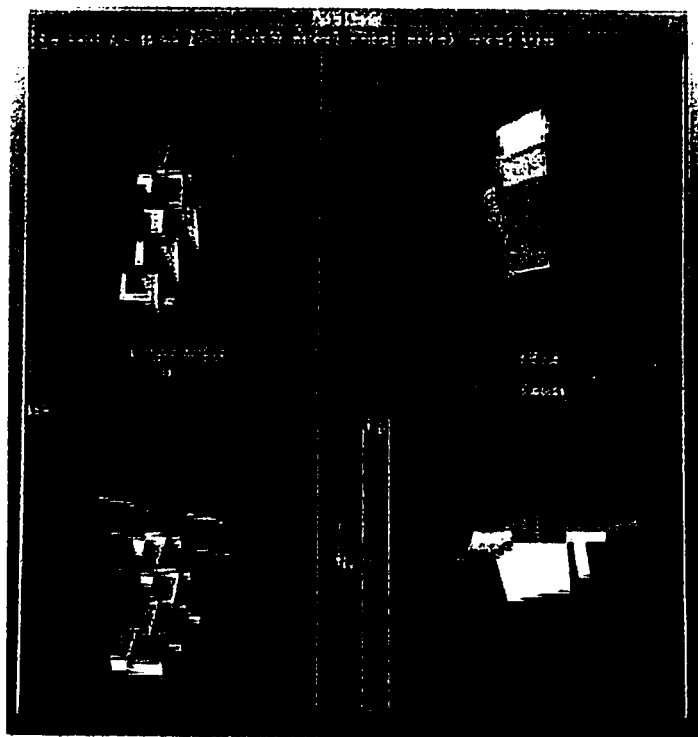


Fig. 5.5 Multiple simultaneous views of spine segment (T5-T9).

5.5 Models of Vertebra

Surgeons viewing 3D models of human spines would like the most realistic rendition of the human spine as possible (Mahood, 1997). However, limitations of computer hardware and software often force a compromise between the level of detail in the 3D model, and the speed of rendering on a computer console. Another limitation is the amount of information known about the model. ORIS determines vertebra body position and orientation only.

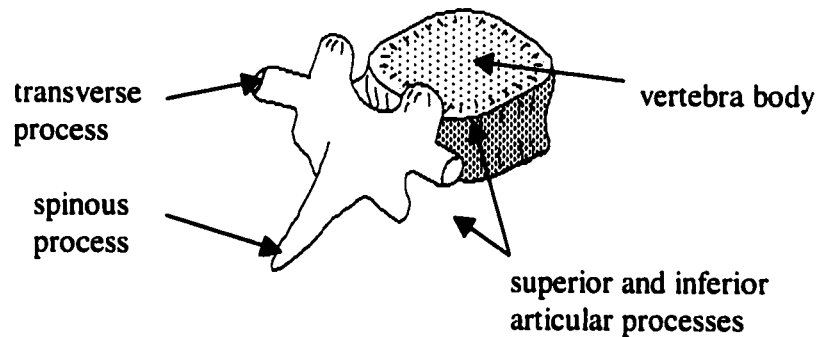


Fig. 5.6 Dominant features of vertebra.

The above model (Figure 5.6) shows the dominant features of a typical vertebra. The vertebra body, followed by the spinous and transverse processes, are the more dominant features. While ORIS returns no information on spinous and transverse processes, when rendered they convey important orientation information.

ORIS thoracic and lumbar vertebra dimensions were taken from research by Panjabi (Panjabi, 1991, 1992). Panjabi's vertebrae were taken from twelve cadavers of male and female adults ranging from 19 to 59 years in age. These were not scoliotic vertebrae. Hence vertebra deformations, that may occur in scoliosis patients, were not

included in Panjabi's study. Vertebra deformations would not alter the ORIS visualization display because stereo x-rays would take into account any deformations the vertebra may have. By maintaining the relative orientation and positional difference between the triad and vertebra, the vertebra position and orientation can always be determined.

Various vertebral models were developed, each meant to convey graphical vertebra information in a slightly different but meaningful way. While some models convey a more realistic depiction of the spine, they may not allow complex rotations and translations to be applied to the visual without slowing the computer console to an unacceptably slow speed. Addressing the limitations of the existing hardware, software, model complexity, and acceptable rendering speeds, various geometric 3D vertebra models were developed and compared. These models, and their respective advantages and disadvantages are now presented.

5.5.1 Wire Frame model

The simplest and most readily drawn model (Figure 5.5) is a skeletal view of the vertebral body. This transparent model of the vertebra allows the spine to be rendered very quickly while undergoing translations and rotations in real-time. While quickly rendered, the model lacks depth and feel when viewed at certain angles. In views where vertebra would normally occlude other vertebra, the transparency of the wire frame model can prevent the determination of which objects in the image are close and which are far. The wire frame model is excellent for setting up points of view of the spine, but not good at providing realistic looking vertebra model. An example of the wire frame model rendering vertebra T5-T9 is shown in Figure 5.7.



Fig. 5.7 Model of spine segment T5-T9 using wire frame model.

5.5.2 Positional model

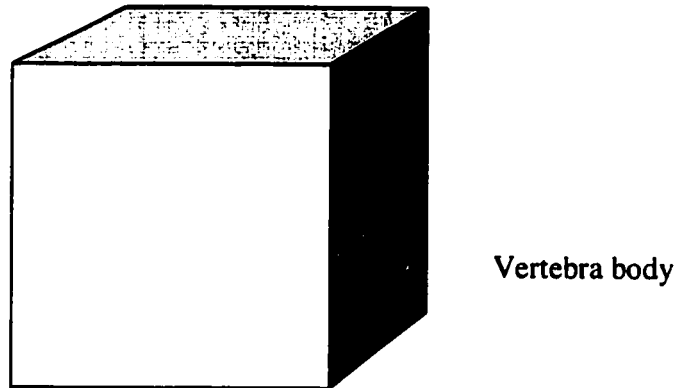


Fig. 5.8 Positional model of vertebra.

The positional model (Figure 5.8) is a solid version of the wire frame model. It also represents the entire vertebra with only the vertebra body. The positional model is solid allowing it to make use of 3D lighting effects. Three-dimensional lighting conveys depth information through the models shaded sides. After the wire frame, the positional model is the simplest most easily rendered vertebra model. While lighting effects do provide basic orientation information, features like transverse and spinous processes would provide more orientation information if drawn. Currently, the user is left without a sense of direction about which is the front or back of the spine since there are no other identifiable features. This model is the fastest solid model for rendering. Figure 5.9 shows what the positional model looks like rendering a segment of a spine.

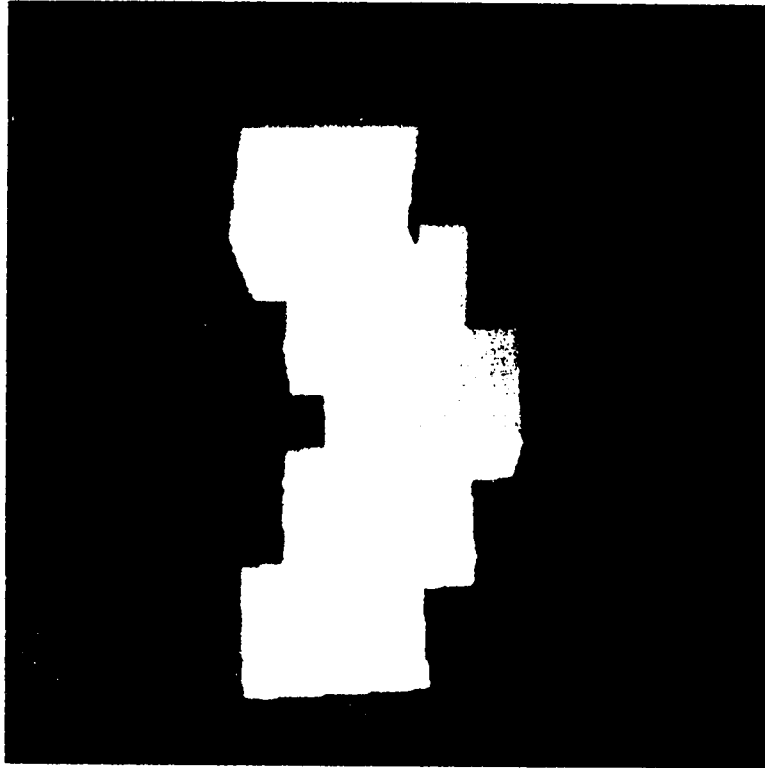


Fig. 5.9 Model of spine segment T5-T9 using positional model.

5.5.3 Orientation model

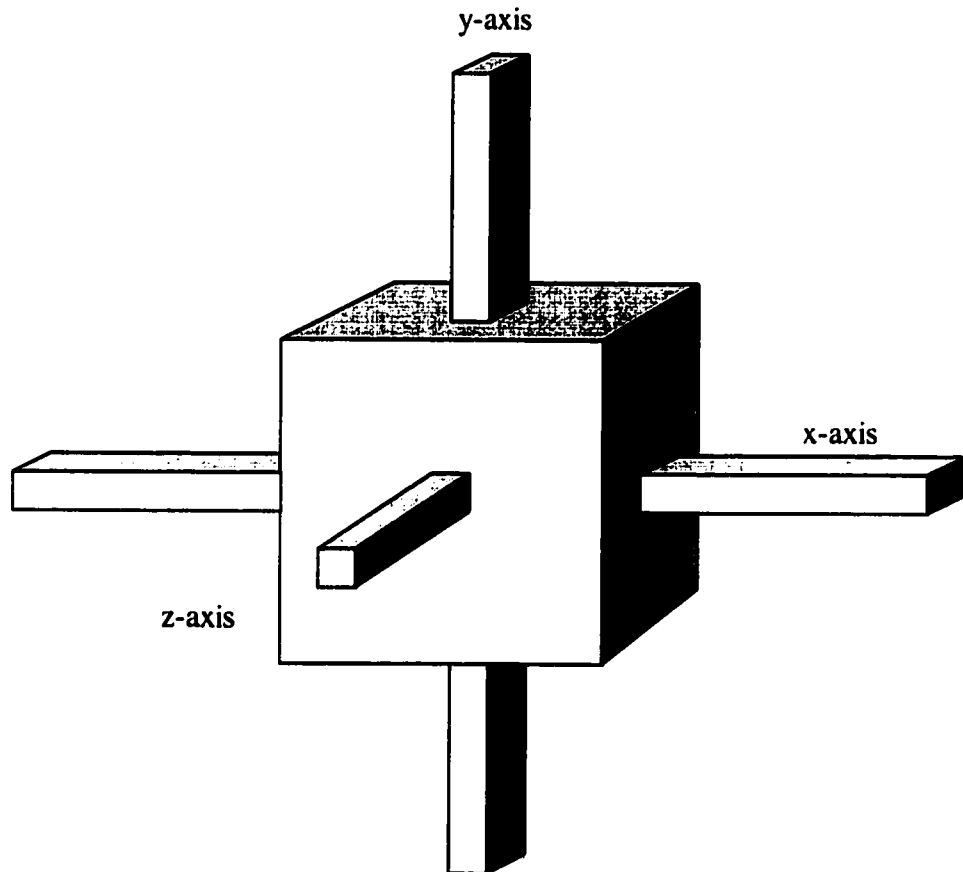


Fig. 5.10 Orientation model of vertebra.

The orientation model, shown in Figure 5.10, conveys not only position information but orientation information about individual vertebra as well. Solid bars representing the local vertebra xyz axes can be toggled ON/OFF. The axes passing through the vertebra body more readily display any abnormal rotation of vertebra relative to their neighbors. This allows rapid identification of vertebrae not properly aligned. The disadvantages of this representation are the lack of feel about which is the front and back of the spine as well as the longer rendering time. As in the positional model, spinous and transverse processes are not rendered. This model,

shown in Figure 5.11, is useful for analysis when searching for vertebra not properly aligned.

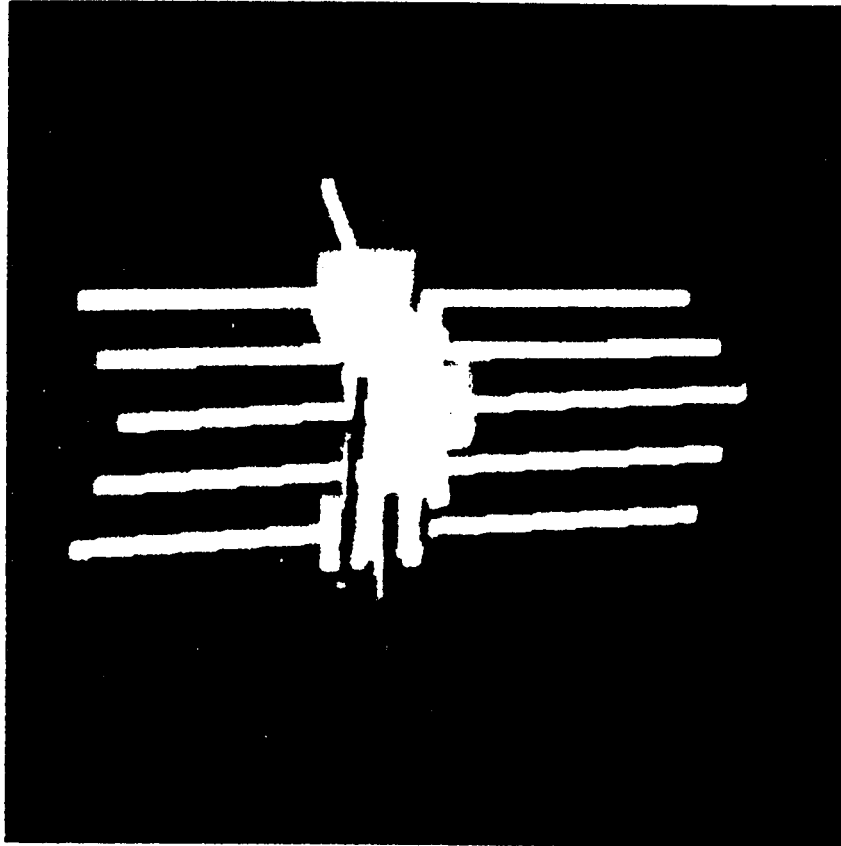


Fig. 5.11 Model of spine segment T5-T9 using orientation model.

5.5.4 Geometric model

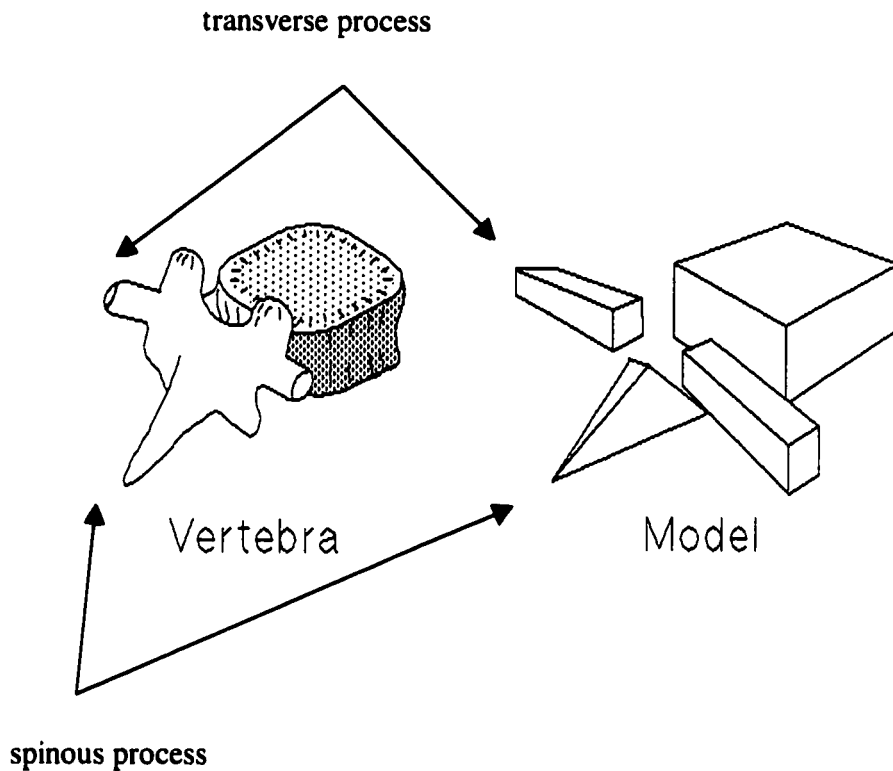


Fig. 5.12 Geometric model representation of vertebra including spinous and transverse processes.

The geometric model, shown in Figure 5.12 on the right, is the most complete and realistic of the spinal models. The dominant vertebra features (spinous and transverse processes) have been included and contribute a realistic look that was lacking in previous models. It should be noted that ORIS makes no measurements of transverse and spinous process features. They have been included only to provide extra orientation information. The transverse and spinous processes provide a more complete model of the vertebra leaving little doubt about which is the front or back of the spine. The geometric model is the most visually appealing model because it most closely resembles the actual vertebra and provides the most realistic looking spine. Additional orientation information can be added by toggling on the *xyz* axes found in the orientation model (solid bars passing through the local vertebra). The only

consequence of the more complicated model is the longer rendering time. Figure 5.13 shows what the display looks like when rendered with the geometric model.

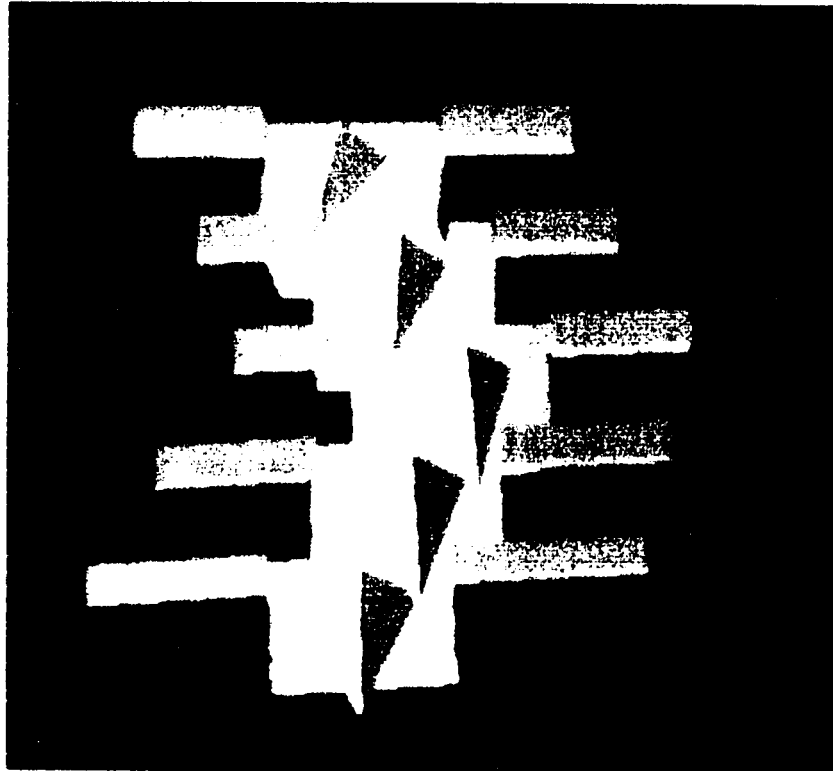


Fig. 5.13 Model of spine segment T5-T9 using geometric model.

5.5.5 Rendering times

An experiment was conducted to quantify the difference in rendering times between the previously described vertebra models. A five-segment spine (T5-T9) was chosen as the object to be tested for rendering. Each vertebra model underwent 100 rotations (50 about the x-axis and 50 about the y-axis). One hundred rotations were chosen to sufficiently allow differences in model rendering time to become obvious. Using a stopwatch, each model was continuously rendered until completion of the rotations. Once the models had completed the rotations, their times were recorded and are shown in Table 5.1.

Model	Wire Frame	Position	Orientation	Geometric
100 rotations	27.24	51.44	106.45	74.47

Table 5.1 Time to render each vertebra model (all times are in seconds).

As expected, the more complicated geometric shapes took longer to render. The wire frame model was almost twice as fast as its solid counterpart the positional model. The orientation model took twice as long as the positional model and ~25% longer than the geometric model.

5.5.6 Comparison of models

All the described vertebra models have their respective advantages and disadvantages. The wire frame model was excellent at quickly displaying the spine and was the fastest model for on screen manipulations. The positional model improved on the wire frame by adding 3D lighting effects at the cost of a doubling in rendering time. The orientation model best highlighted individual vertebra that had abnormal vertebra rotations and was designed with the intention to be used as an analysis tool. Its exceedingly long rendering time made this model inappropriate for rapid on screen model manipulations. The most realistic model was the geometric model. The geometric model provided the most realistic rendition of the spine. While not as fast as the positional model for rendering, its added spinous and transverse processes make the model more desirable for viewing.

Among surgeons, the geometric model was the most popular (Mahood, 1997) because it was the most realistic. Through discussion, the indications were that the best models for viewing the spine were the:

- wire frame model
- geometric model

The wire frame for its rapid onscreen manipulation ability and the geometric model for its realistic portrayal of the vertebra. When used as a clinical tool, the spine would be manipulated into position using the wire frame model, and then rendered with full lighting effects in 3D using the geometric model.

The more graphical information required to display an object, the more time required to render and manipulate that object on a computer screen. That was the tradeoff made between the various models. The detail of the model is directly related to the speed of rendering. With current technology this is a serious concern when rendering 3D models. However, with computers ever becoming faster, the tradeoff between these relatively simple models will eventually become less of a concern. For this reason, the geometric model will be the most useful to surgeons as computers increase their rendering speeds.

6 CONCLUSIONS AND RECOMMENDATIONS

The final chapter of this work is broken into three parts. The first section highlights the research completed and the results obtained. Potential areas of future research and how to build on this work and the work of Bhalla follow. Conclusions based on the author's experience constitute the final section.

6.1 Summary of Results

This work continued the research begun by Bhalla regarding the use of stereo-vision cameras to make intraoperative measurements during corrective scoliosis surgery (Bhalla, 1995). Research was continued in three distinct areas. Tests to determine the accuracy of ORIS (Operating Room Imaging System) were conducted. A triad vertebra model was developed to relate triad positions and orientations to respective vertebra. Additional features were added to the visualization stage of ORIS and various geometric representations of vertebra were investigated. Work done in each of these areas is summarized below.

ORIS accuracy

Experiments were done to determine the accuracy of a stereo-vision imaging system (ORIS) used to track the three-dimensional motion of artificial markers rigidly attached to vertebrae during scoliosis surgery. Displacements and rotations of artificial triad markers were made and recorded by ORIS. Results indicated that ORIS has an accuracy of +/- 1 mm. Measurements were least accurate along the z-axis running passing through the cameras. Initially, rotations about the z-axis were undetectable by ORIS. Modifications to the software have been made to correct this.

Triad vertebra model

A model relating the positions and orientations of triad markers to respective vertebrae was developed. Because ORIS measures artificial triad marker positions and orientations, data must be translated into vertebrae positions and orientations for spine visualization. Stereo x-rays were used to obtain the geometric relationship between triads and vertebrae. Results indicated that the triad to vertebra model worked well when provided accurate data. However, stereo x-rays were not sufficiently accurate in supplying data required for the model. A more accurate method for measuring triad vertebra vectors and vertebra body orientations must be found before the model will accurately predict vertebra position and orientation.

Visualization

Additional features were added to the visualization stage of ORIS. Data can now be read directly from Bhalla's matching correspondence software. Multiple simultaneous views of the spine were added. Three of the four spine views are static, while one dynamic window can be manipulated to change the users point of view. The loading of multiple stage visualization information from various stages of the operation has been included. This allows different stages of a surgery to be loaded and compared visually. Optimal geometric representations of vertebra models were investigated. Results showed that a wire frame model was most popular for dynamically altering the view of the spine in real-time. For static viewing the more detailed geometric model was most popular because of its solid 3D light rendering capabilities, as well as its more realistic physical portrayal of the spine by the inclusion of dominant vertebra features like the spinous and transverse processes.

6.2 Recommendations for future work

This section provides the authors recommendations for future research based on his experience with the project and its limitations. A thorough understanding of the theory, related literature, and what has been done in the past should preclude further research in this area. These recommendations cover ORIS as a whole, and not only topics researched in this work.

1. Improved feature detection

An unacceptable amount of time is currently spent detecting the triad features in the stereo images. Detection time could be greatly reduced if only one detection mask was required (currently ten are used). If a material could be found that would make the triad balls stand out more from the OR background, the reduction in computational time would be significant. Edge detection and preprocessing of images would no longer be required. Possible solutions would be investigating various materials and paints to coat triad balls to enhance their detection. Another option may involve the use of the Infrared VICOM system used in the Gait Lab at the Glenrose Hospital. By coating triad balls with a reflective tape and using infrared cameras, VICOM would quickly and accurately locate triad ball features and separate them from the background. Reducing the time spent in feature detection will be a major factor in approaching real-time feedback in the OR.

2. Camera Calibration

The length of time required for stereo camera calibration could be reduced. Currently, images are captured on a Macintosh to make use of the frame grabber. Points are then measured and digitized as calibration data. This data is then ported to an IBM RS/6000 workstation to make use of the calibration routines written in FORTRAN and C. If the frame grabber and programs could be consolidated onto

one platform and written into one language, a significant amount of time would be saved in the camera calibration process. Porting camera calibration code into one 'shoot and calibrate' software program will be very useful for future researchers.

3. Combine DETECT-POINT, MATCH-POINT and SHOW-POINT

It would be useful if Bhalla's feature detection program DETECT-POINT, the correspondence program MATCH-POINT, and the visualization software SHOW-POINT could be combined into one package. This would allow stereo images to be fed into one program that could then calculate all the vertebrae positions and orientations. Combining all the separate elements of ORIS into one program is one of the issues that will have to be addressed before real-time feedback in the OR will be feasible.

4. Real-time implementation

Work can also continue integrating all of ORIS's components into a single, self-contained, real-time computer platform for making intraoperative measurements. Much thought will have to be given in choosing the platform to handle ORIS's considerable computational needs. The system will have to be capable of the following:

- capturing and processing full stereo images in real-time
- handling the combined computational burden of a program containing versions of Bhalla's feature detection/matching software and 3D visualization software
- rendering full 3D models of the spine in real-time (20-30 frames/second)

5. Triad to vertebra model

To make the triad vertebra model fully functional, an accurate method of obtaining the required model data will have to be found. The inaccuracies of stereo x-rays prevented the model from accurately calculating vertebrae positions and orientations. The model worked well when supplied accurate data from the electromagnetic digitizer (FOB). The FOB can not make the required measurements for the model in the OR because vertebra features required for digitization are not exposed during surgery. Future research could focus on ways of modifying the model so that features not available to the FOB during OR are not required.

6. Visualization

To make the ORIS more appealing to users, future work should be spent on improving the Graphical User Interface (GUI). Making the GUI of ORIS easy to use and user friendly will play an important role acceptance of ORIS as a useful clinical tool.

6.3 Conclusions

A stereo-vision system developed for the intraoperative monitoring of scoliosis surgery (Bhalla, 1995) was improved. Improvements can be categorized into three sections :

- determination of the accuracy of the Operating Room Imaging System (ORIS)
- development of a geometric model relating artificial triad markers to vertebral positions and orientations
- improved 3D visualization tools and vertebra model representation

For each of the above areas, well-defined goals were laid out, literature was surveyed, and solutions were proposed and implemented. As real-time feedback becomes more important, feature detection time will have to be reduced significantly. Bhalla's suggestions of using the FFTs and root triad ball image templates have real merit. Foresight will also be important in picking one computer to run all software and image capturing for real-time feedback in the OR. The computer would ideally be small (laptop preferably), powerful (rapid visualization), and able to handle real-time image capturing.

This work improves the feasibility of using stereo-vision in the OR. While much work remains, I sincerely believe that this approach will one day develop into a standard tool for the 3D intraoperative monitoring of scoliosis surgeries.

REFERENCES

- B. Andre, J. Dansereau, H. Labelle. Effect of radiographic landmark identification errors on the accuracy of three-dimensional reconstruction of the human spine. *Medical & Biological Engineering & Computing*, Vol.30, pages 569 - 575, 1992.
- H. Akbarally. 3D robot sensing from sonar and vision. *Proceedings - IEEE International Conference on Robotics and automation*, Vol.1, pages 686 - 691, 1996.
- M. Asher. The Cobb angle should be used in the management of scoliosis. *Intl. Symp. on 3D Scoliotic Deformities*, pages 57-58, 1992.
- S.T. Ballard and C.M. Brown. *Computer Vision*. Prentice Hall, Inc., 1982.
- K. Bhalla. *A Stereo-Vision System for the Intraoperative Monitoring of Scoliosis Correction*. (Master of Science Thesis, University of Alberta, Canada, 1995).
- K. Bhalla. *MATCH-POINT: An Algorithm for Point Feature Extraction and Registration in Stereoscopic Images*. Tech Report (Course CMPUT 509) for Dr. A. Basu, Computing Science, University of Alberta, Canada, 1994.
- K. Bhalla. *Stereopsis: Some issues involving 3D measurements*. Tech. Report (Course EE 602) for Dr. N.G. Durdle, Electrical Engineering, University of Alberta, Canada, 1994.
- K. Bhalla, N.G. Durdle, A.E.Peterson, J. Raso, D. Hill, and X. Li. Automatic feature detection and correspondence in a stereo-vision application. *IEEE Conference on Systems, Man and Cybernetics*, pages 3537-3542, 1995
- R. Behringer. Real-time 3D reconstruction of road curvature in far look-ahead distance from analysis of image segmentation. *Proceedings of SPIE - The International Society for Optical Engineering*, Vol. 2646, pages 172-179, 1995.
- J. Buchanan. *Personal Communication*. Dept. of Computing Science, University of Alberta, Edmonton, Canada, 1996.
- K. Chu. *Dynamic Visualization of the Spine using OpenGL*. EE602, Dept. of Electrical Engineering, University of Alberta, Canada, 1995.
- J.R. Cobb. Outline for the Study of Scoliosis. *Instructional Course Lectures, American Academy of Orthopedic Surgeons*, pages 175-261, 1948.

- E.R. Davies. On the noise suppression and image enhancement characteristics of the median, truncated median and mode filters. *Pattern Recognition Letters*, pages 87-97, 1988.
- E.R. Davies. *Machine Vision: Theory, Algorithms, Practicalities*. Academic Press, 1990.
- U.R. Dhond and J.K. Aggarwal. Structure from stereo. *IEEE Trans. On Systems, Man, and Cybernetics*, v.19, no.6, pages 1489-1510, 1989.
- N.G. Durdle(*), J. Raso, and D. Hill. *Personal Communication*. (*)Dept. of Electrical Engineering, University of Alberta; Rehabilitation Technology, Glenrose Hospital, Edmonton, Canada, 1996-97.
- O. Faugeras. *Three-Dimensional Computer Vision*. MIT Press, Cambridge, 1993.
- Ascension Technology Corporation, Burlington, Vermont, USA. *Flock of Birds*.
- J. Foley, A. van Dam, S. Feiner, J. Hughes. *Computer Graphics Principles and Practice*. 2nd Ed. Addison-Wesley, 1993.
- G. De Giorgi, A. Gentile, and G. Mantriota. Three-dimensional study of the spine: Our ten year experience. Intl. Symposium. On 3-D Scoliotic Deformities, pages 71-80, 1992.
- N. Glossop, R. Hu. Assessment of Vertebral Body Motion During Spine Surgery. *SPINE Vol 22, No. 8*, pages 903-909, 1997.
- R.C. Gonzales and R.E. Woods. *Digital Image Processing*. Addison-Wesley Publishing Company, 1992.
- R.C. Gonzalez and P. Wintz. *Digital Image Processing*. Addison-Wesley Publishing Company, 1987.
- W.E.L. Grimson. Computational experiments with a feature based stereo algorithm. *IEEE Trans. on Pattern Analysis and Machine Intelligence*, pages 17-34, 1985.
- S. Han, Modelling of 3D object considering internal heat source. *Proceeding of SPIE - The International Society for Optical Engineering*. Vol. 2742, pages 169-176, 1996.
- R. Johnson. *Miller & Freud's Probability & Statistics for Engineers*. Prentice Hall, 1994.

H. Labelle, J. Dansereau, C. Bellefleur, J. De Guise, C. Rivard, and I.A.F. Stokes. 3-D Correction obtained with the C-D procedure during surgery. *Intl. Symp. on Three-dimensional Analysis of Spinal Deformities*, pages 349-351, 1995.

C. Landry, J.A. de Guise, J. Dansereau, H. Labelle, R. Zeller, W. Skalli, F. Lavaste. A Methodology for the 3D Description of the Deformation Patterns of Scoliotic Vertebrae. *Research into Spinal Deformities 1*, IOS Press, pages 339-341, 1997.

J. Mahood. *Personal Communication*. Dept. of Surgery, University of Alberta Hospitals, Edmonton, Canada, 1997.

B. Mehta, S. Rajani. 3D modelling and analysis of human bones : generating 3D models to accommodate varying material properties for finite element analysis. *American Society of Mechanical Engineers, Petroleum Division. Vol. 77, No. 5*, pages 117-125, 1996.

M. Mehta. The Cobb angle should not be used in the management of scoliosis. *Intl. Symp. on 3D Scoliotic Deformities*, page 59, 1992.

R.T. Morrissy. *Atlas of Pediatric Orthopaedic Surgery*. J.B. Lippincott Company, 1992.

M. Neuwirth. *The Scoliosis Handbook : a consultation with a specialist*. 1st Ed. New York. : H. Holt and Co., 1996.

M. Panjabi, K. Takata, V. Goel, D. Federico, T. Oxland, J. Duranceau, M. Krag. Thoracic Human Vertebrae Quantitative Three-Dimensional Anatomy. *SPINE Vol. 16, No. 8*, pages 892-901, 1991.

M. Panjabi, K. Takata, V. Goel, T. Oxland, J. Duranceau, M. Krag, M. Price. Human Lumbar Vertebrae Quantitative Three-Dimensional Anatomy. *SPINE Vol. 17, No. 3*, pages 299-306, 1992.

A. Peterson. *Personal Communication*. Dept. of Civil Engineering, University of Alberta, Edmonton, Canada, 1994-95.

W. Press, P. Flannery, S. Teukolsky, W. Vetterling. *Numerical Recipes in C - The Art of Scientific Computing*. Cambridge University Press, 1988.

H.K. Ramapriyan. A multilevel approach to sequential detection of pictorial pictures. *IEEE Trans. on Computers*, v.25, no.1, 1976.

G.C. Robin. *Scoliosis*. Academic Press, Inc. New York. N.Y. 1973.

N. Schommer. *Stopping scoliosis : the complete guide to diagnosis and treatment*. Rev. ed. Garden City Park, N.Y. : Avery Pub Group, 1991.

W. Smith, N. Vakil, S. Maislin. Correction of Distortion in Endoscope Images. *IEEE Transactions of Medical Imaging, Vol. 11, No.1*, pages 117-122,1992.

J.J.Spiegelman and S. Woo. A rigid-body method for finding centers of rotation and angular displacements of planar joint motion. *J. Biomechanics Vol. 20, No. 7*, pages 715-722, 1987.

D. Sultan, J.A. De Guise, J. Dansereau, H. Labelle. Computer Animation of the Scoliotic Deformation Process. *Three-dimensional Analysis of Spinal Deformities*. Pages 75 - 80, 1995.

S.J. Treadwell, K.S. Booth, C.W. Reilly, B.J. Sawatzky, and S.B. Jang. Three-dimensional analysis of scoliosis surgery using stereophotogrammetry. *Intl. Symp. on Three-dimensional Analysis of Spinal Deformities*, pages 95-100, 1995.

B. Vandegriend, D. Hill, J. Raso, N.G. Durdle, and Z. Zhang. Application of computer graphics for the assessment of spinal deformities. *Medical & Biological Engineering & Computing*, pages 163-167, 1995.

David Vernon. *Machine Vision - Automated Visual Inspection and Robot Vision*. Prectice Hall (UK), 1991.

A. Watt. *Fundamentals of Three-Dimensional Computer Graphics*. Addison-Wesley. 1989.

Ed. S.L. Weinstein. *The Pediatric Spine: Principles and Practice*. Raven Press, 1994.

P.R. Wolf. *Elements of Photogrammetry*. McGraw-Hill Book Company, 1983.

APPENDIX A SYSTEM SPECIFICATIONS

This appendix describes system specifications in terms of the software development and platform used.

Software Information

Programming Language : ANSI C

Operating System : UNIX

Compiler : gcc

Platform : IBM RS/6000

Graphics Support : OpenGL (Hardware assisted on the IBM RS/6000)

Software Available With : Dr. N.G. Durdle, Dept. of Electrical Engineering,
University of Alberta, Edmonton, Alberta, Canada. T6G 2G7

Visualization Software

Directory Name : ShowPoint

Executable Name : sp

Vertebra triad model Software

Directory Name : TriadVertModel

Executable Name : triad2vert

Hardware Information

Refer Table 2.1

APPENDIX B SOFTWARE MODEL: SHOW-POINT

This appendix outlines the software for SHOW-POINT, the visualization software used to render the 3D model of the spine. All software modules are explained along with their respective routines and functions. A high level description of the various software modules is first presented. Detailed information regarding inputs and outputs of each modules' respective routines are included at the end of the Appendix B along with their flowcharts. Code is heavily documented and contains all other information necessary to make modifications to software. Figure B.1 shows a high level model of the major components of SHOW-POINT.

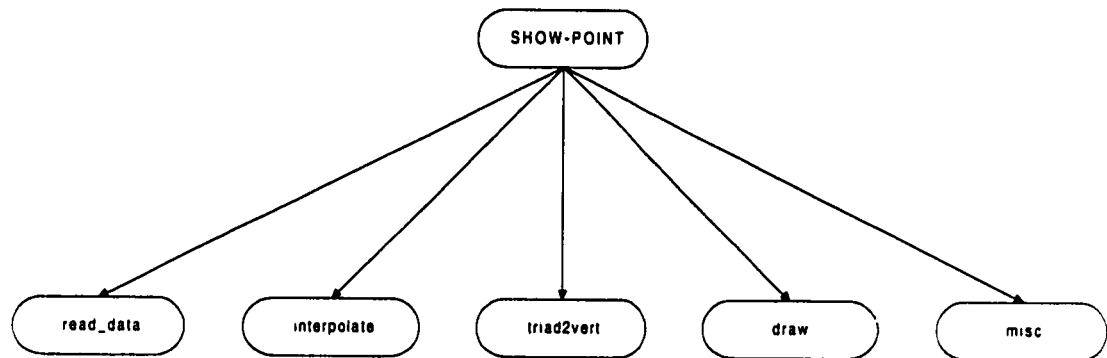


Fig. B.1 SHOW-POINT: Software Modules.

SHOW-POINT

This is the control module for SHOW-POINT. All control and event processing begins and stops here. Graphical user interface, data structure and variable initializations are all taken care of in the **misc** module. Triad positions and orientations and stereo-graphic x-ray data are obtained in the **read_data** module and stored in appropriate data structures. In the **triad2vert** module triad movements are transformed into vertebra movements. To fill in missing data points, the **interpolate** module linearly interpolates the remaining data points. Once vertebra positions and orientations are determined, vertebra models are rendered on screen in the **draw** module depending on user specified settings. Control remains in main until user changes model characteristics through the graphical user interface.

read_data

Reads in the triad position and orientation generated by ORIS and the stereo-graphic x-ray data relating the triads to the vertebrae. Data files are stored in a directory called data and are named Stage0.dat, Stage1.dat, Stage2.dat. Three stages of data are currently supported. X-ray data is stored in TB0.dat. Data is stored in the appropriate data structures and control is returned to main.

interpolate

Interpolates vertebra positions and orientations between known data points. Linear interpolation is used. All interpolated points are calculated and stored in the respective data structures.

triad2vert

Takes the triad position and orientation information with the stereo-graphic x-ray data and determines the new vertebra position and orientation based in the algorithm described in Chapter 4 - Rotation of a point about an arbitrary line in free space. New vertebra positions and orientations are stored and control is returned to main. This module and its routines are shown in Figure B.2. Flowcharts for each triad2vert routine are shown in latter part of Appendix.

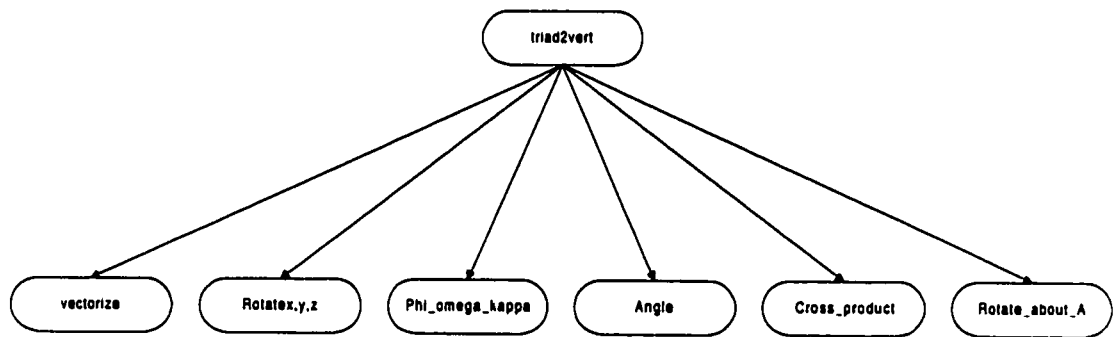


Fig. B.2 triad2vert software module and respective routines.

draw

This routine calls **draw_spine** module to render the wire frame, positional, orientation, or geometric model based on specifications set by the user in the graphical user interface. Once the spine has been rendered, and the **spotlights** have been added, control is returned to main. This module is broken down further in Figure B.3 and Figure B.4. Flowcharts for each draw routine are included at end of Appendix.

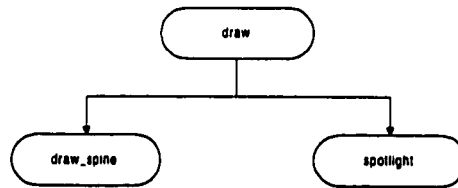


Fig. B.3 draw software module and respective routines.

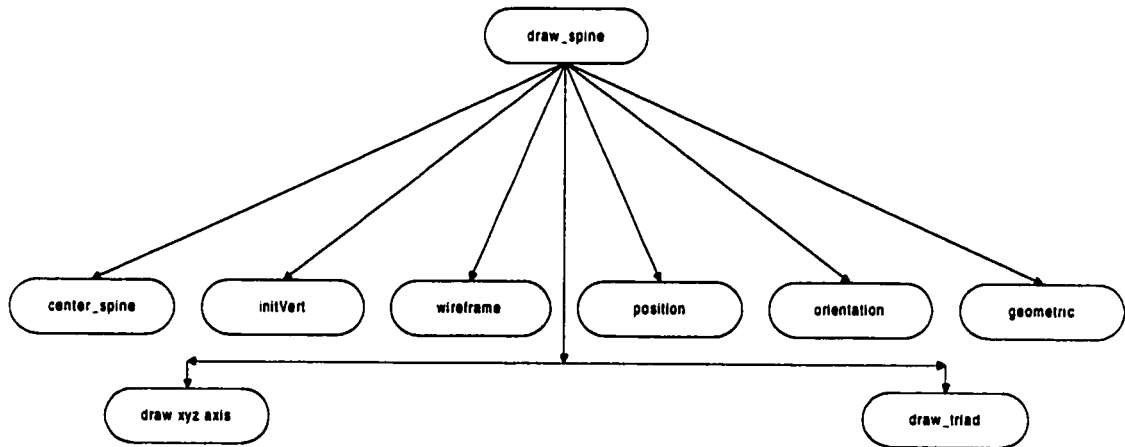


Fig. B.4 draw_spine software module and respective routines.

misc

This module handles the initialization of data structures, OpenGL rendering contexts, graphical user interface widgets and callback structures for SHOW-POINT. These modules are further broken down into routines shown in Figure B.5 and Figure B.6.

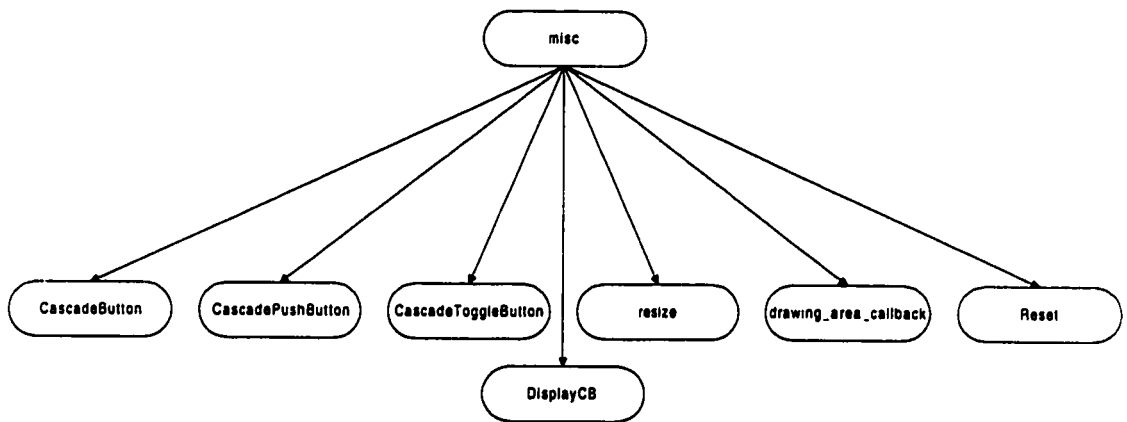


Fig. B.5 misc software module and respective routines.

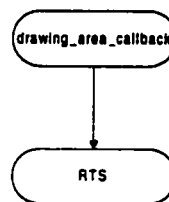


Fig. B.6 drawing_area_callback software module and respective routines.

read_data reads the triad and FOB data (TB_0 and B) required to make the vertebra model

Input data structures to hold triad and FOB data

Output void

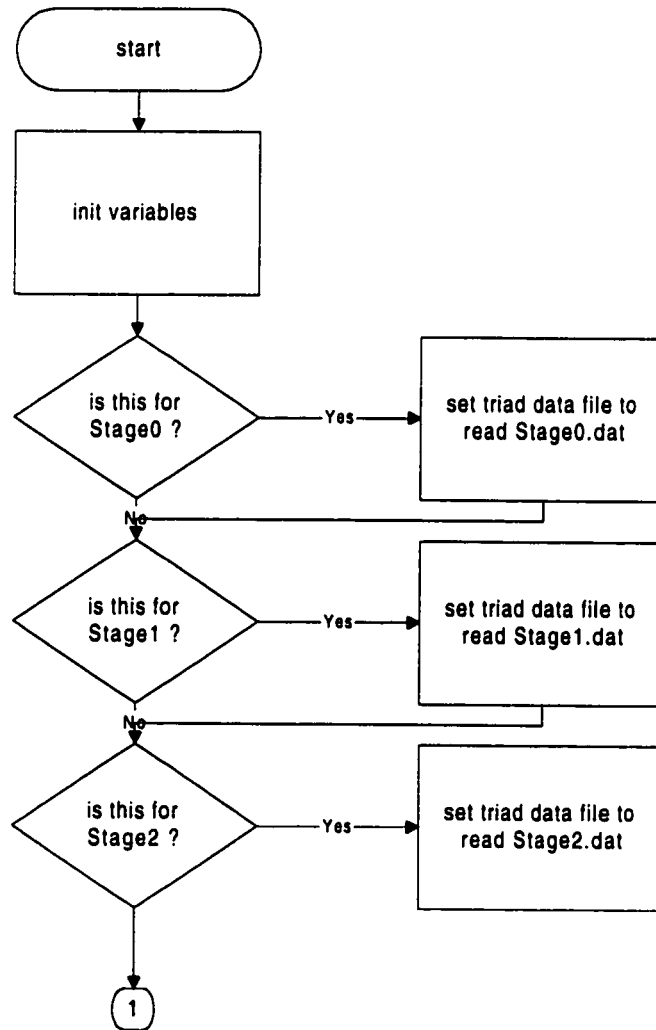


Fig. B.7 Read_data flowchart.

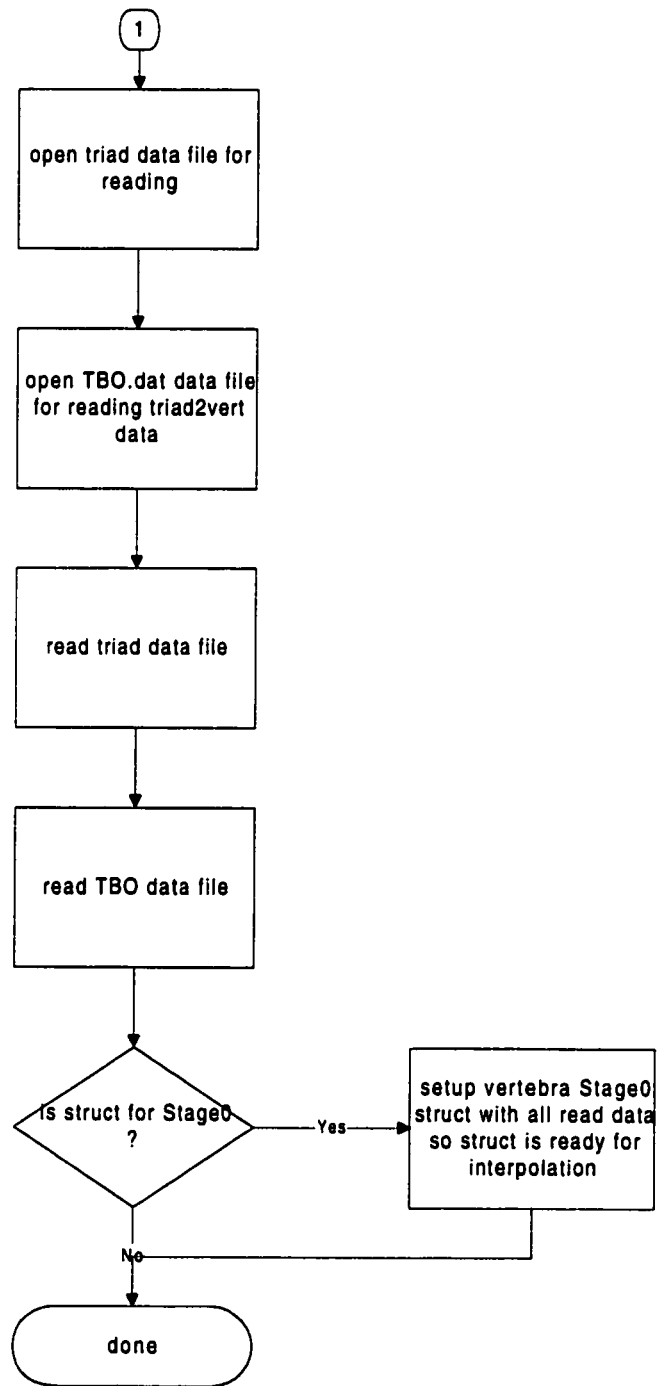


Fig. B.7 Read_data flowchart.

interpolate linearly interpolates between vertebra data points calculated from triad2vert

Input data structure holding vertebra position and orientation information

Output void

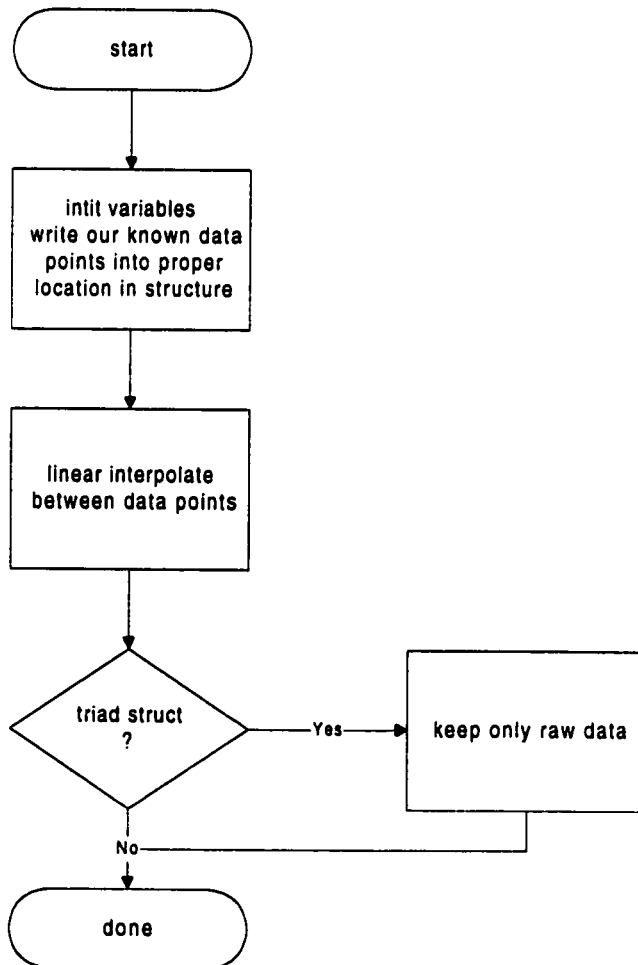


Fig. B.8 Interpolate flowchart.

APPENDIX C TRIAD2VERT FLOWCHARTS

This Appendix contains all flowcharts used in the triad2vert software. Triad2vert takes the triad position and orientation data and transform in into vertebra position and orientation data as explained in Chapter 4. The algorithm to rotate a point about an arbitrary line forms the basis of the module. Each routine flowchart is presented along with its purpose, inputs and outputs. All code was heavily documented for future programmers.

vectorize

Converts a vector of orientation $\phi\omega\kappa$ into a unit vector. This routine is used in the triad2vert program for converting polar expressions into their unit vector form.

Input 4x1 matrix containing angles $\phi\omega\kappa$

Output 4x1 matrix containing unit vector of $\phi\omega\kappa$

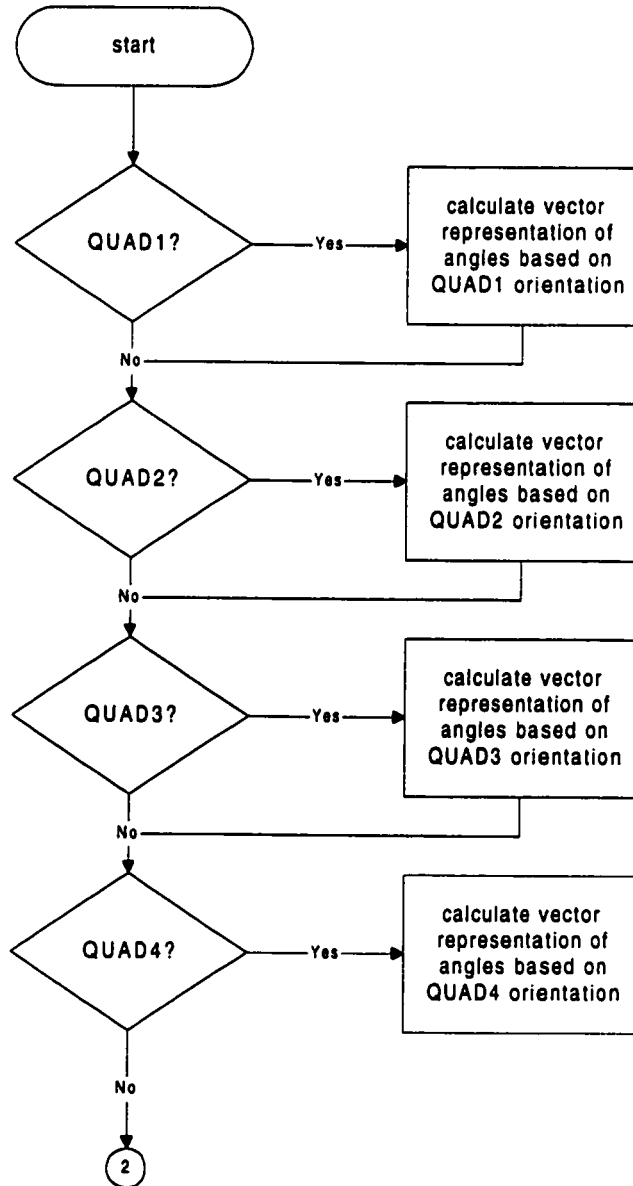


Fig. C.1 Vectorize flowchart.

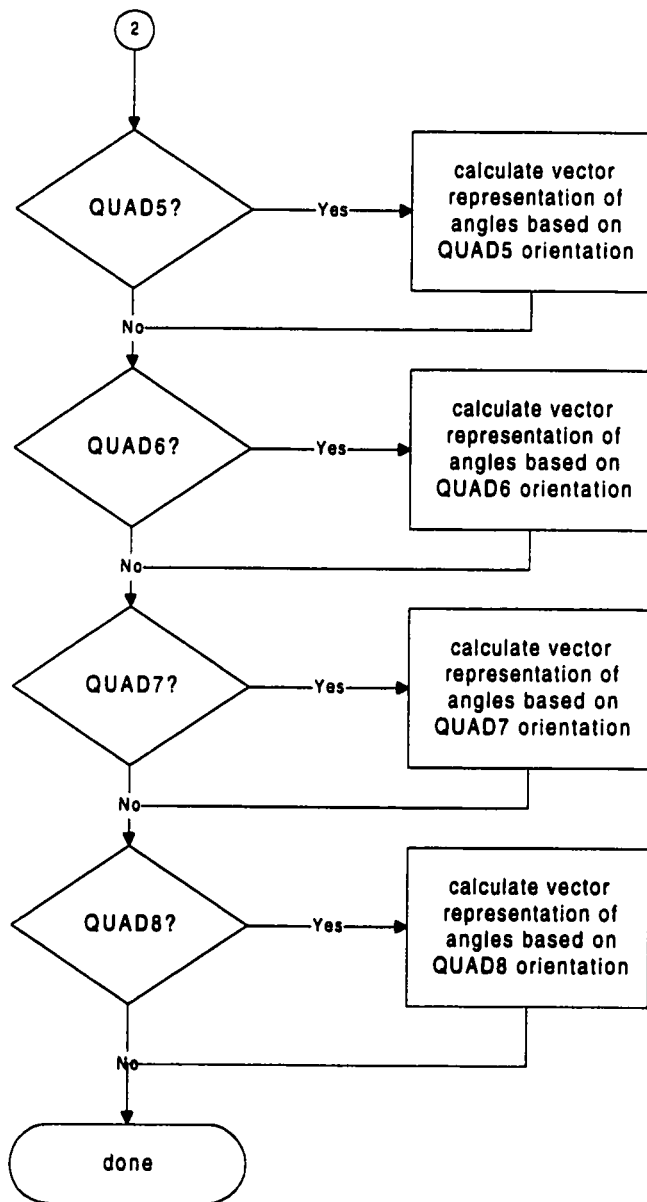


Fig. C.1 Vectorize flowchart.

Rotate_x rotates a 3D point about the x-axis according to

$$R_x = \begin{bmatrix} 1 & 0 & 0 & 0 \\ 0 & \cos\theta & \sin\theta & 0 \\ 0 & -\sin\theta & \cos\theta & 0 \\ 0 & 0 & 0 & 1 \end{bmatrix}$$

Input 4x1 matrix containing point to be rotated

size of angle rotation

Output new rotated point position

Rotate_y rotates a point about the y-axis according to

$$R_y = \begin{bmatrix} \cos\theta & 0 & -\sin\theta & 0 \\ 0 & 1 & 0 & 0 \\ \sin\theta & 0 & \cos\theta & 0 \\ 0 & 0 & 0 & 1 \end{bmatrix}$$

Input 4x1 matrix containing point to be rotated

size of angle rotation

Output new rotated point position

Rotate_z rotates a point about the z-axis according to

$$R_z = \begin{bmatrix} \cos\theta & \sin\theta & 0 & 0 \\ -\sin\theta & \cos\theta & 0 & 0 \\ 0 & 0 & 1 & 0 \\ 0 & 0 & 0 & 1 \end{bmatrix}$$

Input 4x1 matrix containing point to be rotated

size of angle rotation

Output new rotated point position

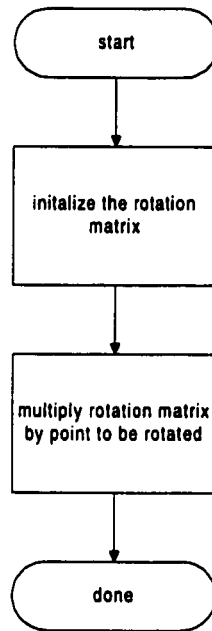


Fig. C.2 Rotate_x, Rotate_y, Rotate_z flowcharts.

phi_omega_kappa calculates the angles $\phi\omega\kappa$ describing the orientation of a vector

Input 4x1 matrix vector to calculate $\phi\omega\kappa$ for

Output 4x1 matrix vector containing $\phi\omega\kappa$ describing that vector

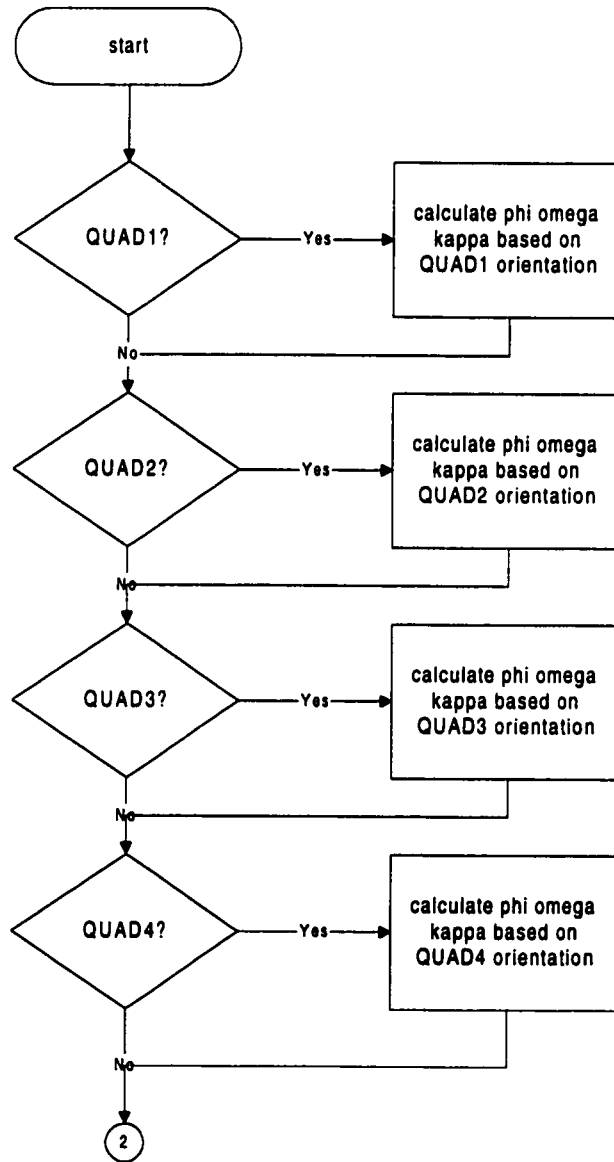


Fig. C.3 Phi_omega_kappa flowchart.

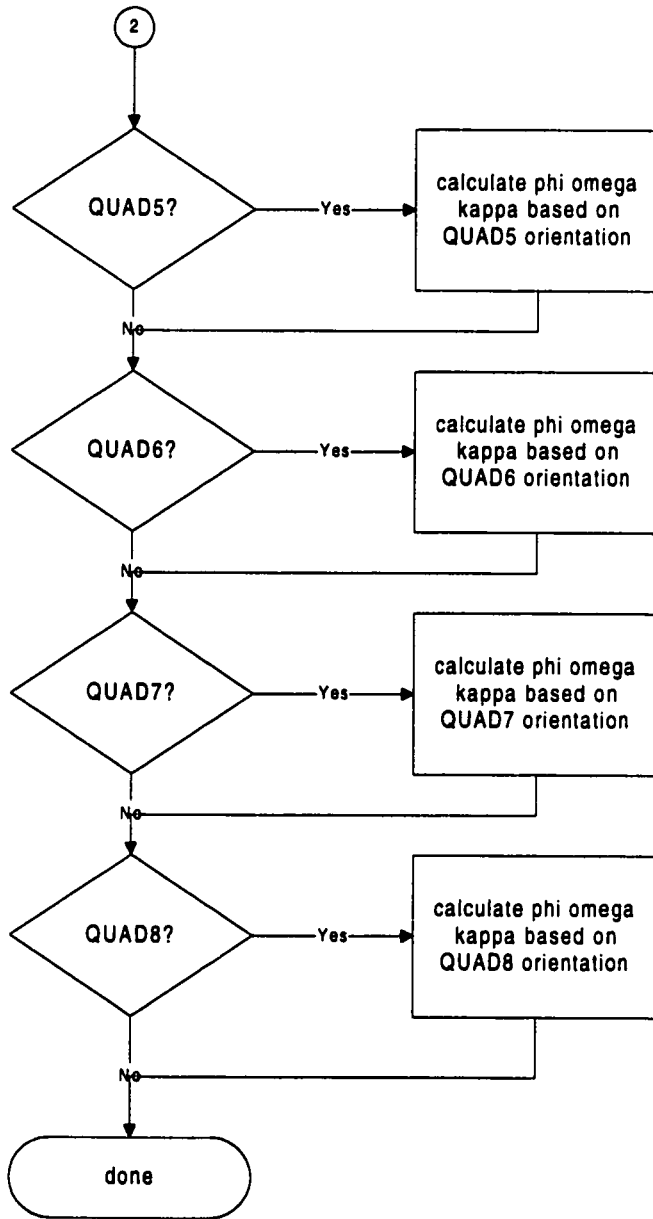


Fig. C.3 Phi_omega_kappa flowchart.

angle calculates the angle theta between two vectors

Input two 4x1 vectors to calculate the angle between and the one 4x1 vector representing the cross product of the two vectors

Output the angle theta

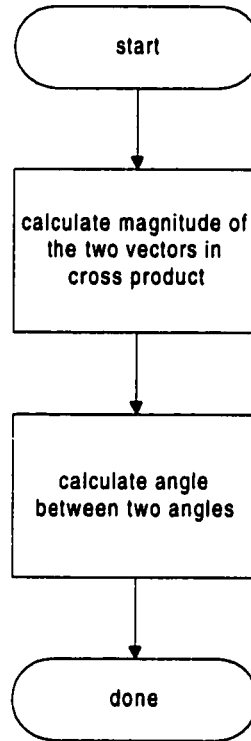


Fig. C.4 Angle flowchart.

cross_product calculates the cross product between two vectors

Input two 4x1 matrix vectors to take cross product of

Output 4x1 matrix vector representing the cross product

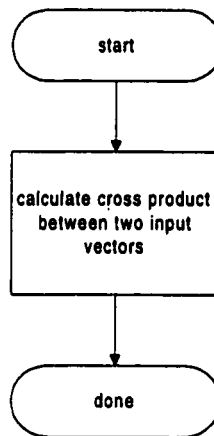


Fig. C.5 Cross_product flowchart.

Rotate_about_A Rotates the body vector **B** about an axis of rotation **A**

Input 4x1 matrix vector **B**

Output new 4x1 matrix vector **B** orientation

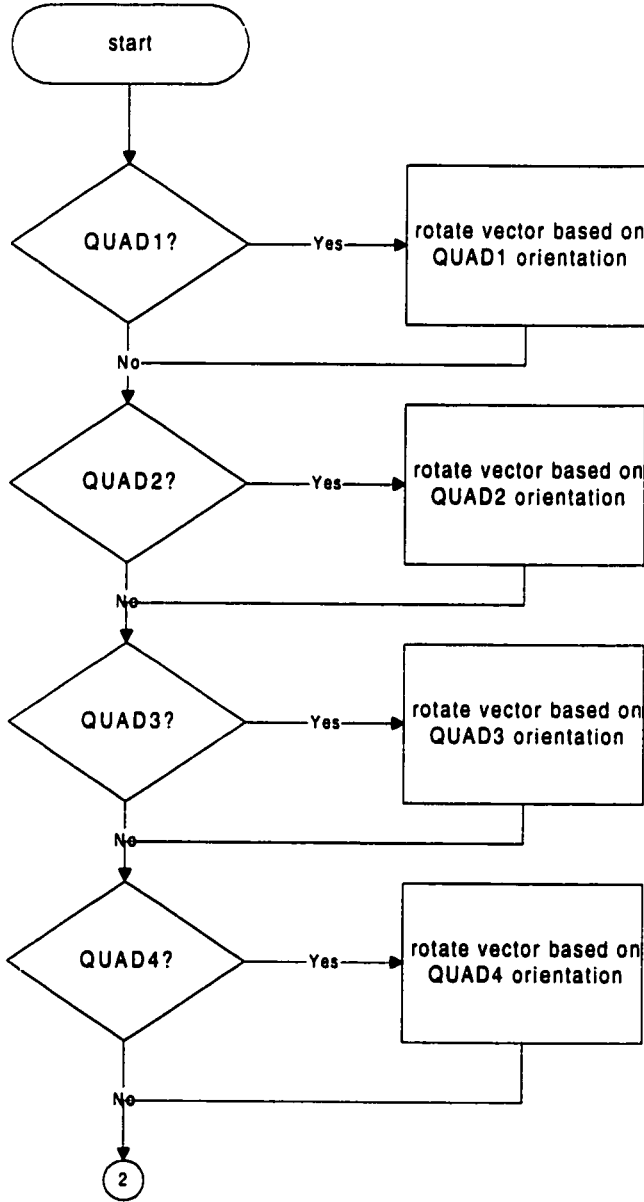


Fig. C.6 Rotate_about_A flowchart.

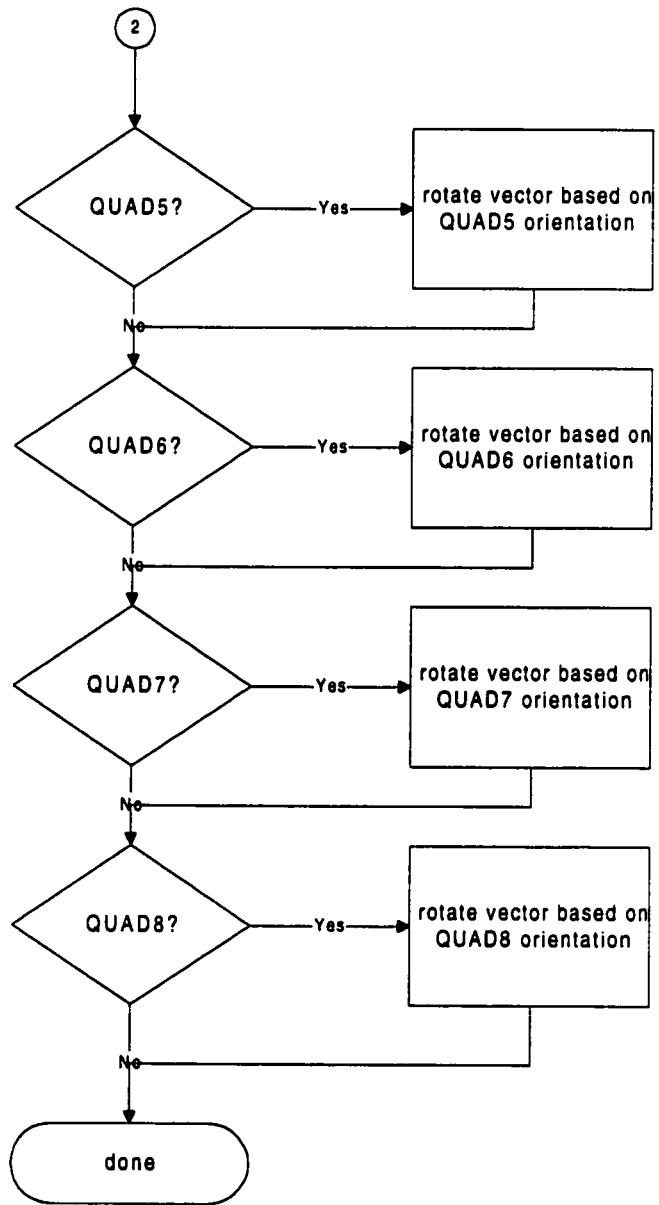


Fig. C.6 Rotation_about_A flowchart.

APPENDIX D DRAW MODULE FLOWCHARTS

Draw is the module from **SHOW-POINT** that renders the spine in 3D on the computer console. The appropriate vertebra model is rendered depending on specification set by the user in the graphical user interface. After the spine has been rendered, control is returned to the **SHOW-POINT** module. Flowcharts are presented describing the purpose of the routine, along with their respective inputs and outputs.

centerSpine finds the middle vertebra of the spine in the data structure, then shifts the position of the spine to display in the middle on the screen

Input pointers to hold the position of the first, middle and last vertebra

Output void

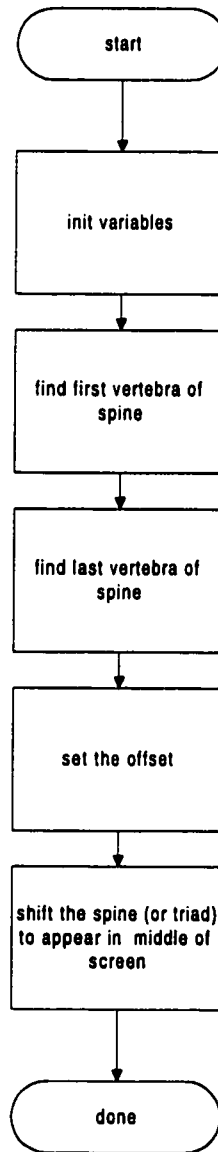


Fig. D.1 CenterSpine flowchart.

initVert initializes a data structure setting the vertebra dimensions specified by Panjabi (Panjabi, 1991, 1992)

Input data structure to holding vertebra dimensions

Output data structure initialized with vertebra dimensions

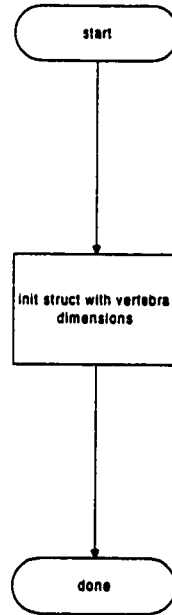


Fig. D.2 InitVert flowchart.

wireFrame draws the wire frame model of vertebra based on supplied dimensions

Input vertebra dimensions and specific vertebra to be drawn

Output void

position draws the positional vertebra model based on supplied dimensions

Input vertebra dimensions and specific vertebra to be drawn

Output void

geometric draws the geometric vertebra model based on supplied dimensions

Input vertebra dimensions and specific vertebra to be drawn

Output void

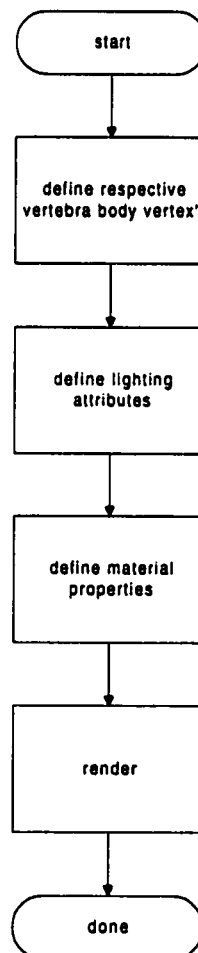


Fig. D.3 WireFrame, position, geometric flowcharts.

draw_triad draws a triad vector represented as an arrow based on supplied dimensions

Input specific vertebra to draw triad on

Output void

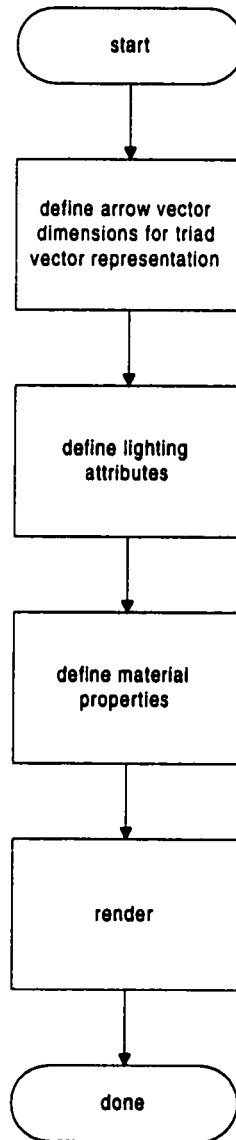


Fig. D.4 Draw_triad flowchart.

draw_xaxis draws the x,y,z axis for the orientation model and other models that can be toggled ON/OFF in the GUI

draw_yaxis

draw_zaxis

Input void

Output void

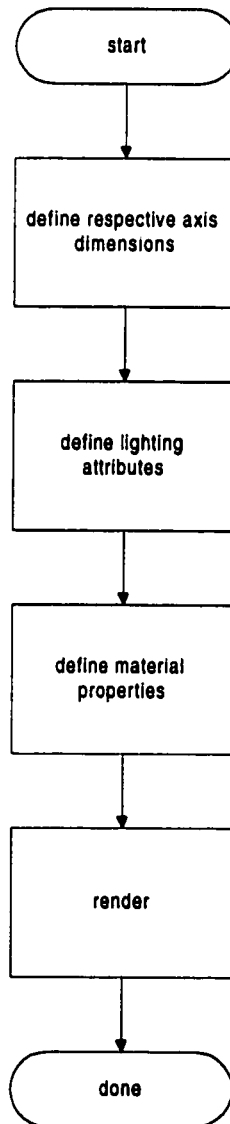


Fig. D.5 Draw_xaxis, draw_yaxis, draw_zaxis flowchart.

spotlight

defines the four non-rotating light positions for adding 3D light effects to model

Input void

Output void

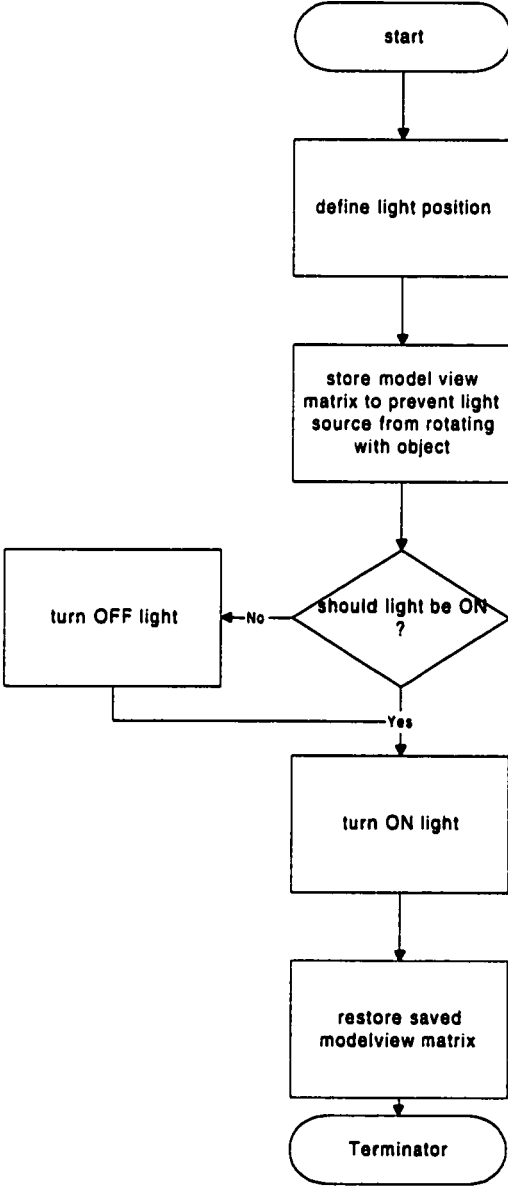


Fig. D.6 Spotlight flowchart.

draw handles all drawing to the four windows

Input widget holding glxcontext to be draw

Output void

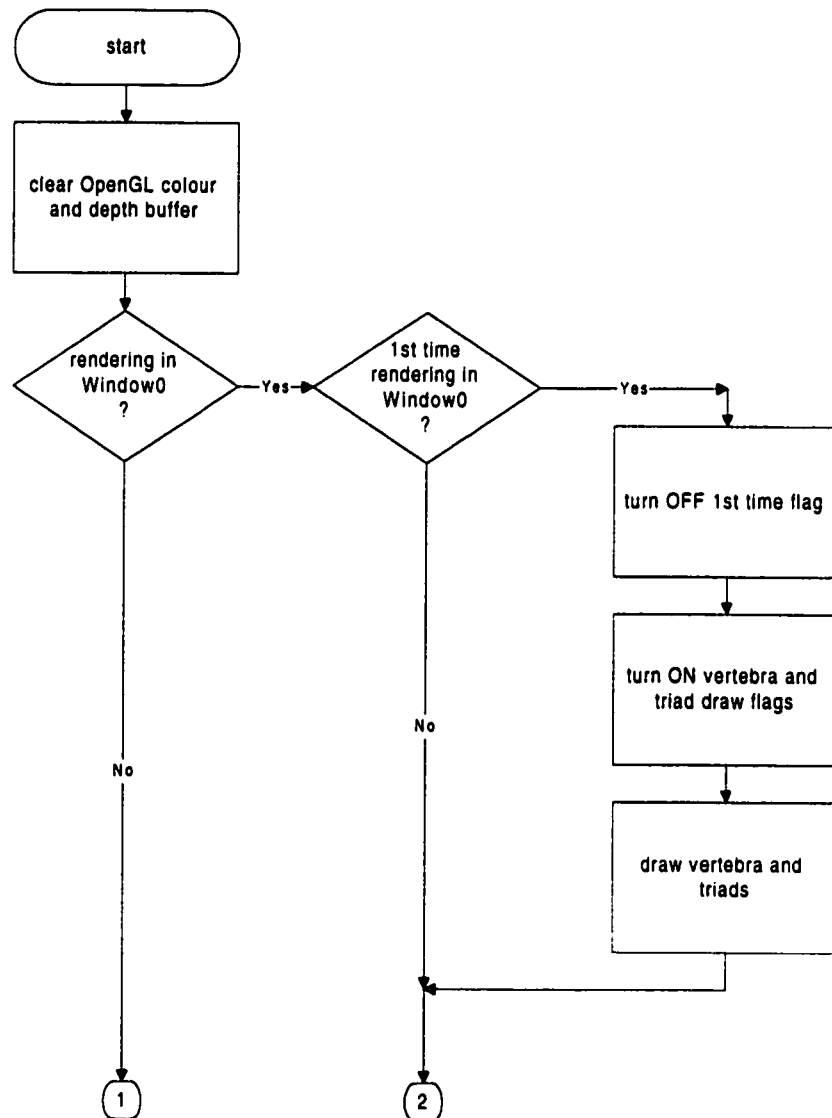


Fig. D.7 Draw flowchart.

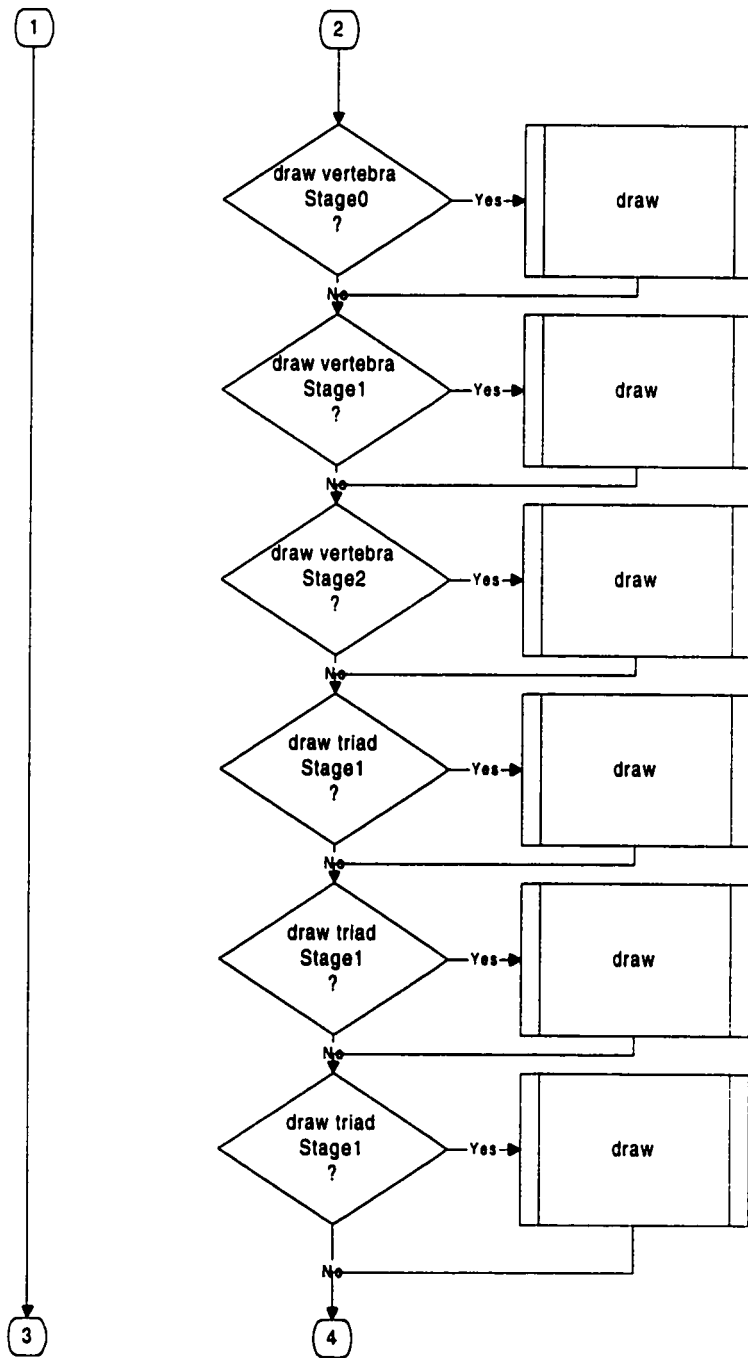


Fig. D.7 Draw flowchart (continued).

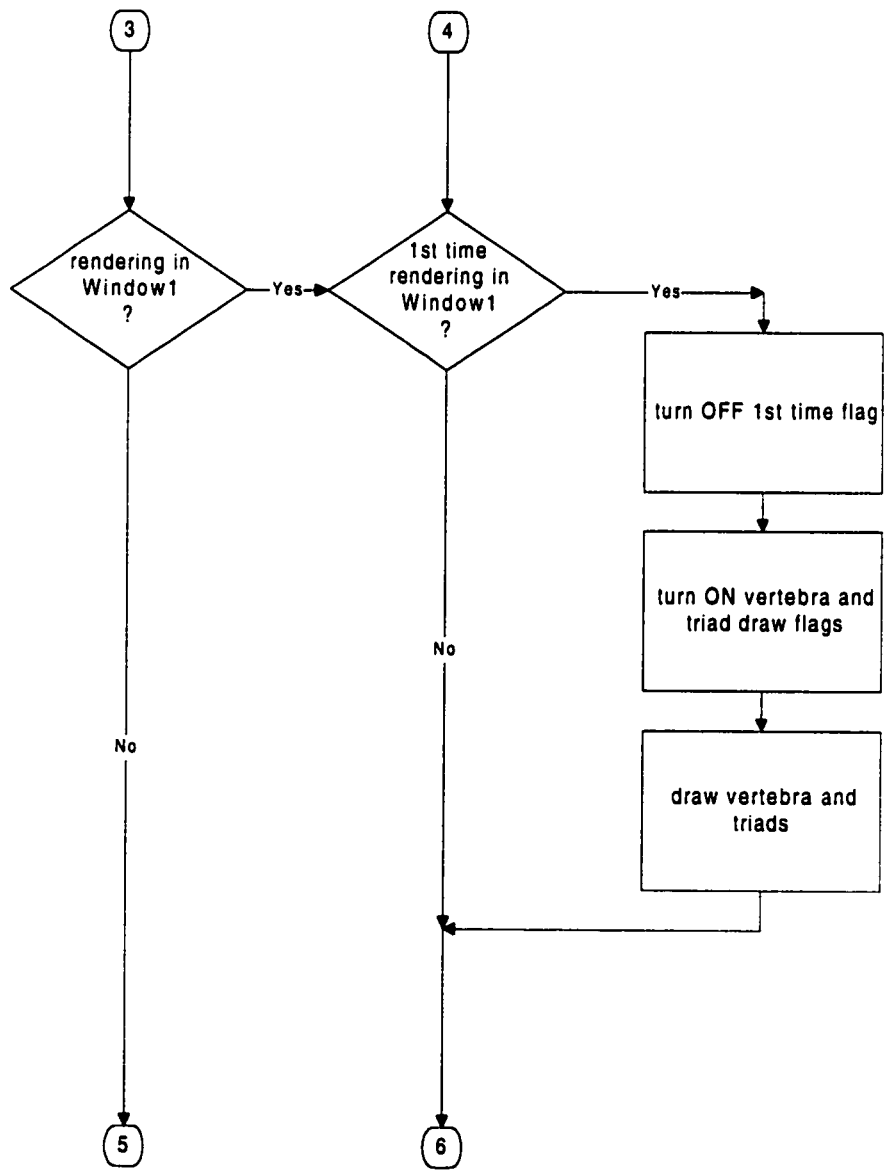


Fig. D.7 Draw flowchart (continued).

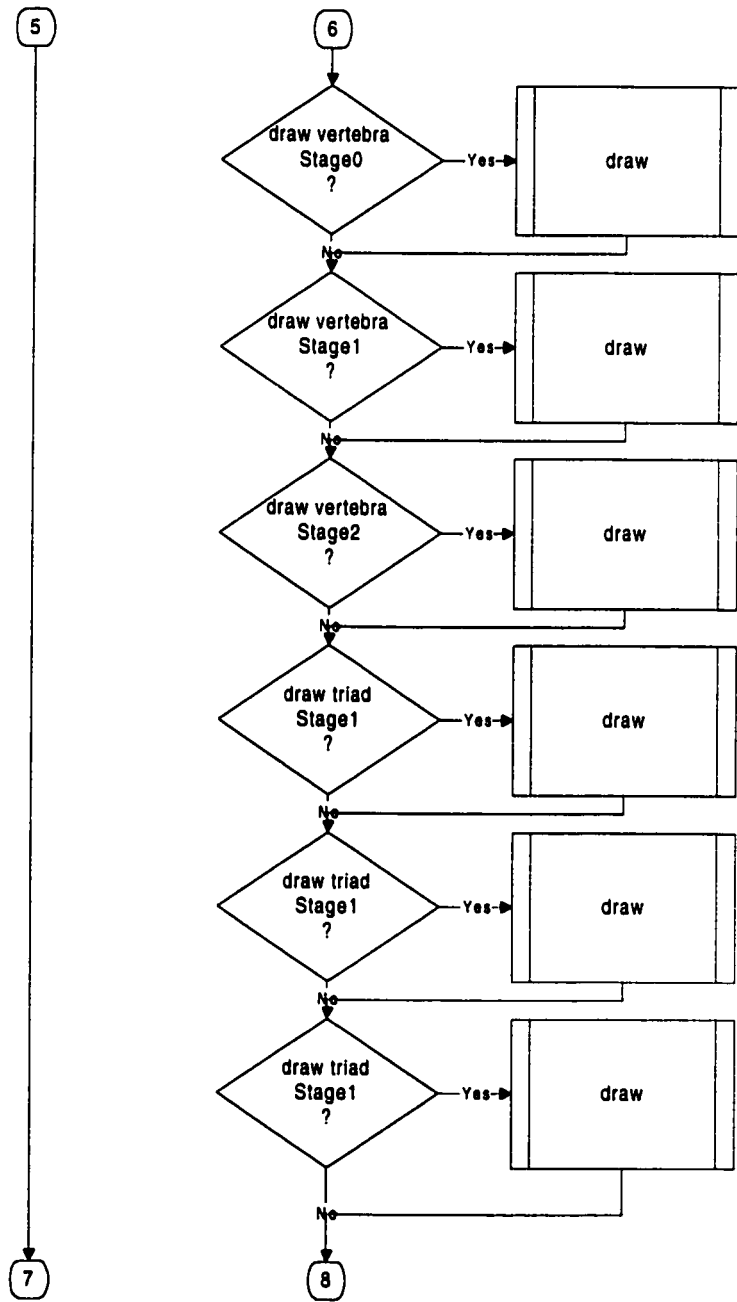


Fig. D.7 Draw flowchart (continued).

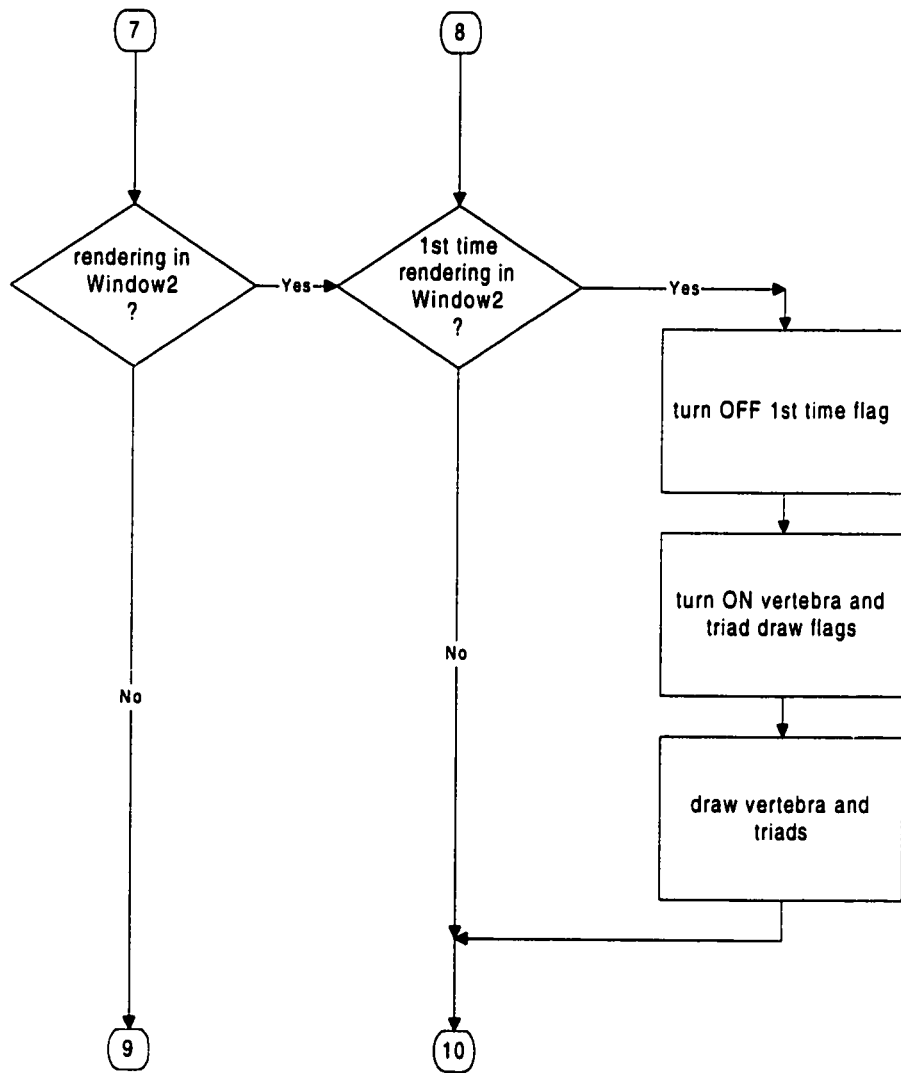


Fig. D.7 Draw flowchart (continued).

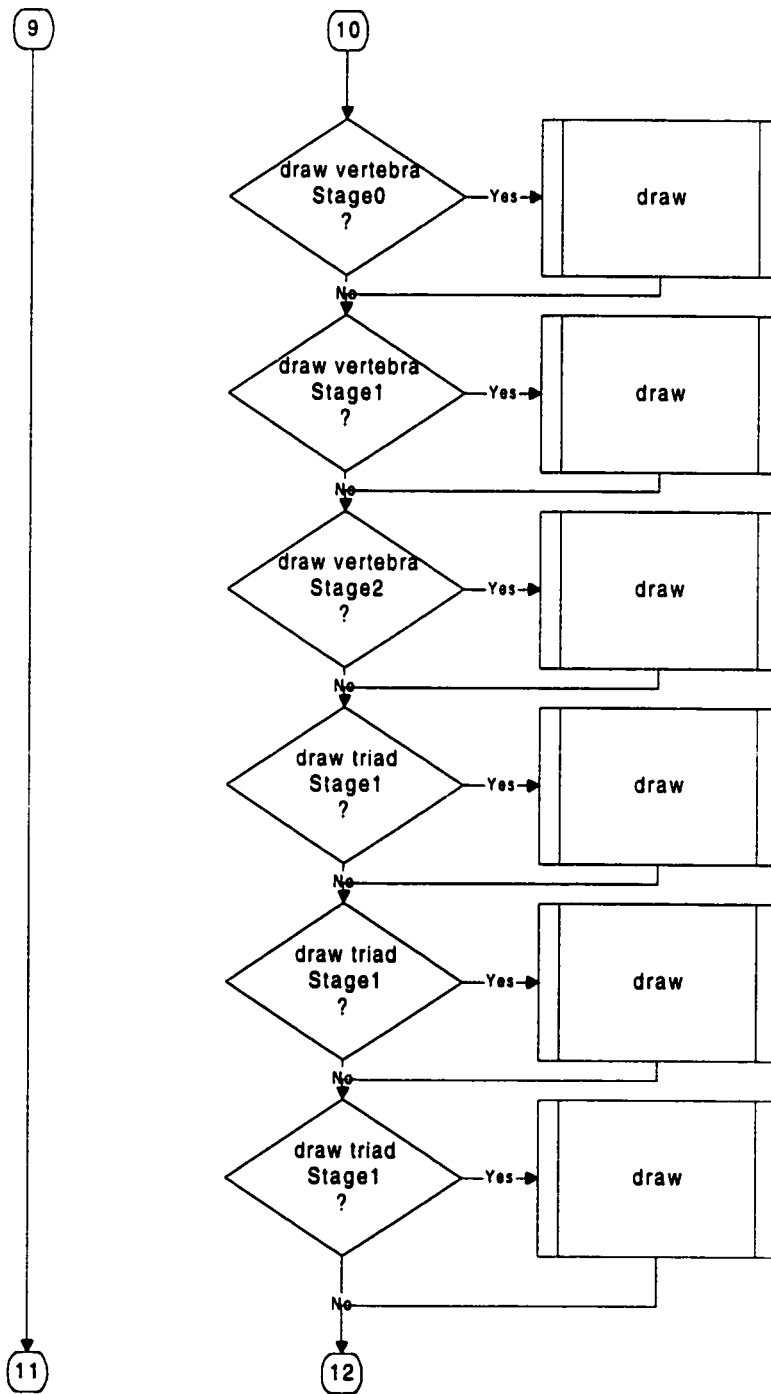


Fig. D.7 Draw flowchart (continued).

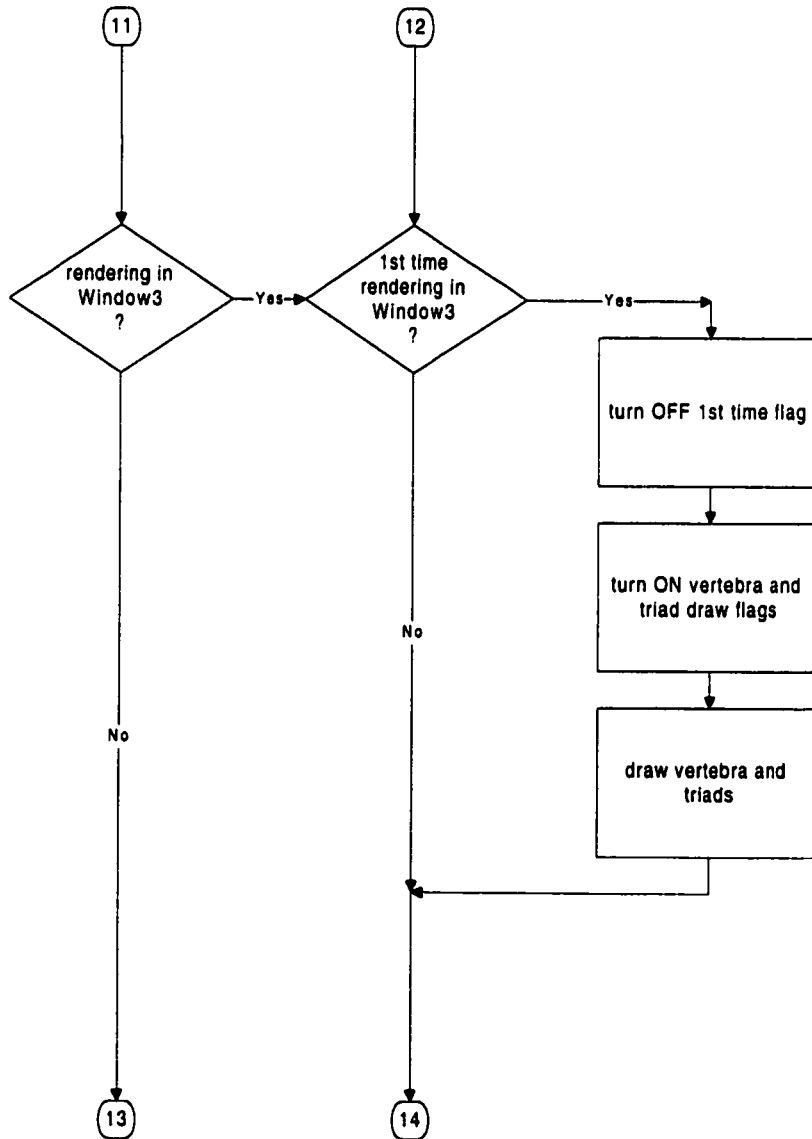


Fig. D.7 Draw flowchart (continued).

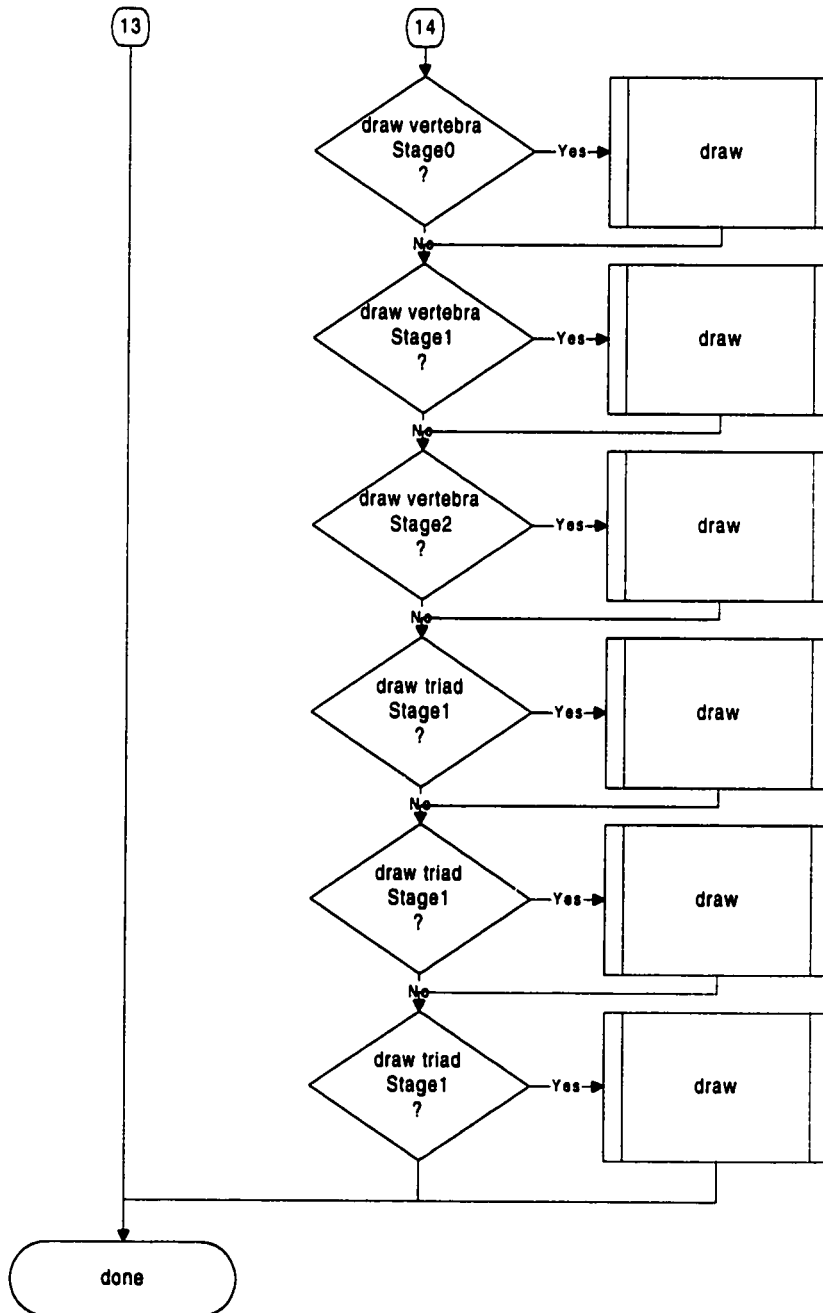


Fig. D.7 Draw flowchart.

draw_spine draws the vertebra model setting up the position and orientation of each vertebra. Model rendered is specified by user in GUI

Input data structure containing position and orientation information of each vertebra

Output void

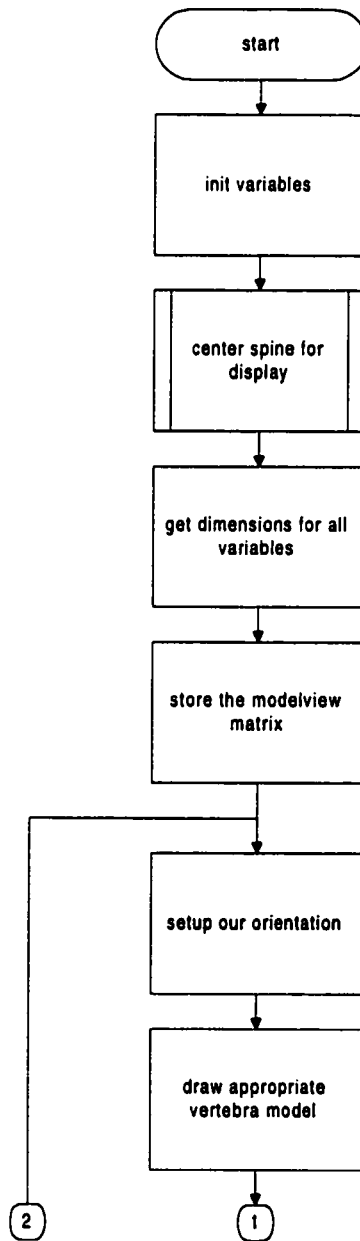


Fig. D.8 Draw_spine flowchart.

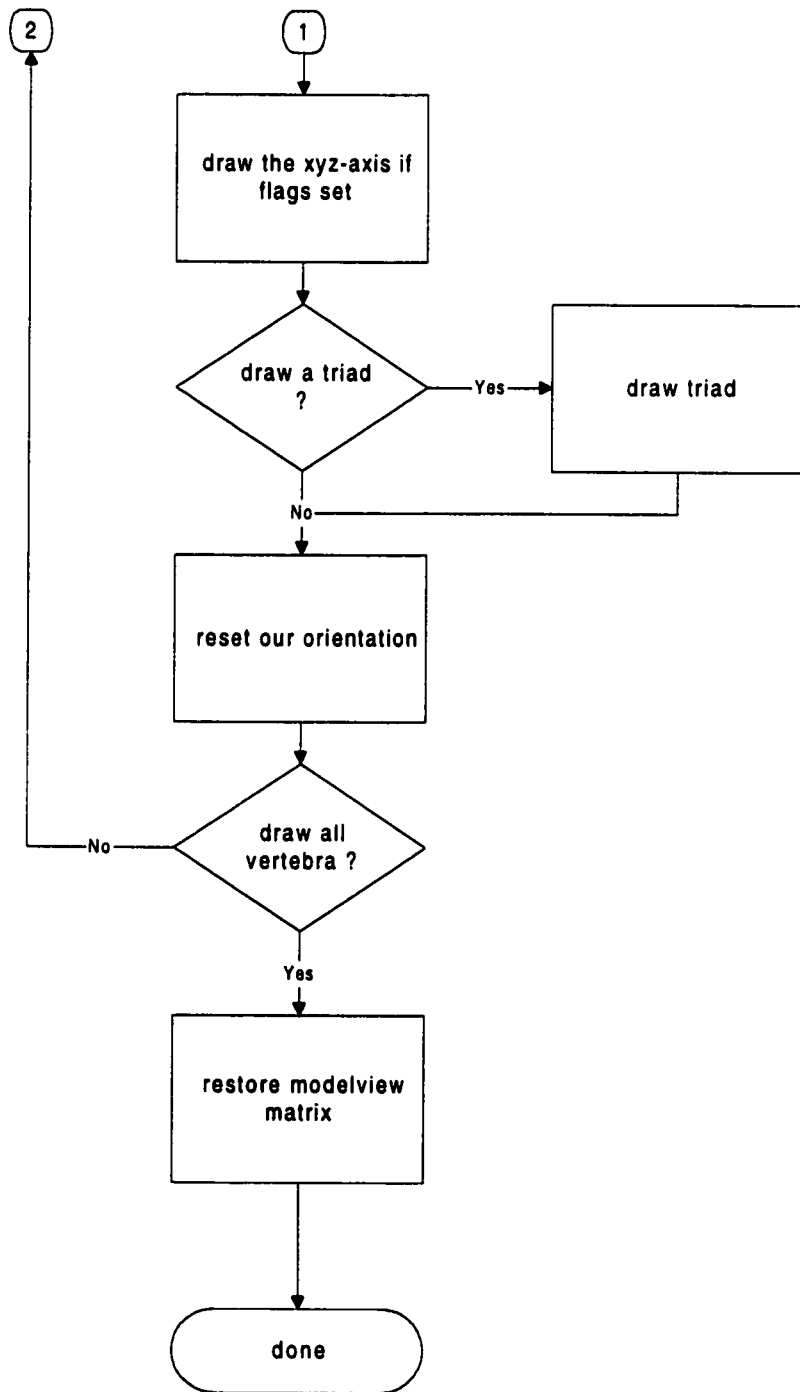


Fig. D.8 Draw_spine flowchart.

APPENDIX E MISC MODULE FLOWCHARTS

The **misc** module contains routines that handle **SHOW-POINT** variable initialization, setup the data structures, create the OpenGL rendering context widgets, and handle the creation of the graphical user interface. The flowcharts are presented explaining their purpose, inputs and outputs.

RTS handles all user commands to modify 3D model on screen

Input character key indicating desired user action

Output void

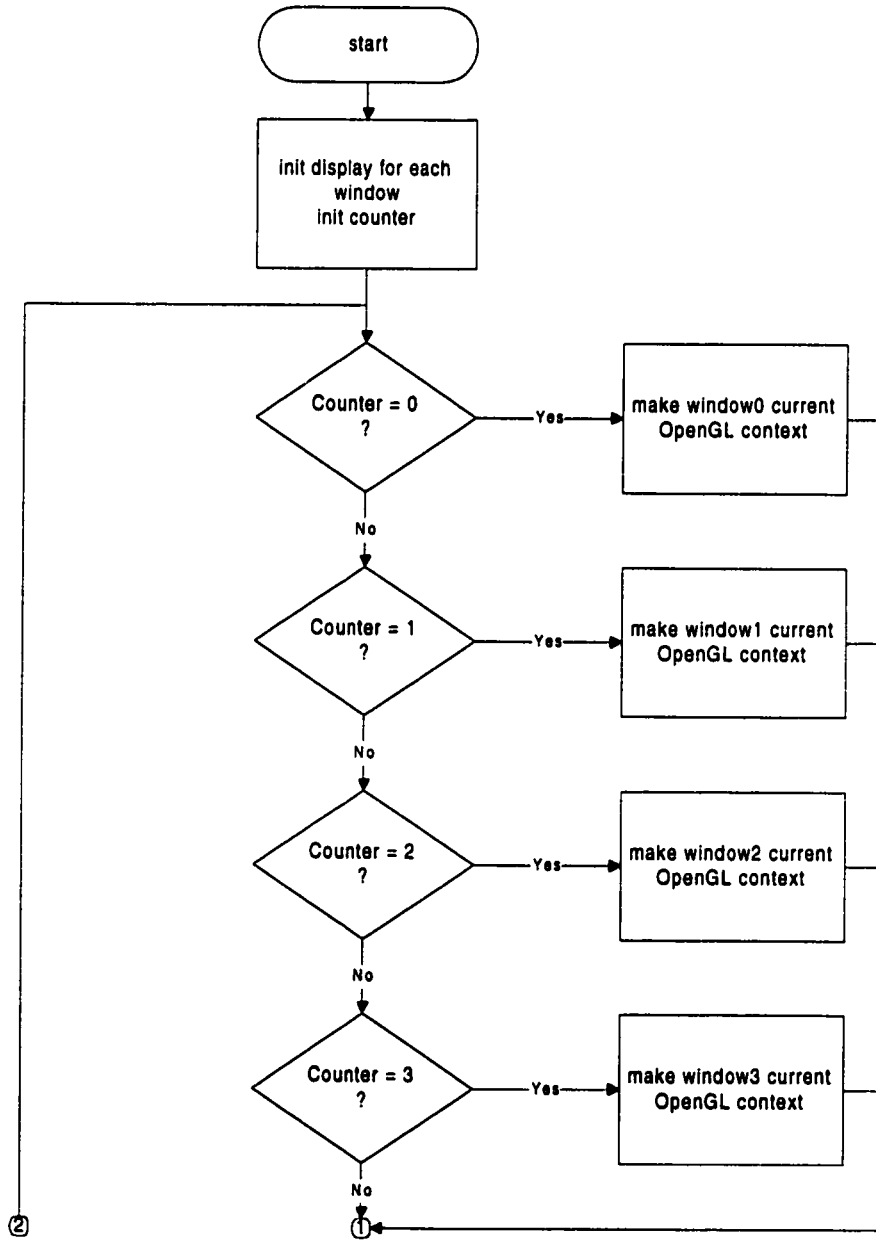


Fig. E.1 RTS flowchart.

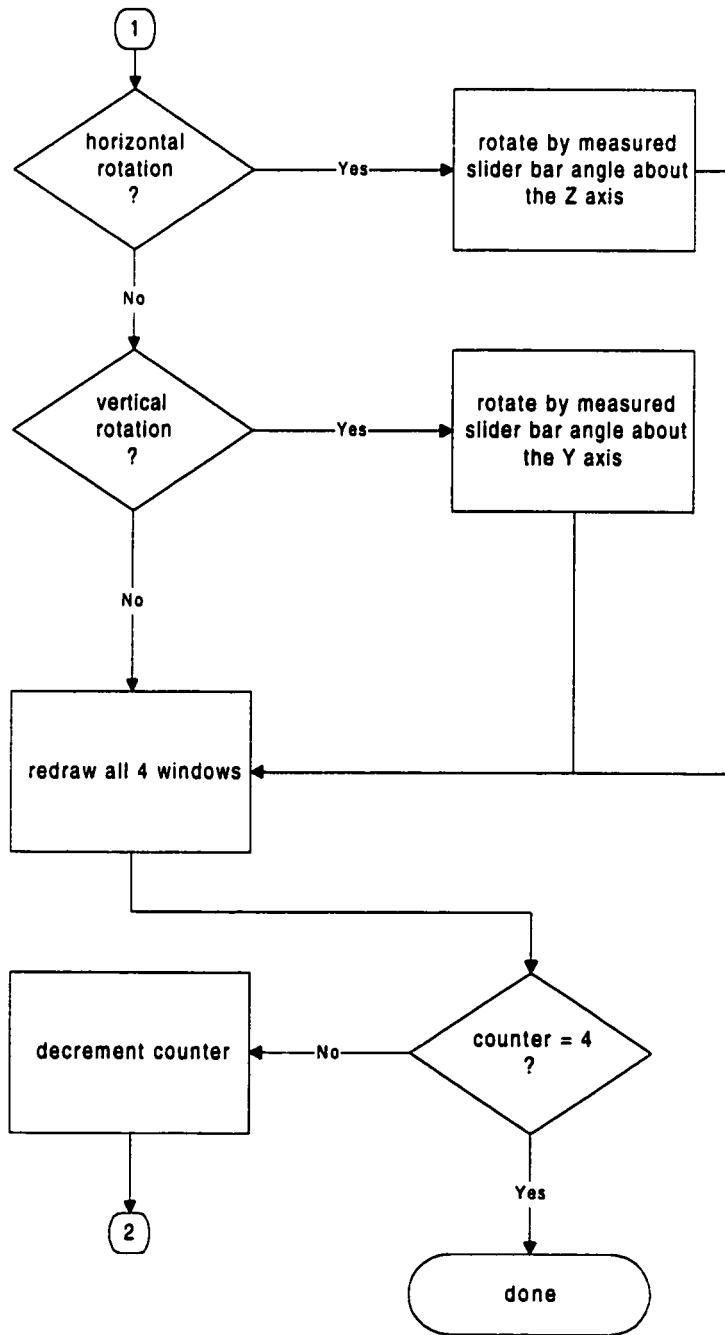


Fig. E.1 RTS flowchart.

Reset resets the views of the four windows to their default settings

Input window the character applies to and relevant X window parameters

Output void

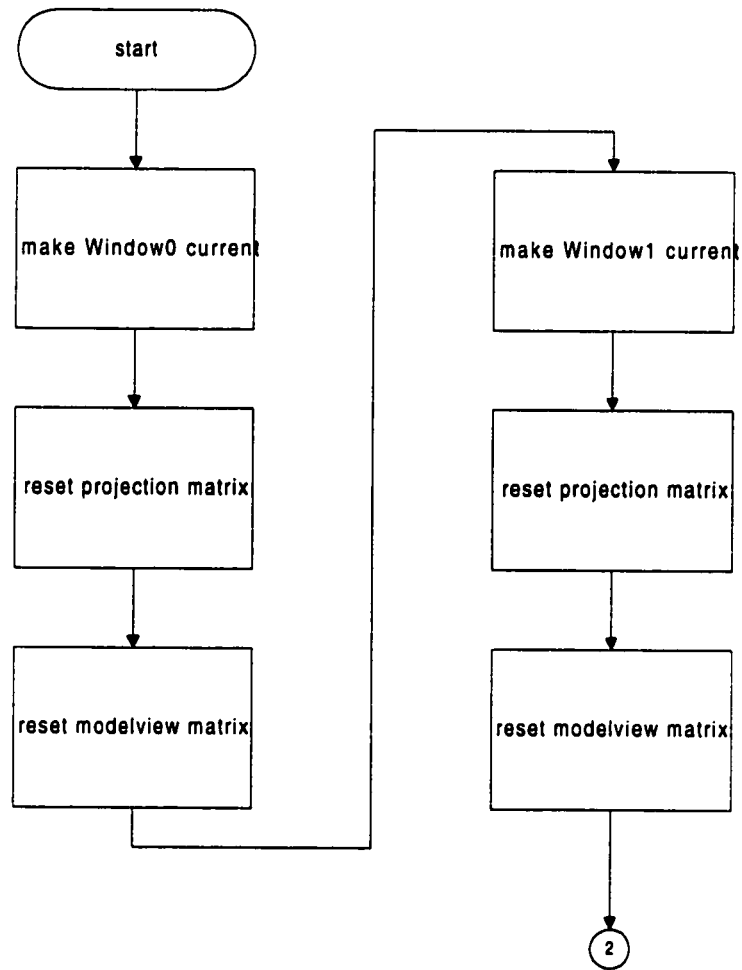


Fig. E.2 Reset flowchart.

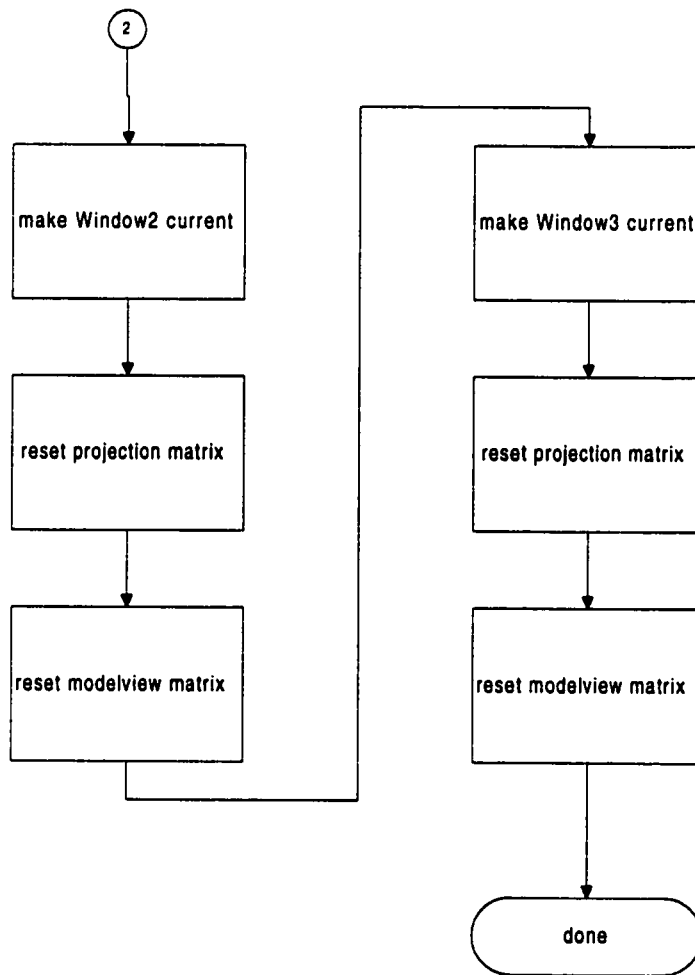


Fig. E.2 Reset flowchart.

drawing_area_callback invokes the user commands specified in RTS

Input window the character applies to and relevant X window parameters

Output void

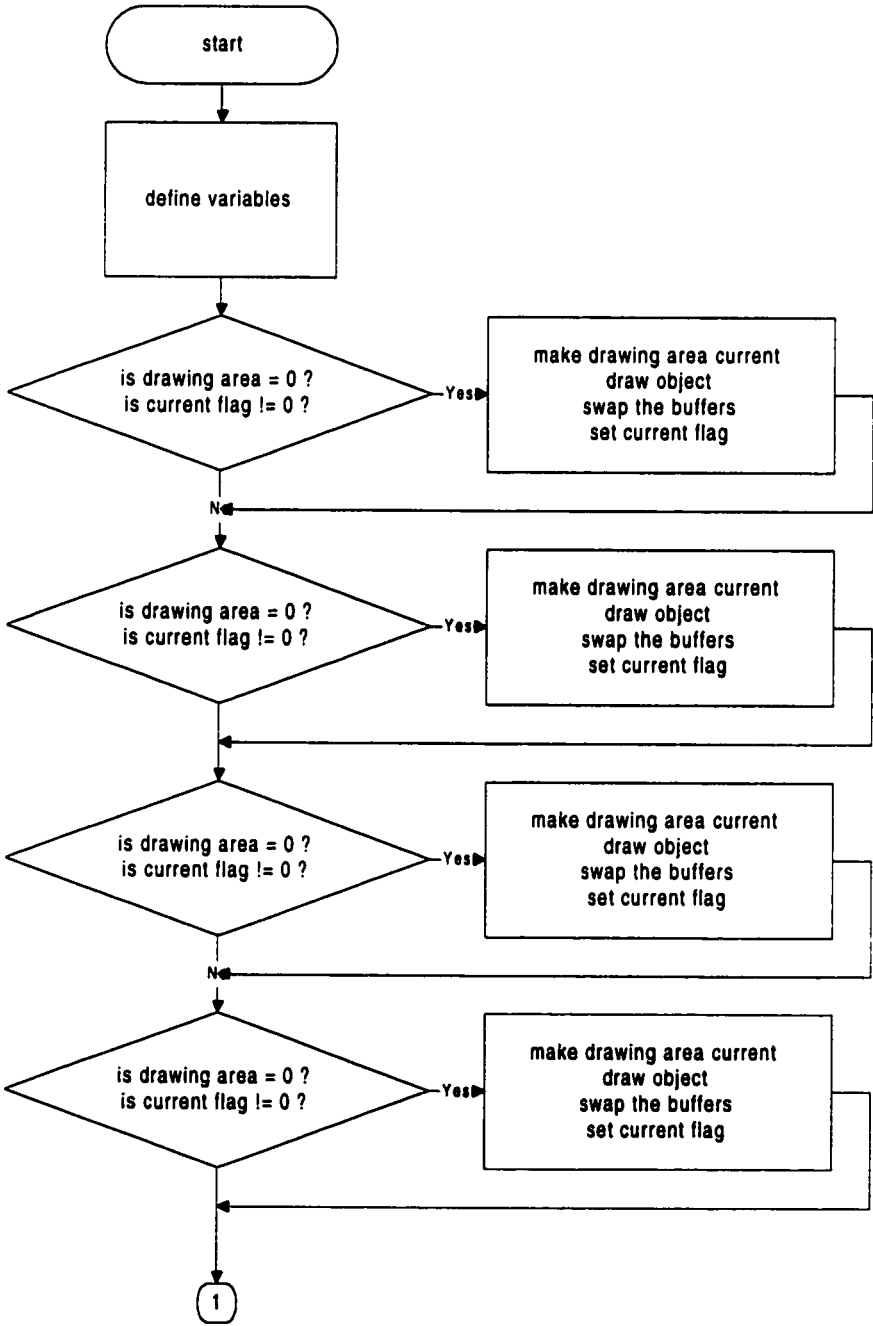


Fig. E.3 Drawing_area_callback flowchart.

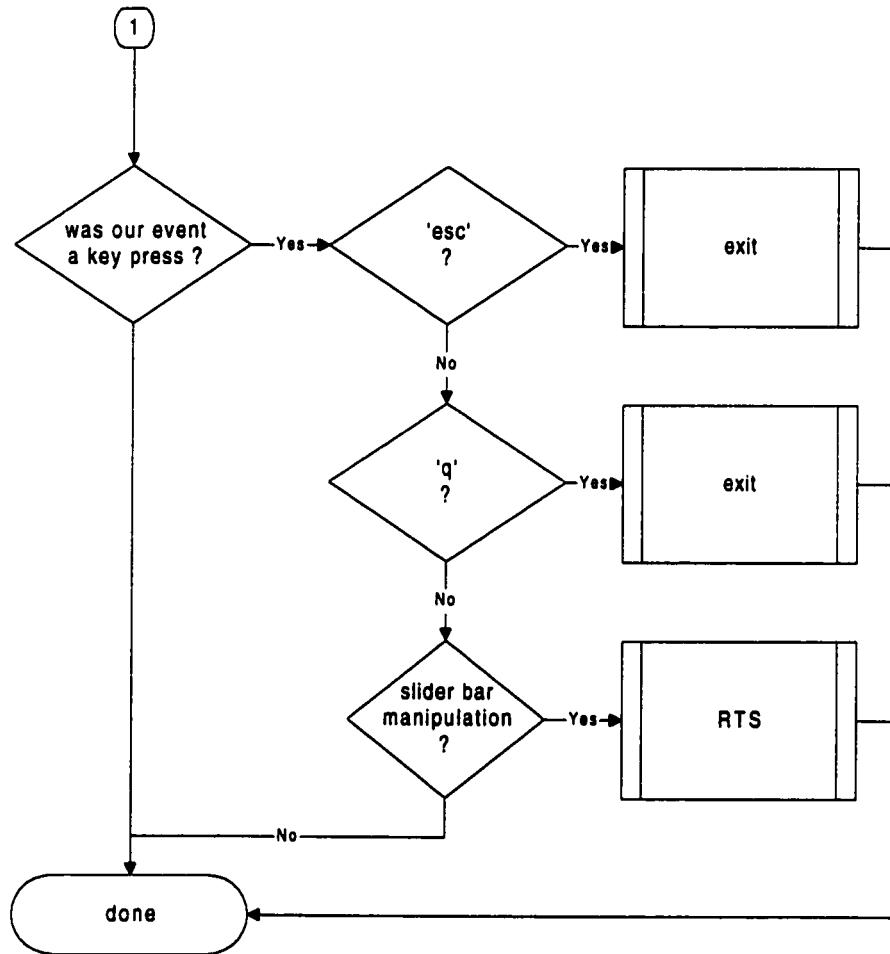


Fig. E.3 Drawing_area_callback flowchart.

CreateCascadeButton creates a Motif cascade button

Input Xwindow button parameters

Output widget containing button

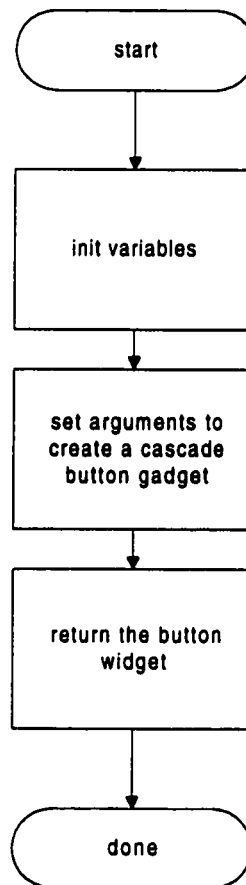


Fig. E.4 CascadeButton flowchart.

CreatePushButton creates a Motif push button

Input Xwindow button parameters

Output widget containing button

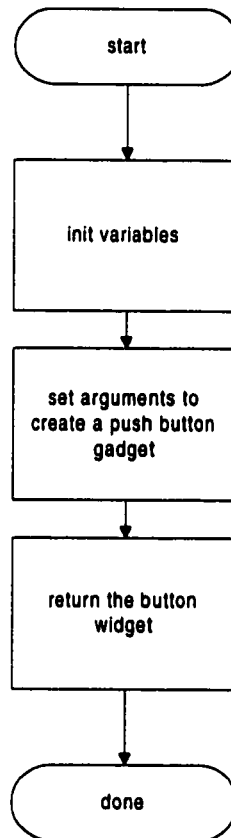


Fig. E.5 CascadePushButton flowchart.

CreateToggleButton creates a Motif toggle button

Input Xwindow button parameters

Output widget containing button

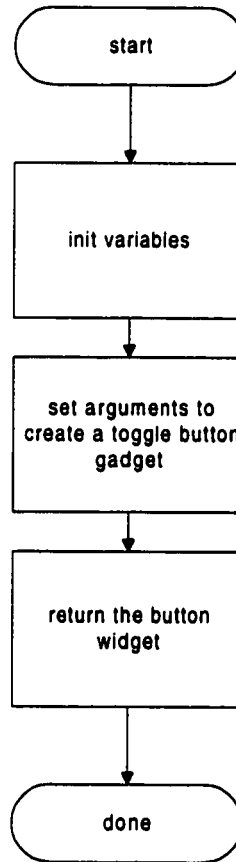


Fig. E.6 CascadeToggleButton flowchart.

DisplayCB toggles flags indicating current stages to be rendered, and type of object to be displayed

Input widget to be drawn and relevant X window parameters

Output void

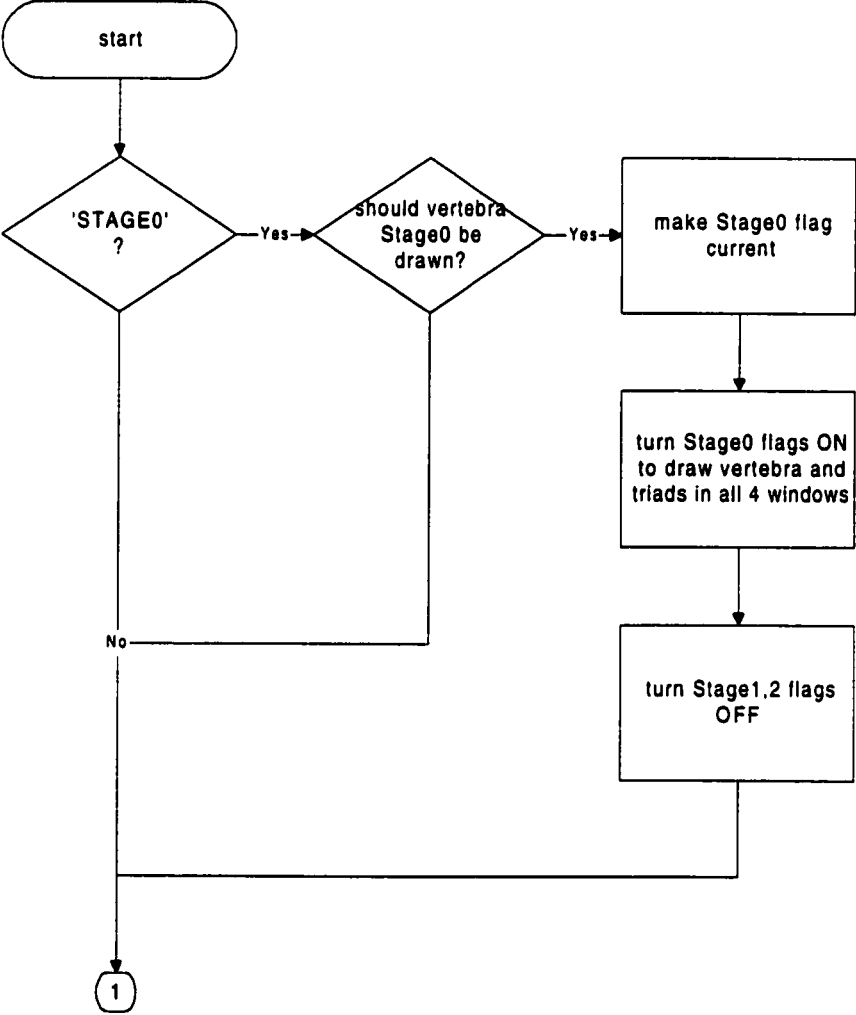


Fig. E.7 DisplayCB flowchart.

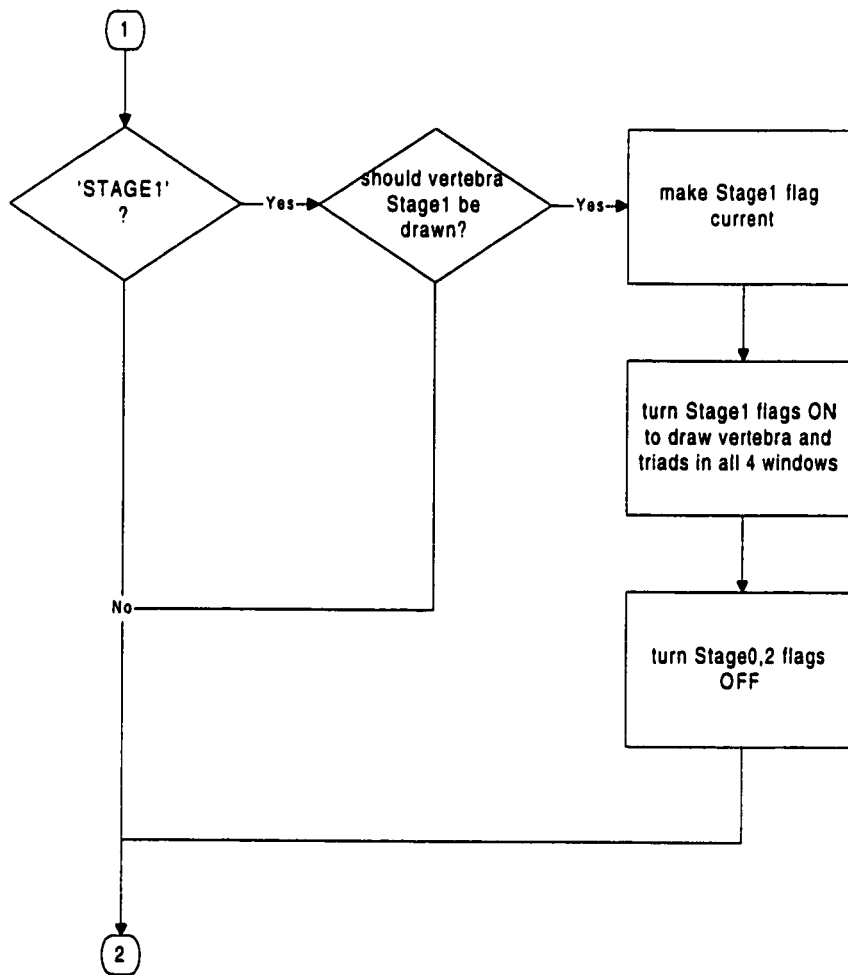


Fig. E.7 DisplayCB flowchart (continued).

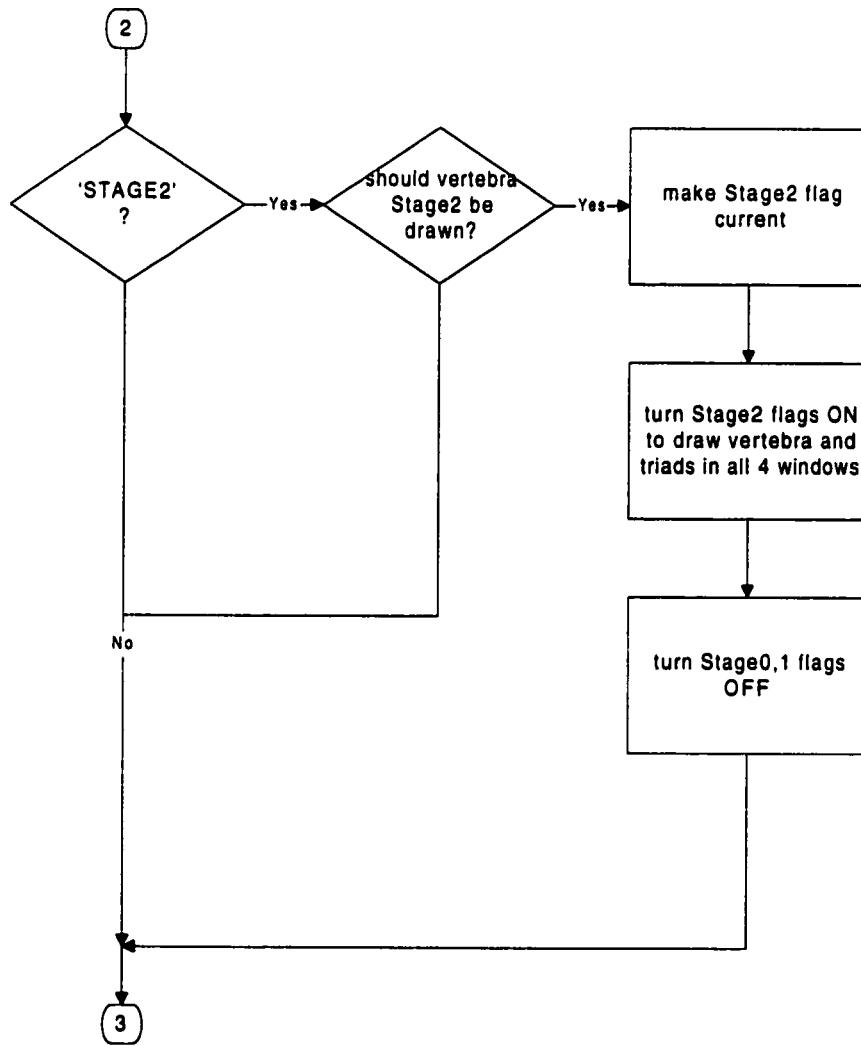


Fig. E.7 DisplayCB flowchart (continued).

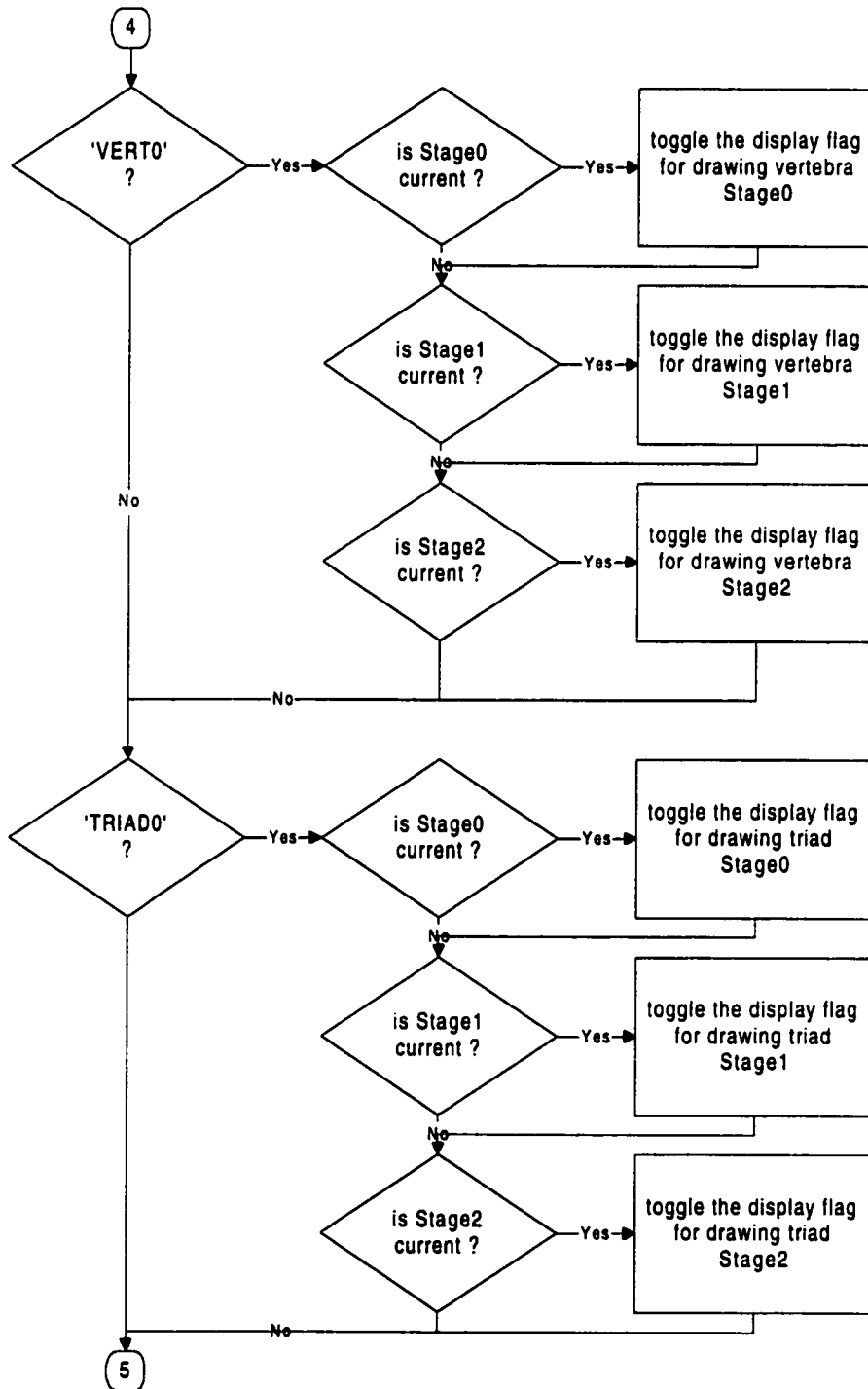


Fig. E.7 DisplayCB flowchart (continued).

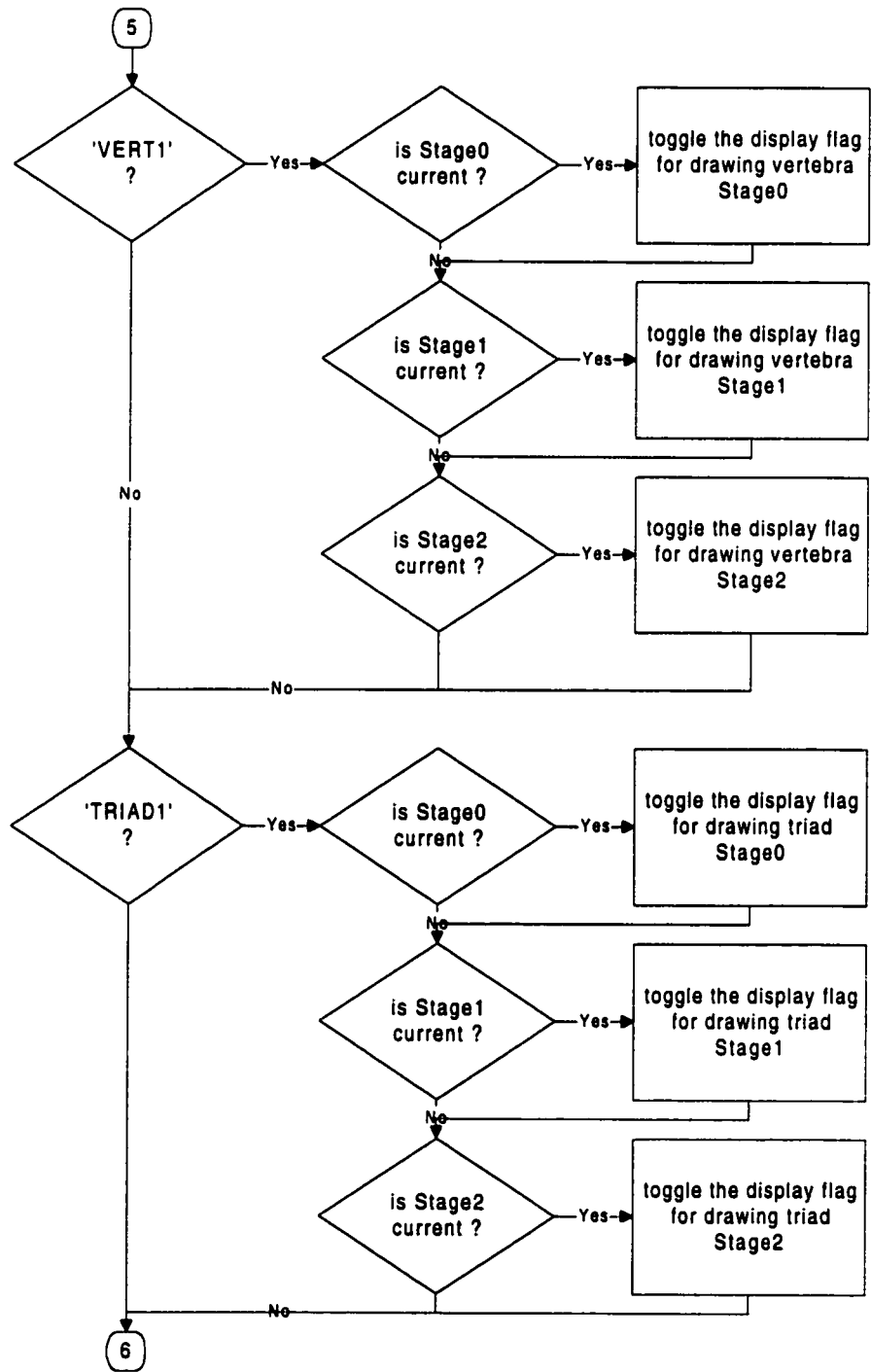


Fig E.7 DisplayCB flowchart (continued).

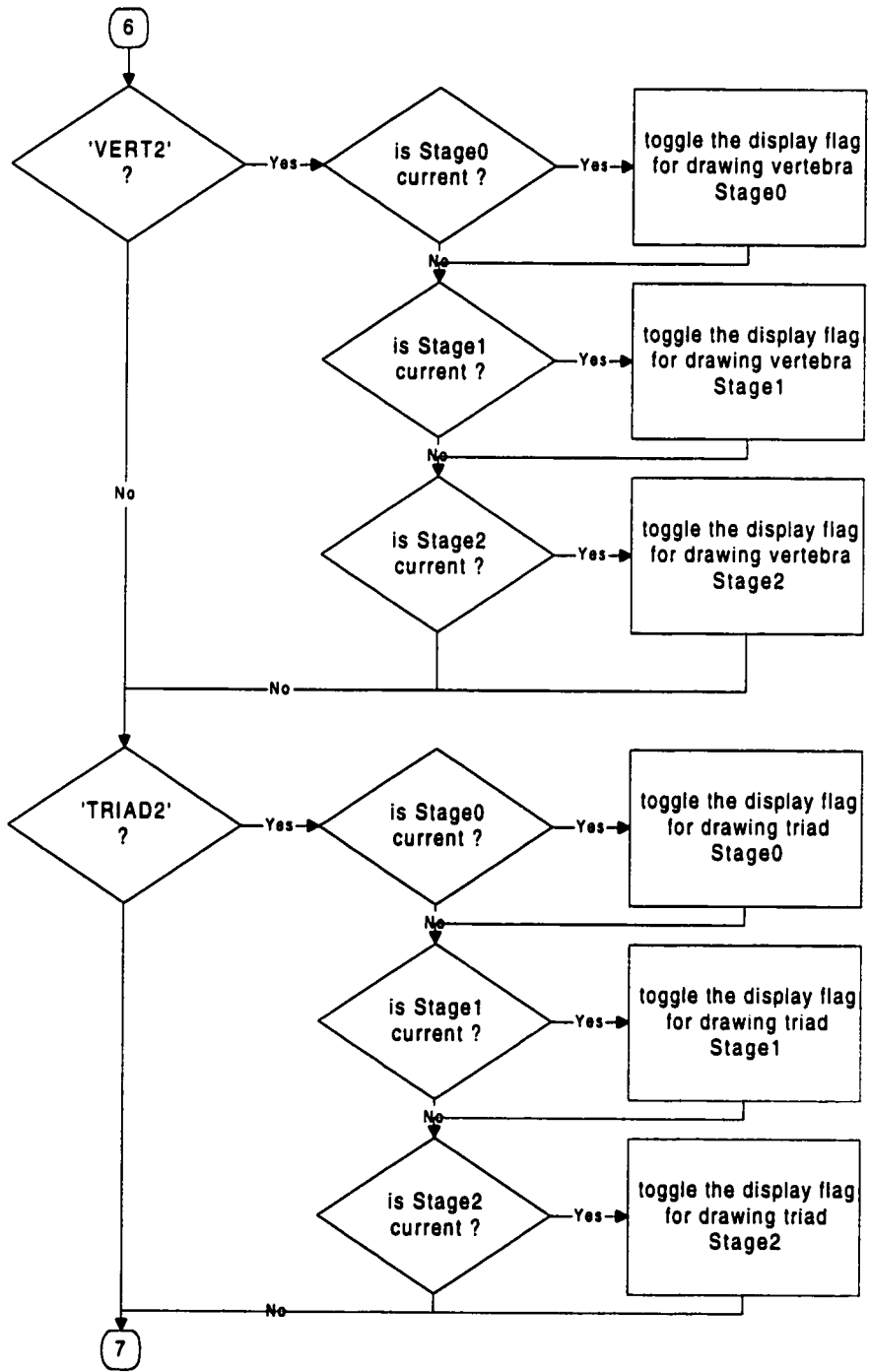


Fig. E.7 DisplayCB flowchart (continued).

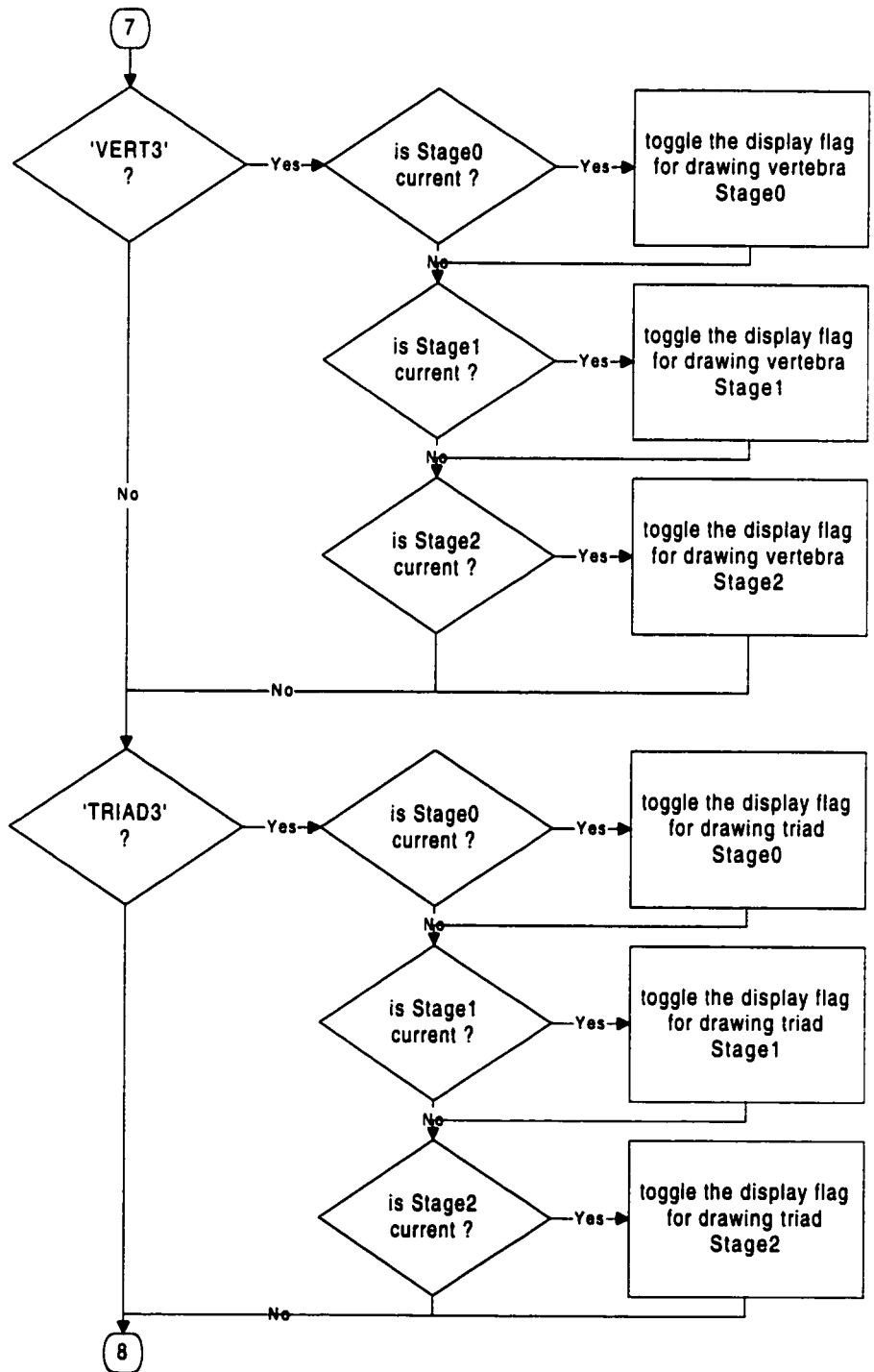


Fig. E.7 DisplayCB flowchart (continued).

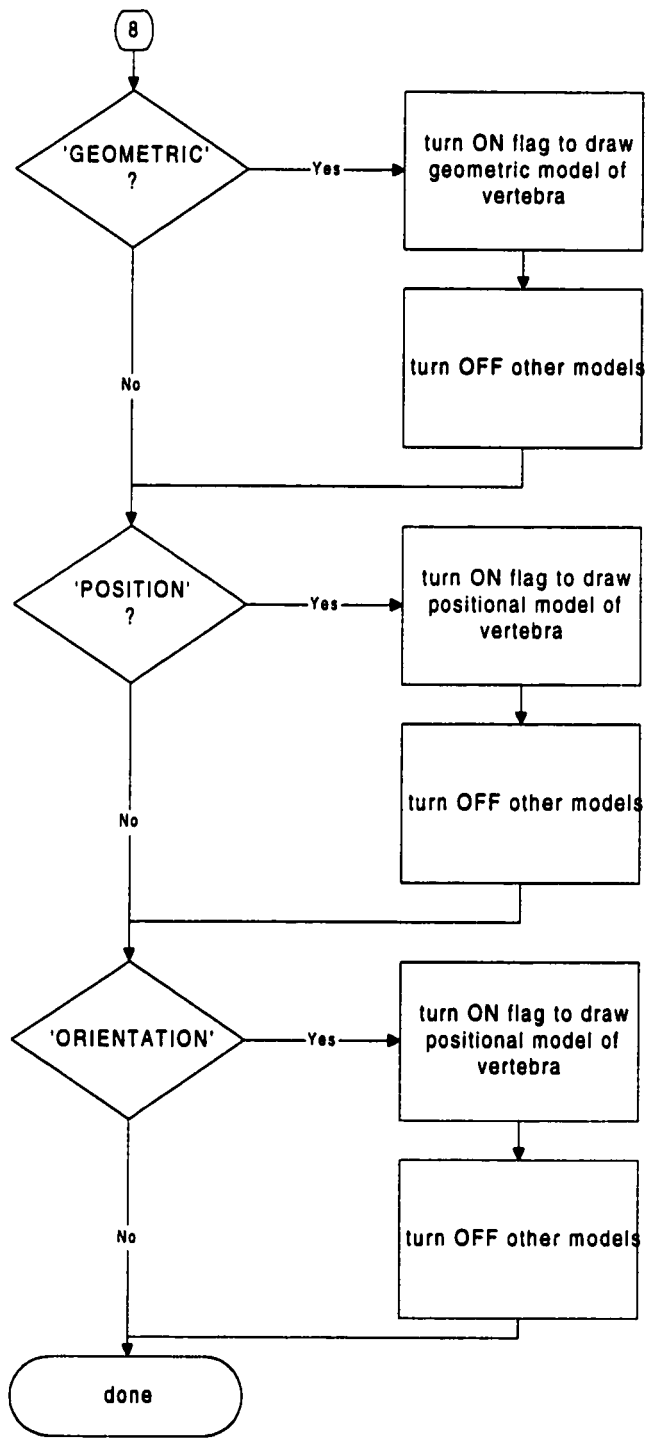
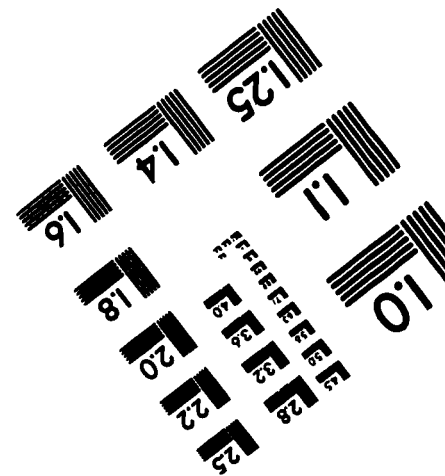
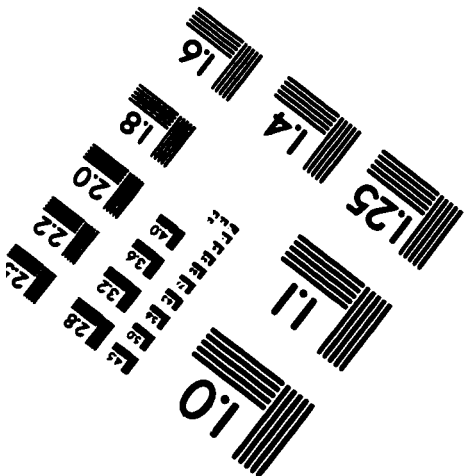
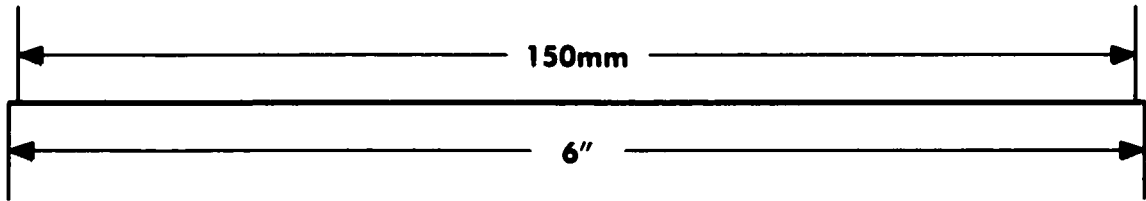
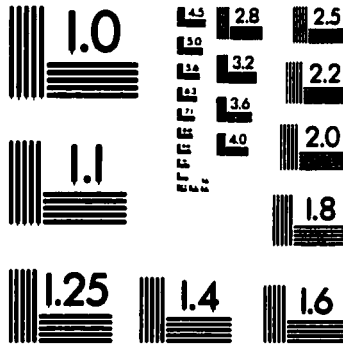
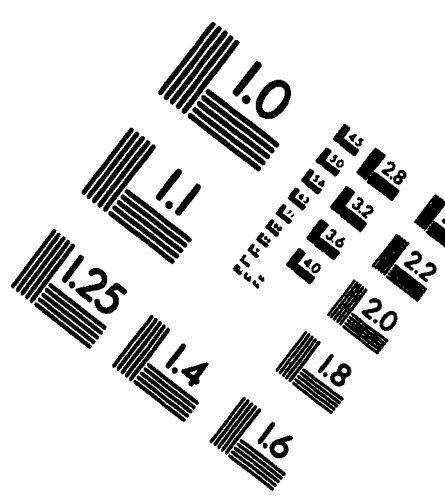
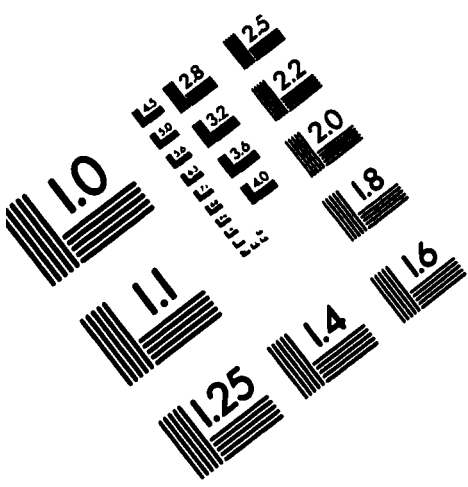


Fig. E.7 DisplayCB flowchart.

IMAGE EVALUATION TEST TARGET (QA-3)



APPLIED IMAGE, Inc
1653 East Main Street
Rochester, NY 14609 USA
Phone: 716/482-0300
Fax: 716/288-5989

© 1993, Applied Image, Inc., All Rights Reserved